Assessing annual urban change and its impacts on evapotranspiration

Heng Wan

Dissertation submitted to the faculty of the Virginia Polytechnic Institute and State University in partial fulfillment of the requirements for the degree of

Doctor of Philosophy

In

Geospatial and Environmental Analysis

Yang Shao, Chair

Lynn M. Resler

James B. Campbell

Xinwei Deng

May 12th, 2020

Blacksburg, Virginia

Keywords: urban change, NDVI, machine learning, evapotranspiration

Assessing annual urban change and its impacts on evapotranspiration

Heng Wan

ABSTRACT

Land Use Land Cover Change (LULCC) is a major component of global environmental change, which could result in huge impacts on biodiversity, water yield and quality, climate, soil condition, food security and human welfare. Of all the LULCC types, urbanization is considered to be the most impactful one. Monitoring past and current urbanization processes could provide valuable information for ecosystem services evaluation and policy-making.

The National Land Cover Database (NLCD) provides land use land cover data covering the entire United States, and it is widely used as land use land cover data input in numerous environmental models. One major drawback of NLCD is that it is updated every five years, which makes it unsatisfactory for some models requiring land use land cover data with a higher temporal resolution. This dissertation integrated a rich time series of Landsat imagery and NLCD to achieve annual urban change mapping in the Washington D.C. metropolitan area by using time series data change point detection methods. Three different time series change point detection methods were tested and compared to find out the optimal one.

One major limitation of using the above time series change point detection method for annual urban mapping is that it relies heavily on NLCD, thus the method is not applicable to near-real time monitoring of urban change. To achieve the near real-time urban change identification, this research applied machine learning-based classification models, including random forest and Artificial Neural Networks (ANN), to automatically detect urban changes by using a rich time series of Landsat imagery as inputs.

Urban growth could result in a higher probability of flooding by reducing infiltration and

evapotranspiration (ET). ET plays an important role in stormwater mitigation and flood reduction, thus assessing the changes of ET under different urban growth scenarios could yield valuable information for urban planners and policy makers. In this study, spatial-explicit annual ET data at 30-m resolution was generated for Virginia Beach by integrating daily ET data derived from METRIC model and Landsat imagery. Annual ET rates across different major land cover types were compared, and the results indicated that converting forests to urban could result in a huge deduction in ET, thus increasing flood probability. Furthermore, we developed statistical models to explain spatial ET variation using high resolution (1m) land cover data. The results showed that annual ET will increase with the increase of the canopy cover, and it would decrease with the increase of impervious cover and water table depth.

Assessing annual urban change and its impacts on evapotranspiration

Heng Wan

GENERAL AUDIENCE ABSTRACT

Motoring past and current urbanization processes is of importance in terms of ecosystem services evaluation and policy-making because urban growth has huge impacts on the environment. First, this dissertation designed and compared three different methods for annual urban change mapping in Washington D.C. metropolitan area by using a rich time series of Landsat imagery and National Land Cover Database (NLCD). Then, machine-learning based classification models were implemented to achieve near real-time urban change identification. Finally, spatially-explicit evapotranspiration (ET; the sum of evaporation and transpiration, representing water evaporated from the earth's surface, and water transpired by plants, respectively) data for Virginia Beach, a case study location, were generated and annual ET rates for major land cover types were compared to assess the urbanization's impacts on ET.

ACKNOWLEDGEMENT

I would like to thank the following individuals and organizations who have contributed to this dissertation. Without their efforts and help, I could not accomplish this complex dissertation about assessing annual urban change and its impacts on evapotranspiration.

First, I would like to express my sincere gratitude to my advisor, Dr. Yang Shao. Without Dr. Shao's guidance, I would not have completed my dissertation so smoothly. Dr. Shao gave me total freedom to choose research topics that I am interested in, and always encouraged me to think critically and develop new skills when I was facing obstacles during my research. He is always patient, wise, and inspiring when I need suggestions and advice for both research and common life. I would also like to thank my committee members, Dr. Lynn Resler, Dr. James B. Campbell, and Dr. Xinwei Deng, for their excellent services in my committee and their support of my research.

Next, I would like to thank Dr. Daniel McLaughlin, Dr. Shyam Ranganatham, and Dr. Xia Cai for their contribution to this dissertation, especially on the fourth chapter. Dr. McLaughlin has given me constructional advice in refining this dissertation while Dr. Ranganathan and Dr. Cai provided valuable advice on the statistical analysis part of this dissertation chapter. I also express my very great appreciation to Dr. Carolyn Copenheaver and Dr. Lisa Kennedy for their detailed guidance on research methodologies when taking their independent study courses, which have contributed to this dissertation.

I also want to thank The Nature Conservancy and Poole Endowment Fund, Department of Geography and GEA program, Virginia Tech for providing funding to support my research. I acknowledge help from Virginia Information Technology Agency and the Tree Canopy Assessment to Virginia Beach for providing high-resolution LiDAR-derived DEM data and land

use land cover data for my dissertation.

Finally, I want to thank my mother, Sulan He, and my father, Wenbin Wan, for their encouragement and support throughout my study. I'd also like to thank my friend, Yanran Wei, for her suggestion in the statistical analysis part of this dissertation. Thank you all for your help and support!

TABLE OF CONTENTS

Chapter 1. Introduction, literature review, and statement of purpose

1.1 BACKGROUND

Land use and land cover change (LULCC) is an essential element of global environmental change and it has significant impacts on many aspects of ecosystem processes and functions at local, regional, and global scales (Turner et al. 1994; Lambin et al. 2003; Wu et al. 2013). Over the past several decades, agricultural extensification and intensification, deforestation, and urbanization have been increasingly impacting over half of the ice-free Earth surface (Kates et al. 1990). Numerous published studies have suggested that LULCC has important implications for biodiversity, water yield and quality, climate, soil condition, food security and human welfare (DeFries et al. 2004; Deng et al. 2014; Messina & Walsh 2001; Muñoz-Rojas et al. 2015; Roy & Srivastava 2012; Staudt et al. 2013; Yuan 2008). Although urban areas only constitute a small portion of the global land surface, urbanization is widely considered as the most intensive and important LULCC type (Mustard et al. 2004). Land transformations from forest and other natural lands to urban are typically irreversible and may lead to many ecosystem service related problems such as deterioration of water and air quality (Kalnay & Cai, 2003; Yuan 2008), loss of biodiversity (McKinney 2002), spread of invasive species (Alston & Richardson 2006), and habitat fragmentation (Radeloff et al. 2005). With the rapid migration of population to urban areas, urbanization processes have been accelerating during the past decades (Chen et al. 2014). Monitoring past and current urban extent and urbanization processes are of critical importance for assessing ecosystem services and supporting policymaking.

The impacts of urbanization on the hydrologic cycle are of critical importance because urbanization could cause more floods by reducing evapotranspiration (ET) and infiltration via impervious surfaces, leading to huge economic losses and threatening people's lives (De Roo et

al., 2001; Suriya and Mudgal, 2012). Urbanization at the sacrifice of urban forests is of major concern in terms of stormwater management and flood control. Urban forests have higher evapotranspiration rate compared to other major land cover types. They contribute to water removal, thus reduce flood risk (Jim and Chen, 2009). Quantifying ET changes caused by urbanization could provide valuable information for urban planners and policy-makers in regards to stormwater management and flood control (Voyde et al., 2010).

1.2 AN OVERVIEW OF PAST URBAN MAPPING EFFORTS

Increasing awareness of the importance of urbanization leads to numerous efforts in urban mapping using remote sensing data. Landsat imagery, along with many other satellite data, are now routinely used in characterizing urban extents and spatial structures (Anderson 1976; Herold et al. 2003; Taubenböck et al. 2012). With the launch of the IKONOS-2 by Space Imaging in 1999, high resolution (e.g., meters or sub-meter) satellite imagery became available for urban analysis (Sawaya et al., 2003). Such urban mapping efforts have been trending from local scale to regional scale and many researchers focused their studies on monitoring urban dynamics (Klein et al., 2012; Mishra et al. 2010; Lambin 1997). The global scale urban mapping is still a significant challenge due to satellite data availability, computational cost, and data quality concerns (Verburg et al., 2011; Yifang et al. 2015). Early global land cover products, mainly those derived from Normalized Difference Vegetation Index (NDVI) of Advanced Very High-Resolution Radiometer (AVHRR), have coarse spatial resolutions of 1km to 1º (DeFries and Townshend 1994; Loveland & Belward 1997). More recently, several global urban map products were generated at 300-m and 500-m resolution using satellite data from SPOT4, MODIS

(Moderate Resolution Imaging Spectroradiometer), and MEdium Resolution Imaging Spectrometer (MERIS) (Bartholome & Belward 2005; Schneider et al. 2010; Arino et al. 2007). In 2014, the spatial resolution was improved to 30 m by the release of a global land cover map named GlobeLand30, focusing on 2000 and 2010 mapping years (Chen et al., 2015).

In the U.S., the National Land Cover Database (NLCD) serves as the major land use land cover database. The products covering the conterminous United States are released every 5 years (e.g., 2001, 2006, 2011, and 2016). Although NLCD are now routinely used in regional and national land change studies (Ahlqvist 2008; Masek et al. 2008), the intrinsic 6-year time gap between the image-capture date and the product-release date often makes NLCD out of date, especially for those areas experiencing fast urbanization processes. Updating NLCD to the annual temporal resolution and near real-time is appealing for a wide range of data users. One approach to update NLCD is to compare and detect changes between the images acquired from the targeted dates and the images from the previous NLCD mapping year (e.g., 2010) (Xian et al., 2009). However, this snapshot change detection method may not be applicable in biologically-complex system due to phenology-induced problems (Lunetta et al. 2002). Also, this method is flawed by its intrinsic undersampling of the temporal series of the spectral information. Thus, multi-temporal land change or time series remote sensing data analyses received increasing attention in both remote sensing image analysis and land change science domains. New urban change detection algorithms, including those based on Normalized Difference Vegetation Index (NDVI) time series data analysis, are of particular interests (Lunetta et al. 2006).

1.3 TIME SERIES DATA ANALYSIS FOR ANNUAL URBAN MAPPING

Mapping annual urban change by updating the annual urban extent of NLCD is promising because NLCD has a relatively high accuracy (overall accuracy greater than 80%) and the resulted dataset could potentially serve a broader range of users since NLCD is the major land use land cover dataset in the U.S. (Wickham et al., 2013). By using two NLCD datasets from different years (e.g., NLCD 2001 and NLCD 2016), all urban change pixels between these two years could be identified, and annual urban change detection can be achieved if specific urban change year could be pinpointed for each urban change pixel.

For annual urban change mapping, Landsat-based NDVI time series data are particularly useful (Liu et al., 2015). NDVI is the indicator of vegetation greenness, with higher NDVI values indicate healthier and denser vegetation conditions (Carlson and Ripley, 1997). Compared with other vegetation index, such as Enhanced Vegetation Index (EVI), NDVI saturates in well-vegetated areas, which is normally considered as a major limitation (Wang et al., 2003). EVI can hardly saturate and is more sensitive to the canopy structural variations, including Leaf Area Index (LAI), canopy type, plant physiognomy, and canopy archietecture (Huete et al., 2002). These variations are considered as noises when talking about urban change detection. Therefore, this saturation limitation of NDVI becomes a merit when dealing with urban change detection problem. NDVI values can be calculated from satellite imagery (e.g., Landsat, MODIS) based on the following equation:

$$\text{NDVI} = \frac{(NIR - RED)}{(NIR + RED)}$$

Where, NIR and RED represent spectral reflectance measurements from the near-infrared band and the red band of the satellite imagery, respectively (Di et al., 1994). Urbanization often starts

with clear cut of forests or removal of agricultural land, and subsequent impervious surface has a low NDVI value, thus causing a huge drop in NDVI value (Esau et al., 2016). The dramatic change of NDVI value linked with urbanization processes enables us to pinpoint urban change year based on the statistical analysis of NDVI time series data (Lunetta et al., 20006; Verbesselt et al., 2010). Accordingly, annual urban mapping can be treated as time series change point detection problem, and various statistical metrics (e.g., mean, and standard deviation of the time series signal) could be used for the detection of change point. For this research, Washington D.C. metropolitan area (Figure 1) is chosen as the study site due to its diverse land cover types and high urbanization rate during the past decades (Sexton et al., 2013).

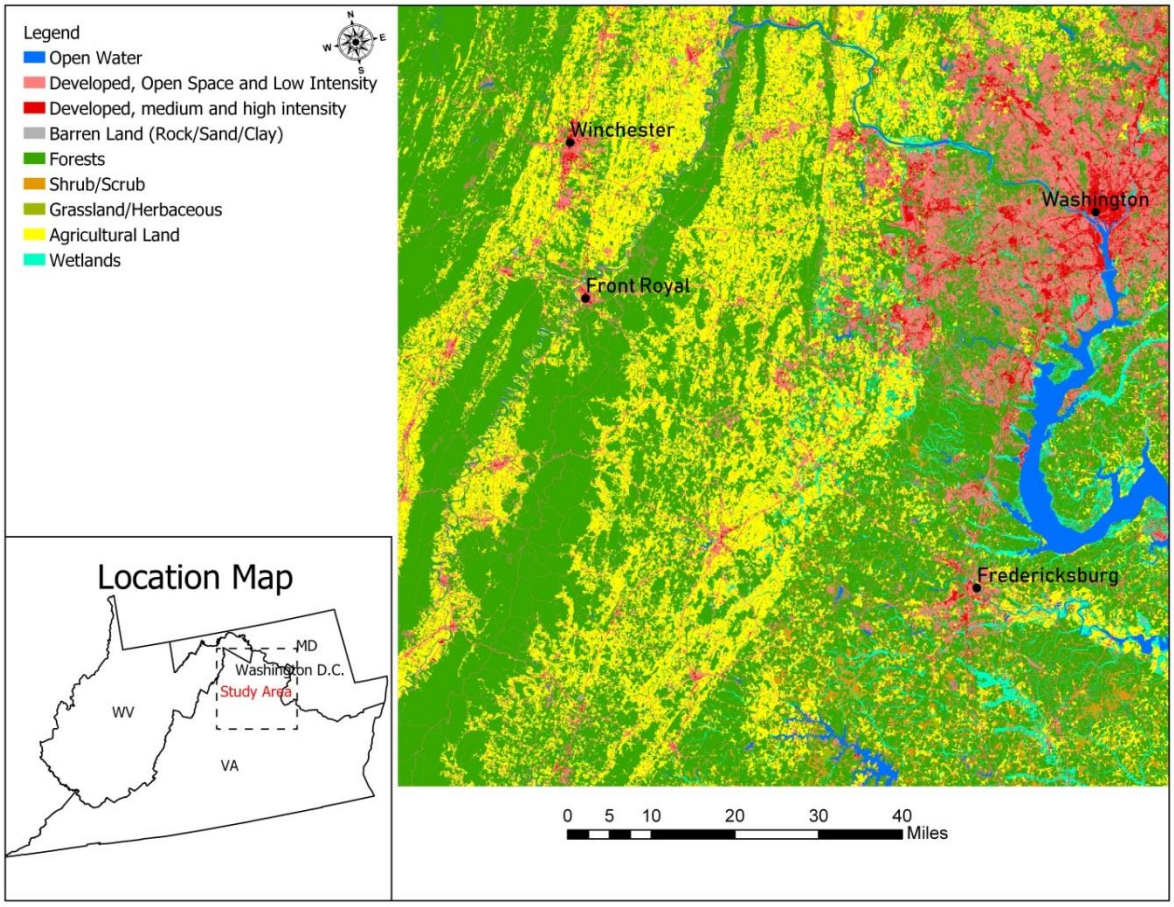

Figure 1. Study area in Washington D.C. metropolitan area

1.4 MACHINE LEARNING

Annual urban mapping via NDVI time series change point detection method relies heavily on the NLCD dataset to first identify all the urban change pixels. Currently, the most up-to-date version of NLCD is for the year of 2016 (Yang et al., 2018), which means annual urban mapping by time series change point detection is not applicable for the year after 2016 (e.g., 2017, 2018). New methods should be explored to deal with this near real-time urban change detection problem.

Recently, machine learning algorithms (e.g., random forest, artificial neural networks) are increasingly used to deal with classification/regression problems, and their performances are often considered superior than traditional statistical methods (Breiman, 2001). The use of machine learning algorithm in remote sensing community is quite common, especially for image classification tasks (McIver and Friedl, 2001; Shao et al., 2012; Vatsavai et al., 2011). For remote sensing researchers, the most important task is to determine how to use one or more machine learning algorithms to solve a problem or achieve higher accuracy. For example, to achieve near real-time urban change detection, researchers should focus on the usage of available data to automate training data development and optimum tuning of algorithms.

1.4.1 RANDOM FOREST CLASSIFIER

A decision tree is a classifier that recursively splits a dataset into smaller subdivisions based on defined rules at each split node (e.g., maximize information gain; Friedl and Brodley, 1997). A random forest classifier consists of various decision trees, where each tree is independent from each other to produce its own classification outputs, and the final classification result is generated by taking the votes of all the decision trees (Pal, 2005). There's low correlation

among trees in random forest because each tree is trained based on a different training dataset randomly sampled with replacement and the features used for splitting data are also randomly selected, thus trees can protect each other from their individual errors (Trawinski et al., 2011). The use of random forest does not require the assumption of normal distribution and can deal with nonlinear classification problems (Lai et al., 2018).

1.4.2 ARTIFICIAL NEURAL NETWORKS

Artificial Neural Networks (ANN) is designed to mimic the biological neural networks that constitute the animal brain (Jain et al., 1996). It consists of numerous nodes (artificial neurons), which form input layer, hidden layer, and output layer, and data signal could be transferred from input layer to hidden layer, and then from hidden layer to output layer through the interconnections between neurons in each layer as shown in figure 2 (Zou et al., 2008). Each connection transfers the output of the previous node as the input of the next node, with a weight to adjust its relative importance, and then the weighted sum could be further processed by the nonlinear function of the next node (Sietsma and Dow, 1991).The training process of ANN is to iteratively update those weights by minimizing the cost function (Majhi and Panda, 2011). ANN is broadly implemented in classification problems due to its noise-tolerant, high learning and generalization characteristics and its excellence in dealing with nonlinear problems (Basheer and Hajmeer, 2000).

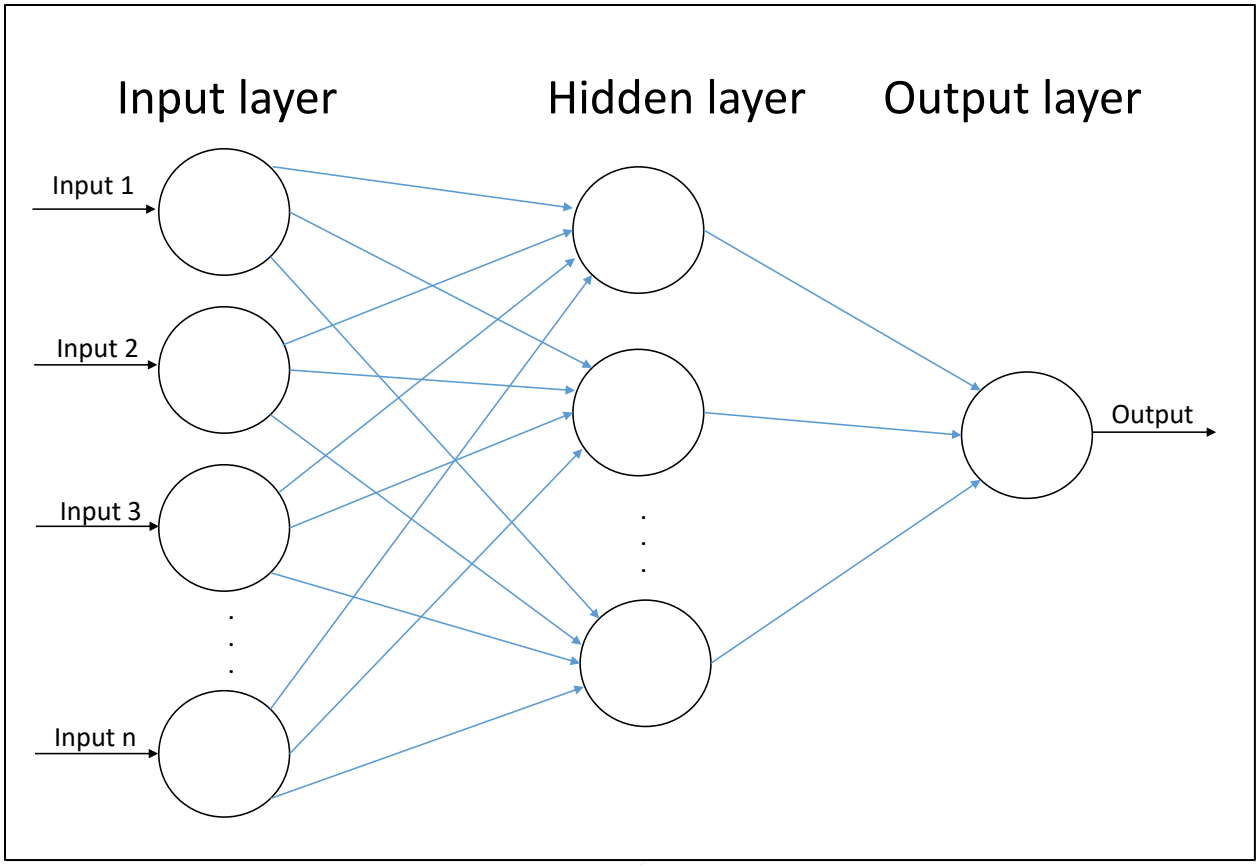

Figure 2. ANN model

1.4.3 SUPPORT VECTOR MACHINE

Support Vector Machine (SVM) can be used for both regression and classification, but it is mainly used for classification problems. SVM algorithm finds out the best hyperplane that separates two data classes in the n-dimensional space (n equals to the number of features used for classification) by using kernel function to reduce calculation intensity (Amari and Wu, 1999). It can be used to deal with nonlinear classification problems and it is robust to outliers (Suykens, 2001.).

1.5 CONSEQUENCES OF URBANIZATION

Urban growth has direct impacts upon water yield and water quality. In this dissertation, urbanization is defined as land cover changes from non-urban categories to urban categories based on the NLCD. Large-scale conversion of forest/grassland to impervious surfaces can drastically affect surface runoff, interception, evapotranspiration, percolation and soil water storage (Weng et al., 2001; Lin et al., 2015). Highly urbanized areas can be more prone to flooding (Weng et al., 2001; McDonald et al., 2011). Production of excess nutrient export generated from urban expansion and intensification contributes to various water quality problems including Harmful algal blooms (HABs) (Paerl et al., 2001). Impacts of urban growth on water yield and water quality can be quantified using coupled urban change analysis and process-based watershed models (e.g., Zhang et al. 2007; Kling et al. 2014). For example, the Soil Water Assessment Tool (SWAT) has been extensively used to assess hydrologic and biogeochemical responses to land use and climate change (Arnold et al. 1998; Neitsch et al. 2002). Implementation of SWAT, or other process-based watershed models, can be challenging for highly developed urban areas because some urban watersheds may have already been heavily disturbed so they could not be fully calibrated. There is a pressing need for developing new approaches to quantify impacts of urban growth on major components of the hydrologic cycle, especially evapotranspiration, which serves as the major water removal agent from the earth's surface.

1.6 METRIC-DERIVED EVAPOTRANSPIRATION

Evapotranspiration (ET) data could be directly quantified through measurements, such as using Eddy Covariance Tower observations (Liu et al., 2013). But ET data obtained from direct

measurement is limited in a relatively small spatial extent, and it is also quite expensive to conduct such measurements (El-Baroudy et al., 2010). When considering about estimating ET over a large area, remote sensing-based method is preferred rather than direct measurement because it cost much less money and labor (Liou and Kar, 2014). Mapping Evapotranspiration at High Resolution with Internalized Calibration (METRIC) is a mature surface energy balance-based model which produces reliable ET estimation by using satellite imagery and ground weather observation data (Allen et al., 2007). With 30-m resolution METRIC-derived daily ET data readily available through Google Earth Engine, this relatively new geospatial data, combined with high temporal resolution (e.g., annual) urban change maps or future urban change simulations, could provide unprecedented opportunities for quantifying major impacts of urban growth on evapotranspiration. In this dissertation, Virginia Beach (Figure 3) is chosen as a case study for assessing urban growth's impacts on evapotranspiration.

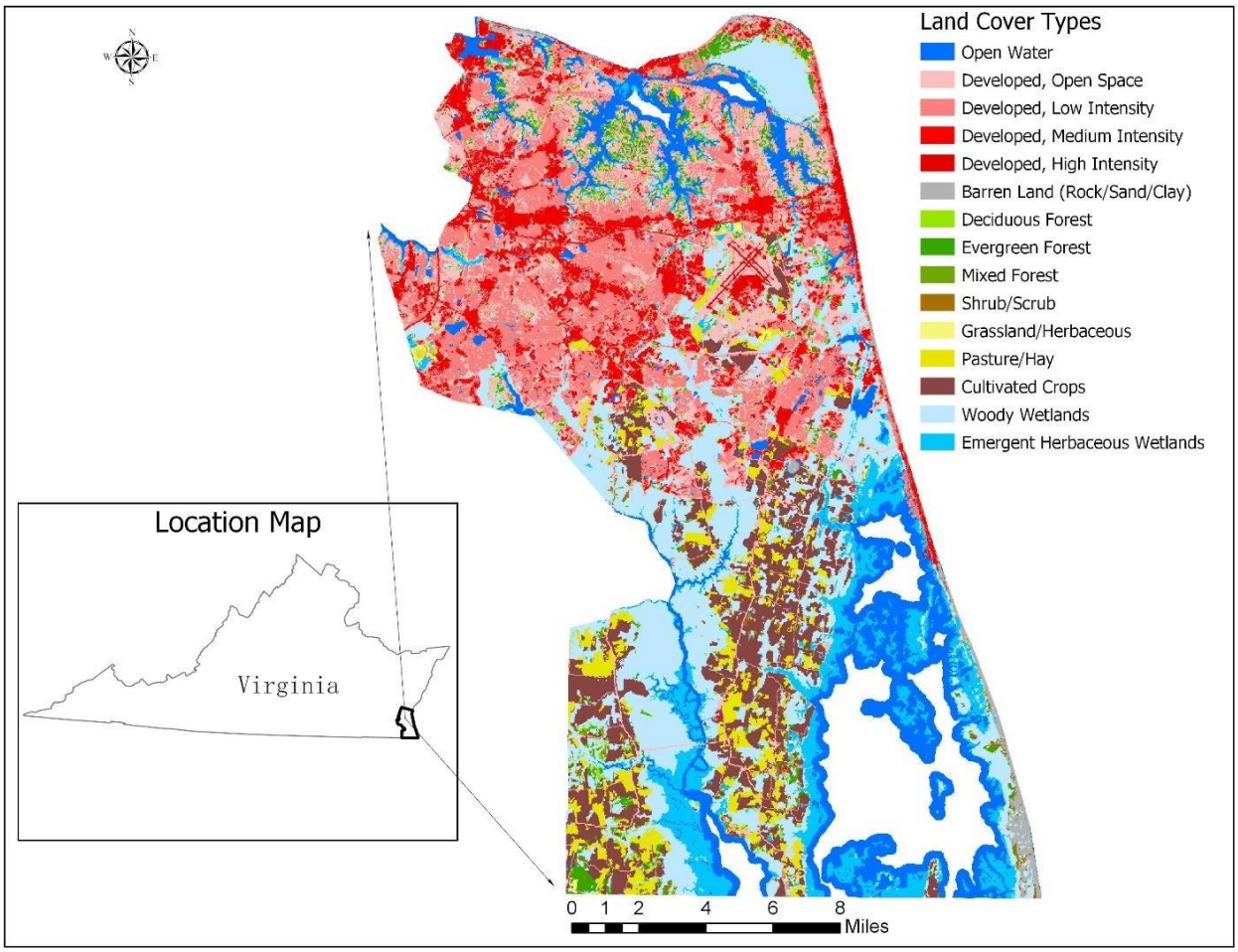

Figure 3. Study area in Virginia Beach

1.7 CHALLENGES OF THE DISSERTATION

Annual urban mapping by analyzing a rich time series of Landsat imagery required dealing with large spatio-temporal datasets. These data processing steps were quite computationally-intensive and time-consuming. Once annual urban mapping was completed, conducting a thorough accuracy assessment emerged as a new challenge because it was hard to find the real urban change years as a reference dataset. The pinpoint of real urban change years required tremendous amount of labor and time to manually monitor LULCC by comparing historic high-resolution imagery from Google Earth.

To quantify urban growth's impacts on evapotranspiration, spatially-explicit annual ET data was generated based on daily ET data from 2000 to 2018. The current Google Earth Engine Evapotranspirtion Flux website does not support batch download of daily ET data, thus downloading such huge dataset was labor-intensive and time-consuming. These daily ET data also suffered from different extents of cloud contamination, and some of the data were flawed by noise and outliers. Before using them to generate annual ET data, data cleaning was implemented for this large dataset of daily ET, which required lots of computational capability and time.

1.8 STATEMENT OF PURPOSE AND SIGNIFICANT OF RESEARCH

Land use land cover data plays an important role in environmental modeling, such as ecological models, climatic models, and hydrological models (Hepinstall-Cymerman et al., 2009; Miller et al., 2007; Pielke et al., 2011). Currently, the broadly used NLCD is updated every five years, which might not satisfy some environmental models requiring higher temporal resolution (Foresman et al., 1997). Annual urban mapping based on NLCD could provide land use land cover data with a higher temporal resolution, which could be beneficial for those environmental models, and it can also help us have a better understanding about urbanization processes (Yin et al., 2014).

Urbanization could increase the flood probability and severity mainly by decreasing evapotranspiration and infiltration (De Roo et al., 2001; Suriya and Mudgal, 2012). Assessing evapotranspiration changes under different urban growth scenarios could potentially provide valuable information for urban planning and stormwater management.

The main goals for this project are to:

- Develop annual urban change map using a rich time series of satellite imagery from 1988 to 2017 and NLCD products.
- Achieve near real-time urban change detection using NDVI time series data and machine learning algorithms
- Use high spatial-temporal resolution geospatial data to assess impacts of urban growth on evapotranspiration.

1.9 STRUCTURE OF THE DISSERTATION

This dissertation is organized into five chapters. Chapter 1 gives basic introduction and literature review about LULCC and its impacts on the environment, and it also states the purpose and challenges of this dissertation. Chapter 2 develops and compares three different annual urban mapping algorithms by using a rich time series of Landsat imagery and NLCD. Chapter 3 implements machine learning algorithms on a rich time series of Landsat imagery to achieve near real-time urban change detection. Chapter 4 assesses the evapotranspiration changes under different LULCC scenarios. Chapter 5 concludes all the previously stated studies and identifies major limitations of this dissertation.

1.10 DATA SOURCES

All the data used in this dissertation have been listed in table 1, with their corresponding sources given. For DEM and 0.5-m land cover data, they were directly obtained from Virginia Information Technologies Agency and Tree Canopy Assessment for Virginia Beach, respectively, thus there are no corresponding download links.

Table1. Data sources

Data	**Source**
NLCDs	Multi-Resolution Land Characteristics Consortium (https://www.mrlc.gov/)
Landsat imagery	Earth Explore (https://earthexplorer.usgs.gov/)
Daily ET data	Google Earth Engine Evapotranspiration Flux (https://eeflux-level1.appspot.com/)
DEM	Virginia Information Technologies Agency
Ground water well observations	USGS (https://nwis.waterdata.usgs.gov/va/nwis/gwlevels)
0.5-m land cover data	Tree Canopy Assessment for Virginia Beach

References:

Ahlqvist, O., 2008. Extending post-classification change detection using semantic similarity metrics to overcome class heterogeneity: A study of 1992 and 2001 US National Land Cover Database changes. Remote Sensing of Environment 112, 1226–1241.

Allen, R.G., Tasumi, M., Morse, A., Trezza, R., Wright, J.L., Bastiaanssen, W., Kramber, W., Lorite, I., Robison, C.W., 2007. Satellite-based energy balance for mapping evapotranspiration with internalized calibration (METRIC)—Applications. Journal of Irrigation and Drainage Engineering 133, 395–406.

Alston, K.P., Richardson, D.M., 2006. The roles of habitat features, disturbance, and distance from putative source populations in structuring alien plant invasions at the urban/wildland interface on the Cape Peninsula, South Africa. Biological Conservation 132, 183–198.

Amari, S., Wu, S., 1999. Improving support vector machine classifiers by modifying kernel functions. Neural Networks 12, 783–789.

Anderson, J.R., 1976. A land use and land cover classification system for use with remote sensor

data. US Government Printing Office.

Arino, O., Gross, D., Ranera, F., Leroy, M., Bicheron, P., Brockman, C., Defourny, P., Vancutsem, C., Achard, F., Durieux, L., 2007. GlobCover: ESA service for global land cover from MERIS, in: 2007 IEEE International Geoscience and Remote Sensing Symposium. IEEE, pp. 2412–2415.

Arnold, J.G., Srinivasan, R., Muttiah, R.S., Williams, J.R., 1998. Large area hydrologic modeling and assessment part I: model development 1. JAWRA Journal of the American Water Resources Association 34, 73–89.

Bartholome, E., Belward, A.S., 2005. GLC2000: a new approach to global land cover mapping from Earth observation data. International Journal of Remote Sensing 26, 1959–1977.

Basheer, I.A., Hajmeer, M., 2000. Artificial neural networks: fundamentals, computing, design, and application. Journal of Microbiological Methods 43, 3–31.

Breiman, L., 2001. Statistical modeling: The two cultures (with comments and a rejoinder by the author). Statistical Science 16, 199–231.

Carlson, T.N., Ripley, D.A., 1997. On the relation between NDVI, fractional vegetation cover, and leaf area index. Remote sensing of Environment 62, 241–252.

Chen, M., Zhang, H., Liu, W., Zhang, W., 2014. The global pattern of urbanization and economic growth: evidence from the last three decades. PloS one 9, e103799.

Chen, Jun, Chen, Jin, Liao, A., Cao, X., Chen, L., Chen, X., He, C., Han, G., Peng, S., Lu, M., 2015. Global land cover mapping at 30 m resolution: A POK-based operational approach. ISPRS Journal of Photogrammetry and Remote Sensing 103, 7–27.

DeFries, R.S., Townshend, J.R.G., 1994. NDVI-derived land cover classifications at a global scale. International Journal of Remote Sensing 15, 3567–3586.

DeFries, R.S., Asner, G.P., Houghton, R., 2004. Trade-offs in land-use decisions: towards a framework for assessing multiple ecosystem responses to land use change. Ecosystems and Land Use Change 153, 1–9.

Deng, X., Güneralp, B., Su, H., 2014. Observations and modeling of the climatic impact of land-use changes. Advances in Meteorology 2014.

De Roo, A., Odijk, M., Schmuck, G., Koster, E., Lucieer, A., 2001. Assessing the effects of land use changes on floods in the Meuse and Oder catchment. Physics and Chemistry of the Earth, Part B: Hydrology, Oceans and Atmosphere 26, 593–599.

Di, L., Rundquist, D.C., Han, L., 1994. Modelling relationships between NDVI and precipitation during vegetative growth cycles. International Journal of Remote Sensing 15, 2121–2136.

El-Baroudy, I., Elshorbagy, A., Carey, S.K., Giustolisi, O., Savic, D., 2010. Comparison of three data-driven techniques in modelling the evapotranspiration process. Journal of Hydroinformatics 12, 365–379.

Esau, I., Miles, V.V., Davy, R., Miles, M.W., Kurchatova, A., 2016. Trends in normalized difference vegetation index (NDVI) associated with urban development in northern West Siberia. Atmospheric Chemistry & Physics 16.

Foresman, T.W., Pickett, S.T., Zipperer, W.C., 1997. Methods for spatial and temporal land use and land cover assessment for urban ecosystems and application in the greater Baltimore-Chesapeake region. Urban Ecosystems 1, 201–216.

Friedl, M.A., Brodley, C.E., 1997. Decision tree classification of land cover from remotely sensed data. Remote Sensing of Environment 61, 399–409.

Hepinstall-Cymerman, J., Coe, S., Alberti, M., 2009. Using urban landscape trajectories to develop a multi-temporal land cover database to support ecological modeling. Remote

Sensing 1, 1353–1379.

Herold, M., Goldstein, N.C., Clarke, K.C., 2003. The spatiotemporal form of urban growth: measurement, analysis and modeling. Remote Sensing of Environment 86, 286–302.

Huete, A., Didan, K., Miura, T., Rodriguez, E.P., Gao, X., Ferreira, L.G., 2002. Overview of the radiometric and biophysical performance of the MODIS vegetation indices. Remote Sensing of Environment 83, 195–213.

Jain, A.K., Mao, J., Mohiuddin, K.M., 1996. Artificial neural networks: A tutorial. Computer 29, 31–44.

Jim, C.Y., Chen, W.Y., 2009. Ecosystem services and valuation of urban forests in China. Cities 26, 187–194.

Kalnay, E., Cai, M., 2003. Impact of urbanization and land-use change on climate. Nature 423, 528.

Kates, R. W., B. L. Turner, and W. C. Clark . 1990. The great transformation. 1– 17 B. L. Turner, W. C. Clark, R. W. Kates, J. F. Richards, J. T. Mathews, and W. B. Meyer, editors. The Earth as transformed by human action. Cambridge University Press, Cambridge, England.

Klein, I., Gessner, U., Kuenzer, C., 2012. Regional land cover mapping and change detection in Central Asia using MODIS time series. Applied Geography 35, 219–234.

Kling, H., Stanzel, P., Preishuber, M., 2014. Impact modelling of water resources development and climate scenarios on Zambezi River discharge. Journal of Hydrology: Regional Studies 1, 17–43.

Lai, K., Twine, N., O'brien, A., Guo, Y., Bauer, D., 2018. Artificial intelligence and machine learning in bioinformatics. Encyclopedia of Bioinformatics and Computational Biology:

ABC of Bioinformatics 55, 272.

Lambin, E.F., 1997. Modelling and monitoring land-cover change processes in tropical regions. Progress in Physical Geography 21, 375–393.

Lambin, E.F., Geist, H.J., Lepers, E., 2003. Dynamics of land-use and land-cover change in tropical regions. Annual Review of Environment and Resources 28, 205–241.

Lin, B., Chen, X., Yao, H., Chen, Y., Liu, M., Gao, L., James, A., 2015. Analyses of landuse change impacts on catchment runoff using different time indicators based on SWAT model. Ecological Indicators 58, 55–63.

Liou, Y.-A., Kar, S.K., 2014. Evapotranspiration estimation with remote sensing and various surface energy balance algorithms—A review. Energies 7, 2821–2849.

Liu, S.M., Xu, Z.W., Zhu, Z.L., Jia, Z.Z., Zhu, M.J., 2013. Measurements of evapotranspiration from eddy-covariance systems and large aperture scintillometers in the Hai River Basin, China. Journal of Hydrology 487, 24–38.

Liu, Y., Wang, Y., Peng, J., Du, Y., Liu, X., Li, S., Zhang, D., 2015. Correlations between urbanization and vegetation degradation across the world's metropolises using DMSP/OLS nighttime light data. Remote Sensing 7, 2067–2088.

Loveland, T.R., Belward, A.S., 1997. The IGBP-DIS global 1km land cover data set, DISCover: first results. International Journal of Remote Sensing 18, 3289–3295.

Lunetta, R.S., Ediriwickrema, J., Johnson, D.M., Lyon, J.G., McKerrow, A., 2002. Impacts of vegetation dynamics on the identification of land-cover change in a biologically complex community in North Carolina, USA. Remote Sensing of Environment 82, 258–270.

Lunetta, R.S., Knight, J.F., Ediriwickrema, J., Lyon, J.G., Worthy, L.D., 2006. Land-cover change detection using multi-temporal MODIS NDVI data. Remote Sensing of

Environment 105, 142–154.

Majhi, B., Panda, G., 2011. Robust identification of nonlinear complex systems using low complexity ANN and particle swarm optimization technique. Expert Systems with Applications 38, 321–333.

Masek, J.G., Huang, C., Wolfe, R., Cohen, W., Hall, F., Kutler, J., Nelson, P., 2008. North American forest disturbance mapped from a decadal Landsat record. Remote Sensing of Environment 112, 2914–2926.

McDonald, R.I., Green, P., Balk, D., Fekete, B.M., Revenga, C., Todd, M., Montgomery, M., 2011. Urban growth, climate change, and freshwater availability. Proceedings of the National Academy of Sciences 108, 6312–6317.

McKinney, M.L., 2002. Urbanization, Biodiversity, and ConservationThe impacts of urbanization on native species are poorly studied, but educating a highly urbanized human population about these impacts can greatly improve species conservation in all ecosystems. Bioscience 52, 883–890.

McIver, D.K., Friedl, M.A., 2001. Estimating pixel-scale land cover classification confidence using nonparametric machine learning methods. IEEE Transactions on Geoscience and Remote Sensing 39, 1959–1968.

Messina, J.P., Walsh, S.J., 2001. Simulating land use and land cover dynamics in the Ecuadorian Amazon through cellular automata approaches and an integrated GIS, in: Open Meeting of the Human Dimensions of Global Environmental Change Research Community in Rio de Janeiro, Brazil. pp. 6–8.

Miller, S.N., Phillip Guertin, D., Goodrich, D.C., 2007. Hydrologic modeling uncertainty resulting from land cover misclassification 1. JAWRA Journal of the American Water

Resources Association 43, 1065–1075.

Mishra, V., Cherkauer, K.A., Niyogi, D., Lei, M., Pijanowski, B.C., Ray, D.K., Bowling, L.C., Yang, G., 2010. A regional scale assessment of land use/land cover and climatic changes on water and energy cycle in the upper Midwest United States. International Journal of Climatology 30, 2025–2044.

Muñoz-Rojas, M., Jordán, A., Zavala, L.M., De la Rosa, D., Abd-Elmabod, S.K., Anaya-Romero, M., 2015. Impact of land use and land cover changes on organic carbon stocks in Mediterranean soils (1956–2007). Land Degradation & Development 26, 168–179.

Mustard, J.F., Defries, R.S., Fisher, T., Moran, E., 2004. Land-Use and Land-Cover Change Pathways and Impacts, in: Gutman, G., Janetos, A.C., Justice, C.O., Moran, E.F., Mustard, J.F., Rindfuss, R.R., Skole, D., Turner, B.L., Cochrane, M.A. (Eds.), Land Change Science: Observing, Monitoring and Understanding Trajectories of Change on the Earth's Surface, Remote Sensing and Digital Image Processing. Springer Netherlands, Dordrecht, pp. 411–429. https://doi.org/10.1007/978-1-4020-2562-4_24

Neitsch, S.L., Arnold, J.G., Srinivasan, R., 2002. Pesticides fate and transport predicted by the Soil And Water Assessment Tool (SWAT). Atrazine, Metolachlor and Trifluralin in the Sugar Creek Watershed: BRC Report 3.

Paerl, H.W., Fulton, R.S., Moisander, P.H., Dyble, J., 2001. Harmful freshwater algal blooms, with an emphasis on cyanobacteria. The Scientific World Journal 1, 76–113.

Pal, M., 2005. Random forest classifier for remote sensing classification. International Journal of Remote Sensing 26, 217–222.

Pielke Sr, R.A., Pitman, A., Niyogi, D., Mahmood, R., McAlpine, C., Hossain, F., Goldewijk, K.K., Nair, U., Betts, R., Fall, S., 2011. Land use/land cover changes and climate:

modeling analysis and observational evidence. Wiley Interdisciplinary Reviews: Climate Change 2, 828–850

Radeloff, V.C., Hammer, R.B., Stewart, S.I., Fried, J.S., Holcomb, S.S., McKeefry, J.F., 2005. The wildland–urban interface in the United States. Ecological applications 15, 799–805.

Roy, A., Srivastava, V.K., 2012. Geospatial approach to identification of potential hotspots of land-use and land-cover change for biodiversity conservation. Current Science 1174–1180.

Sawaya, K.E., Olmanson, L.G., Heinert, N.J., Brezonik, P.L., Bauer, M.E., 2003. Extending satellite remote sensing to local scales: land and water resource monitoring using high-resolution imagery. Remote Sensing of Environment 88, 144–156.

Schneider, A., Friedl, M.A., Potere, D., 2010. Mapping global urban areas using MODIS 500-m data: New methods and datasets based on 'urban ecoregions.' Remote Sensing of Environment 114, 1733–1746.

Sexton, J.O., Song, X.-P., Huang, C., Channan, S., Baker, M.E., Townshend, J.R., 2013. Urban growth of the Washington, DC–Baltimore, MD metropolitan region from 1984 to 2010 by annual, Landsat-based estimates of impervious cover. Remote Sensing of Environment 129, 42–53.

Shao, Y., Lunetta, R.S., 2012. Comparison of support vector machine, neural network, and CART algorithms for the land-cover classification using limited training data points. ISPRS Journal of Photogrammetry and Remote Sensing 70, 78–87.

Sietsma, J., Dow, R.J., 1991. Creating artificial neural networks that generalize. Neural Networks 4, 67–79.

Suriya, S., Mudgal, B.V., 2012. Impact of urbanization on flooding: The Thirusoolam sub

watershed–A case study. Journal of Hydrology 412, 210–219.

Staudt, A., Leidner, A.K., Howard, J., Brauman, K.A., Dukes, J.S., Hansen, L.J., Paukert, C., Sabo, J., Solórzano, L.A., 2013. The added complications of climate change: understanding and managing biodiversity and ecosystems. Frontiers in Ecology and the Environment 11, 494–501.

Suykens, J.A., 2001. Nonlinear modelling and support vector machines, in: IMTC 2001. Proceedings of the 18th IEEE Instrumentation and Measurement Technology Conference. Rediscovering Measurement in the Age of Informatics (Cat. No. 01CH 37188). IEEE, pp. 287–294.

Taubenböck, H., Esch, T., Felbier, A., Wiesner, M., Roth, A., Dech, S., 2012. Monitoring urbanization in mega cities from space. Remote Sensing of Environment, Remote Sensing of Urban Environments 117, 162–176. https://doi.org/10.1016/j.rse

Tranwinski, K., Cordon, O., Quirin, A., 2011. On designing fuzzy rule-based multiclassification systems by combining FURIA with bagging and feature selection. International Journal of Uncertainty, Fuzziness and Knowledge-Based Systems 19, 589–633.

Turner, B.L., Meyer, W.B., Skole, D.L., 1994. Global land-use/land-cover change: towards an integrated study. Ambio. Stockholm 23, 91–95.

Vatsavai, R.R., Bright, E., Varun, C., Budhendra, B., Cheriyadat, A., Grasser, J., 2011. Machine learning approaches for high-resolution urban land cover classification: a comparative study, in: Proceedings of the 2nd International Conference on Computing for Geospatial Research & Applications. pp. 1–10.

Verburg, P.H., Neumann, K., Nol, L., 2011. Challenges in using land use and land cover data for global change studies. Global Change Biology 17, 974–989.

Verbesselt, J., Hyndman, R., Newnham, G., Culvenor, D., 2010. Detecting trend and seasonal changes in satellite image time series. Remote sensing of Environment 114, 106–115.

Voyde, E., Fassman, E., Simcock, R., Wells, J., 2010. Quantifying evapotranspiration rates for New Zealand green roofs. Journal of Hydrologic Engineering 15, 395–403.

Yifang, B., Gong, P., Gini, C., 2015. Global land cover mapping using Earth observation satellite data: Recent progresses and challenges. ISPRS Journal of Photogrammetry and Remote Sensing (Print) 103, 1–6.

Wang, Z., Liu, C., Huete, A., 2003. From AVHRR-NDVI to MODIS-EVI: Advances in vegetation index research. Acta Ecologica Sinica 23, 979–987.

Weng, Q., 2001. Modeling urban growth effects on surface runoff with the integration of remote sensing and GIS. Environmental Management 28, 737–748.

Wickham, J.D., Stehman, S.V., Gass, L., Dewitz, J., Fry, J.A., Wade, T.G., 2013. Accuracy assessment of NLCD 2006 land cover and impervious surface. Remote Sensing of Environment 130, 294–304.

Wu, K., Ye, X., Qi, Z., Zhang, H., 2013. Impacts of land use/land cover change and socioeconomic development on regional ecosystem services: The case of fast-growing Hangzhou metropolitan area, China. Cities 31, 276–284.

Xian, G., Homer, C., Fry, J., 2009. Updating the 2001 National Land Cover Database land cover classification to 2006 by using Landsat imagery change detection methods. Remote Sensing of Environment 113, 1133–1147.

Yang, L., Jin, S., Danielson, P., Homer, C., Gass, L., Bender, S.M., Case, A., Costello, C., Dewitz, J., Fry, J., 2018. A new generation of the United States National Land Cover Database: Requirements, research priorities, design, and implementation strategies.

ISPRS Journal of Photogrammetry and Remote Sensing 146, 108–123.

Yin, H., Pflugmacher, D., Kennedy, R.E., Sulla-Menashe, D., Hostert, P., 2014. Mapping annual land use and land cover changes using MODIS time series. IEEE Journal of Selected Topics in Applied Earth Observations and Remote Sensing 7, 3421–3427.

Yuan, F., 2008. Land-cover change and environmental impact analysis in the Greater Mankato area of Minnesota using remote sensing and GIS modelling. International Journal of Remote Sensing 29, 1169–1184.

Zhang, X., Srinivasan, R., Hao, F., 2007. Predicting hydrologic response to climate change in the Luohe River basin using the SWAT model. Transactions of the ASABE 50, 901–910.

Zou, J., Han, Y., So, S.-S., 2008. Overview of artificial neural networks, in: Artificial Neural Networks. Springer, pp. 14–22.

Chapter 2. Mapping annual urban change using time series Landsat and NLCD

2.1 INTRODUCTION

In this chapter, we analyzed NLCD and a rich time series Landsat imagery from 1998 to 2017 to achieve annual urban mapping in Washington D.C. metropolitan area. Three different algorithms have been designed and compared, and the optimal algorithm can detect annual urban change with a high overall accuracy of 89%.

2.2 PUBLICATION

Wan, H., Shao, Y., Campbell, J.B., Deng, X.W., 2019. Mapping annual urban change using time-series Landsat data and NLCD. *Photogrammetric Engineering and Remote Sensing*, 85, 715-724.

The manuscript related to this chapter was published in *Photogrammetric Engineering & Remote Sensing* journal and is shown below:

Mapping annual urban change using time series Landsat and NLCD

Develop annual urban change map using a rich time series of satellite imagery from 1988 to 2017 and NLCD products.

Abstract

Annual urban change information is important for an improved understanding of urban dynamics and continuous modelling of urban ecosystem processes. This study examined Landsat-derived NDVI time series for characterizing annual urban change. To reduce impacts from cloud contamination and missing data, USGS Landsat Analysis Ready Data were processed to derive annual NDVI layers using a maximum value composite (MVC) algorithm. NLCD land cover products from 2001 and 2011 were used as references for generating a decadal urban change mask. Within the decadal urban change mask and using annual NDVI as input, we examined three time-series change detection methods to pinpoint specific year of urban change: (a) minimum-value method, (b) break-point detection, and (c) simple threshold identification. For accuracy assessment, we divided change pixels into urbanization and urban-intensification pixel groups, defined by initial land cover types. We used Google Earth's High-Resolution Imagery Archive as primary reference data for detailed accuracy assessment. Overall, the urbanization pixel group has good change detection accuracies of above 82.0% for all three change detection algorithms. The break-point detection method resulted in the highest overall accuracy of 88.0%. Overall accuracies for urban intensification pixel group were in the range of 35.0%-76.0%, depending on choice of change detection algorithm, length of input time-series, and further division of pixel subgroups.

1. Introduction

Land use and land cover change (LULCC) has been recognized as a main driver of global environmental change. Important consequences of LULCC span a wide range of interconnected domains such as local-regional climate, air and water quality, hydrological cycle and biogeochemical fluxes, biodiversity, and food production (Messina and Walsh, 2001; DeFries et al., 2004; Foley et al., 2005; Yuan, 2008; Roy and Srivastava, 2012; Staudt et al., 2013; Deng et al. 2014; Maimaitiyiming et al., 2014; Muñoz-Rojas et al., 2015). Although urban area only covers a small percentage of the earth's land surface, urbanization is probably the most intensive type of LULCC to alter local and regional environments. Conversion from forest and other natural landscapes to urban are typically irreversible and can lead to many ecological problems including deterioration of water and air quality (Kalnay and Cai, 2003; Yuan, 2008), biodiversity loss (McKinney 2002), introduction and spread of invasive species (Alston and Richardson, 2006), and habitat fragmentation (Radeloff et al., 2005).

Consequences of urban growth have traditionally been treated as local issues, but recent studies suggest that impacts are far-reaching, with regional and global implications (Seto et al., 2012). Currently, over half of the world's population lives in urban environments, which are expected to grow at an unprecedented rate in coming decades, especially in developing countries (Cohen, J.E., 2003; Seto, et al., 2009). Monitoring urban dynamics is of critical importance for ecosystem service assessment.

Increasing awareness of the impact of urbanization on a global scale has motivated numerous urban mapping efforts using satellite remote sensing. Early satellite-based urban mapping applied medium resolution data from Landsat Multi-spectral Scanner System (MSS, 79m), but its coarse spatial resolution presented a significant challenge for detailed urban studies

(Welch, 1982; Barnsley et al., 2003). With the continuous improvement of sensor technology and image processing capabilities, remote sensing data with higher spatial and spectral resolution, such as those from Landsat (TM/ETM/OLI) and SPOT, are now routinely used for urban mapping. The Landsat series of satellite imagery are among the most widely used because of its rich archive and open access (Woodcock et al., 2008). Examples of applications include general land cover mapping (Fung, 1992; Zha et al., 2003; Lo, 2004; Lu et al., 2011; Zhu et al., 2012; Chen et al., 2015), study of urban dynamics (Masek et al., 2000; Yuan et al., 2005; Taubenböck et al., 2012; Zhang and Weng, 2016; Wu and Chin, 2016), urban spatial structure analysis (Herold et al., 2002; Seto and Fragkias, 2005; Wang et al., 2014), and quantification of urban thermal characteristics (Weng et al., 2004; Weng, 2009; Xian and Crane, 2006).

Most previous studies on urban mapping follow a "snapshot" model using 5-10 year mapping intervals. For example, in the U.S., regional- and national-scale urban mapping has been routinely conducted every 5 years (e.g., 2001, 2006, and 2011), as part of the National Land Cover Database (NLCD) development (Homer et al., 2007; Homer et al., 2015). The arbitrary mapping interval, however, is limiting for certain applications requiring land cover data at a higher temporal frequency (e.g., annual). For example, spatially distributed landscape process models and system dynamic models typically favor high temporal frequency land cover map products to support continuous modelling of ecosystem processes and functions (Lunetta et al., 2006; Winz et al., 2009). Forecasting future land cover distributions can also benefit greatly from understanding historical and ongoing urban changes, observed with high temporal frequency (Pontius et al., 2008).

Annual urban map products can be derived using a number of image classification and change

detection techniques. One approach is to conduct image classification for each mapping year. Intrinsic image classification errors and their accumulations over all mapping years make this one-classification-per year method less appealing (Chen et al., 2003). Xian et al. (2009) developed a cost-effective change detection method for updating NLCD every 5 years. Specifically, they first identified areas of land cover change between 2001 and 2006 using a change vector analysis. The change pixels were subsequently classified into new land cover types. Although this method is effective in updating national land cover products at 5-10 year intervals, it is unclear whether it is directly applicable for an annual mapping interval because the associated change vector analysis may not be fully automated. In addition, the use of bi-temporal change detection focuses one image pair a time and does not make full use of rich temporal information (Huang et al., 2010).

An alternative approach for annual urban mapping is to make full use of rich time series but coarser resolution remote sensing data to conduct change detection. For example, using high-temporal MODIS (Moderate Resolution Imaging Spectroradiometer) data as input, Lunetta et al. (2006) examined annual integrated NDVI (Normalized Difference Vegetation Index) for each 250m MODIS pixel to identify newly urbanized area. Change pixels were determined by applying NDVI change thresholds on a 1 year time-step. Through this approach, annual urban mapping is simplified as an annual urban change detection problem. The main limitation of this MODIS NDVI-based annual change detection is associated with MODIS 250m coarse spatial resolution. Time series analysis with 30 m Landsat data can be challenging because Landsat satellite has lower temporal resolution (i.e., 16 days). The U.S. Geological Survey's recent effort in analysis-ready Landsat products significantly improved the potential of Landsat-based time

series analyses by standardizing data from multiple Landsat satellites (TM, ETM, and OLI) (Banskota et al., 2014). The dense Landsat time series stacks from multiple Landsat satellites, combined with carefully designed analytical algorithms, are now increasingly used in characterizing forest disturbance and land cover change at annual intervals (e.g., Huang et al., 2009; Huang et al., 2010; Zhu et al., 2012). Few previously published studies, however, have examined automated annual urban change mapping using the relatively longer Landsat time series data. It is also appealing to develop annual urban maps that maintain an overall consistency with the existing national/regional land cover data, especially when the existing national/regional land cover products have acceptable classification accuracies (e.g., NLCD). Significant resources have been used in generating national/regional products and it is generally more cost-effective to update the existing data than develop a completely new urban map product (Xian et al., 2009).

The purpose of this study is to evaluate annual urban mapping by combined use of time series Landsat data and NLCD. Specifically, we first used decadal NLCD data to identify areas of urban change from 2001-2011. Within the urban change mask, we analyzed NDVI time series from Landsat data, pixel-by-pixel, to identify year of change. We compared three change detection methods using Landsat-derived NDVI time series: (a) minimum-value method, (b) break-point detection, and (c) simple threshold identification. We conducted detailed accuracy assessments for our annual urban maps by visual interpretation of Google Earth's High-Resolution Imagery Archive. In addition, we examined how map accuracies vary when the length of input NDVI time series changes.

2. Methods

2.1 Study Area

The study area (22,500 km^2) covers the northwest portion of the Washington D.C. metropolitan area, northern Virginia, and a small portion of West Virginia (Fig. 1). The Washington D.C. metropolitan area and its suburbs (northern Virginia) are among the fastest growing regions in the US, with an average urbanization rate of 11±2 km^2/year (Sexton et al., 2013). Another reason for choosing this study area is due to its diversity in land cover types, including 2.83% of water body, 16.88% of urban and barren land, 49.05% of forest, 2.45% of shrub and grassland, 25.29% of agriculture, and 3.48% of wetlands in 2001, based on 2001 NLCD data. The robustness of annual urban mapping technique can be tested on varied land cover types. Finally, this study area has a good collection of high spatial resolution images based on Google Earth's High-Resolution Imagery Archive, thereby providing easier implementation of accuracy assessment at higher temporal resolution.

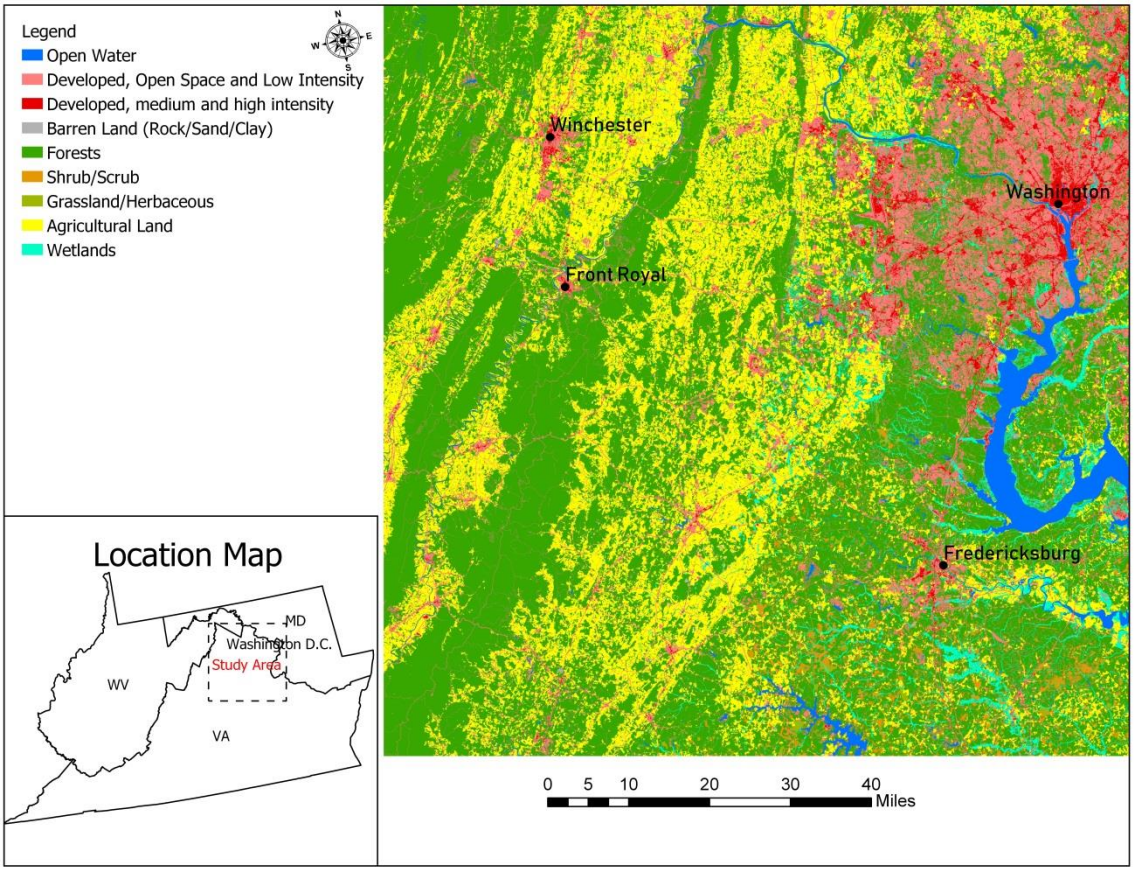

Fig 1. Study area covers the northwest portion of the Washington D.C. metropolitan area, northern Virginia, and a small portion of West Virginia

2.2 Data

A total of 1,292 Landsat Analysis Ready Data (ARD) (h027v009, ARD tile) surface reflectance images from 1988 to 2017 were downloaded from the USGS EarthExplorer (https://earthexplorer.usgs.gov). Each image contains 5,000 x 5,000, 30-meter pixels. We included imagery with substantial cloud/shadow cover as well as Landsat ETM+ SLC-off imagery in our original time series dataset, since for a given image with heavy cloud cover, cloud-free parts of the image can be used to enhance the temporal sampling frequency. A significant number of high quality pixels in the Landsat SLC-off ETM imagery are also useful

for time series data analysis. Therefore, all available Landsat 5, 7, and 8 ARD imagery were obtained to develop a dense time series stack. We also downloaded two recent NLCD map products (NLCD 2001 and NLCD 2011) from the Multi-Resolution Land Characteristics Consortium (http://www.mrlc.gov/). Overall accuracies for NLCD are approximately 85% and individual class accuracies ranged from 79% to 91% for Anderson Level I classes (Wickham et al., 2010).

2.3 Data preprocessing

We derived NDVI for each Landsat image from 1988 to 2017 and stacked all NDVI layers to develop a NDVI time series stack. No additional data preprocessing steps were needed before NDVI calculation because Landsat ARD surface reflectance data come readily processed to the highest scientific standards. The main reason to use NDVI time series for our annual urban mapping was to reduce data dimensionality – one NDVI layer versus six surface reflectance bands. In addition, NDVI is good indicator of vegetation condition and status; new urban development typically involves vegetation clear-cut and NDVI change (Lunetta et al., 2006, Shao et al., 2011).

To reduce cloud contamination, we applied a maximum value composite (MVC) algorithm to the original NDVI time series to derive monthly NDVI layers. Each monthly NDVI layer is a composite image representing the highest observed NDVI value for each pixel in a given compositing month. The same MVC algorithm (Holben, 1986) was used as the compositing algorithm in developing 16-day MODIS NDVI products (Huete et al., 2002); here, we applied it to 30m Landsat time series. The monthly NDVI images appeared to be noisy, with a significant

amount of missing data due to image availability and cloud impacts. Thus, to further reduce cloud impacts and data volume, we applied the MVC algorithm to the NDVI time series to derive annual NDVI layer from 1988 to 2017. The resultant annual NDVI layers were stacked to construct annual NDVI time series – each pixel has 30 NDVI values covering years from 1988 to 2017. We applied a Savitzky-Golay smoothing algorithm to remove pseudo hikes and drops from the annual NDVI time-series. The Savitzky-Golay filter is among the best performers with respect to ease of implementation and robustness of results (Chen et al., 2004; Jia et al., 2014; Shao et al., 2016). Fig. 2 shows the flowchart for the above-described data processing steps.

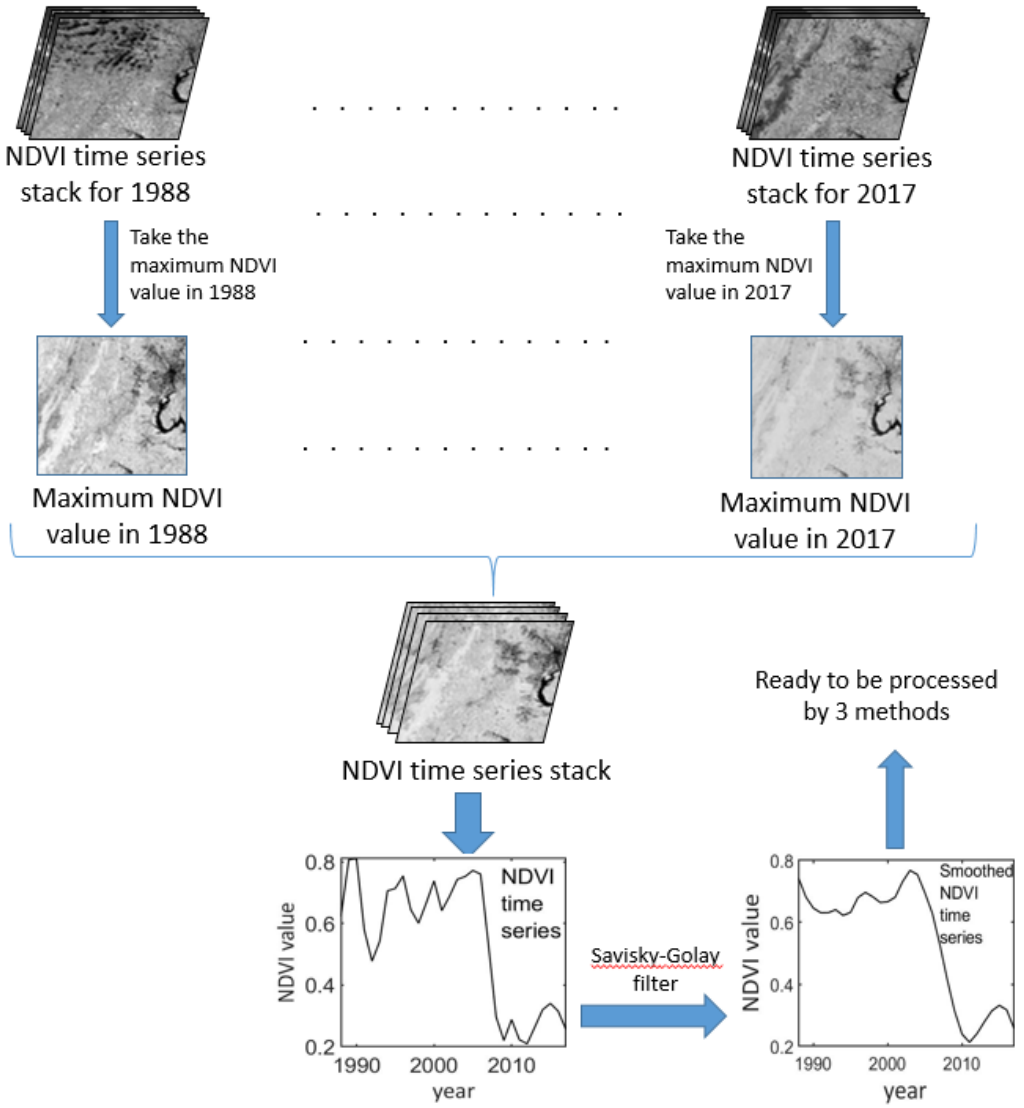

Fig. 2. Flowchart of data preprocessing

2.4 Annual urban mapping

We used NLCD as our primary reference data to evaluate our annual urban mapping methods. Starting with NLCD 2001, each release of NLCD divides urban areas into four classes: (a) developed open space (< 20% impervious cover; class code 21), (b) low-intensity developed (20-49% impervious cover; class code 22), (c) medium-intensity developed (50-79% impervious

cover; class code 23), and (d) high-intensity developed (≥ 80% impervious cover; class code 24) (Homer et al., 2015). By comparing to higher resolution urban map, Irwin and Bockstael (2007) stated that NLCD has relatively low classification accuracy for open space and low intensity urban classes, mainly due to limitations of 30m Landsat resolution. Therefore, it is more realistic to focus on medium-high intensity urban pixels (NLCD classes 23 and 24) for better mapping accuracy. Using 2001 NLCD and 2011 NLCD as reference, we identified all pixels influenced by urbanization processes (from non-urban land cover to medium-high intensity urban) and pixels influenced by urban intensification processes (from open space/low intensity urban to medium-high intensity urban) during the 10-year time period. These NLCD-derived urban change pixels were principal targets for further detection of their corresponding urban change years.

In the following section, we describe three time series analyses used for identifying the specific year of urban change. For each time series change detection method, we examined input data for two time series, 1998-2014 and 1988-2017, to evaluate how length of input NDVI time series affect mapping accuracy.

Minimum-value method

For the minimum-value method, our assumption was that the minimum NDVI value within each NDVI time series should match well with specific urban change year. It is expected to see a significant decrease of the NDVI value if a forest/agricultural pixel is converted to a medium-high intensity urban pixel. Similarly, NDVI values typically decrease, probably with a smaller amplitude, when an open space/low intensity urban pixel is further intensified to medium-high intensity urban.

We used 40 randomly selected urban change pixels (i.e., training data points) to conduct an initial assessment of this minimum-value method, using Google Earth's High-Resolution Imagery Archive as reference. It should be noted that urban change can be a multi-year process from the beginning of clear-cutting to the completion of construction. We used beginning of clear-cutting as 'ground truth' for urban change. We found that there was typically a three-year time lag between the minimum-value year and the observed urban change year from Google Earth. In other words, NDVI values may continue to decrease from beginning of clear-cutting and reach its lowest value in the next 2-3 years, depending on duration of construction activities. Therefore, we simply applied the 3-year adjustment to correct the time lag for the minimum-value method.

Break-point method

For each MVC NDVI time series, the specific urban change year could serve as a break point dividing the whole time series into two segments. This break point should maximize the difference between the mean values of the two segments. To be specific, the identified urban change year should result in a maximum value of $\mu_1 - \mu_2$, where μ_1 is the mean of the time series segment ranging from starting year to the year of urban change and μ_2 is the mean of the time series segment ranging from the urban change year to the ending year of time series.

Simple-threshold identification

Another approach to identify a specific change year in a time series NDVI is to specify a threshold value. Scanning the annual MVC NDVI from the beginning of the time series, the year

where NDVI value first dropped below the threshold value can be defined as the urban change year.

We evaluated potential threshold values by examining the histogram plots of MVC NDVI values for various NLCD 2001 land cover categories. Fig. 3(a) shows the distribution of MVC NDVI (2001) values for medium-high intensity urban pixels. A large proportion of medium-high intensity urban pixels have relatively low MVC NDVI values (e.g., 0.1-0.7). Conversely, the vegetation pixels (e.g., forest and agricultural lands) and open space pixels typically have high MVC NDVI values greater than 0.6 (Fig. 3b and 3c). Therefore, it is reasonable to specify a threshold value of 0.6 to separate medium-high intensity urban and the other land cover classes. For a given NDVI time series, once the MVC NDVI value dropped below 0.6, it would imply an urban change event in that year. We started with a 0.6 threshold, then evaluated different threshold values ranging from 0.5 to 0.7 for sensitivity analysis. This simple threshold method may not produce accurate results for detecting urban intensification processes that involve changes from low intensity urban (NLCD class = 22) to medium-high intensity urban, because low intensity urban class shows a largely scattered NDVI distribution (0.1-0.9) (Fig. 3d).

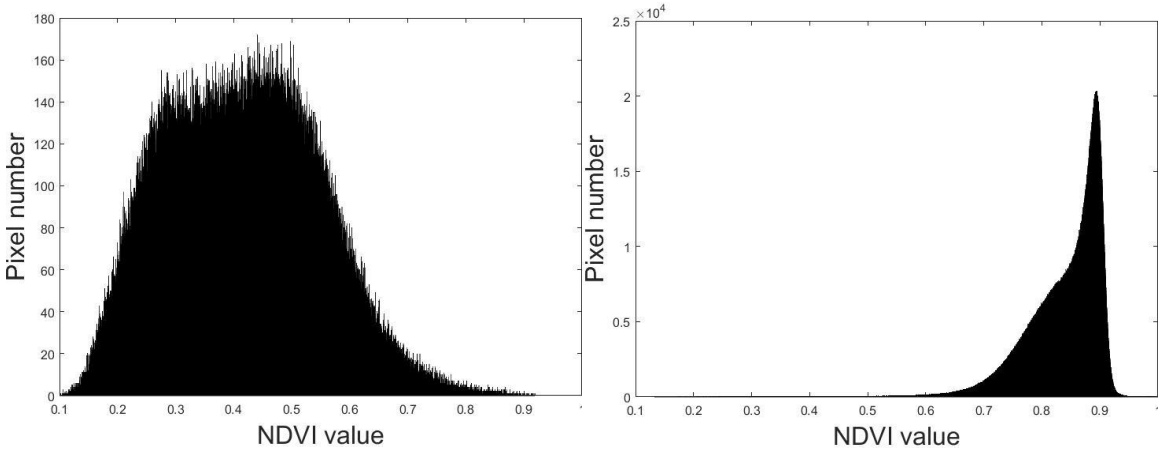

(a) Medium-high intensity urban (b) Vegetation

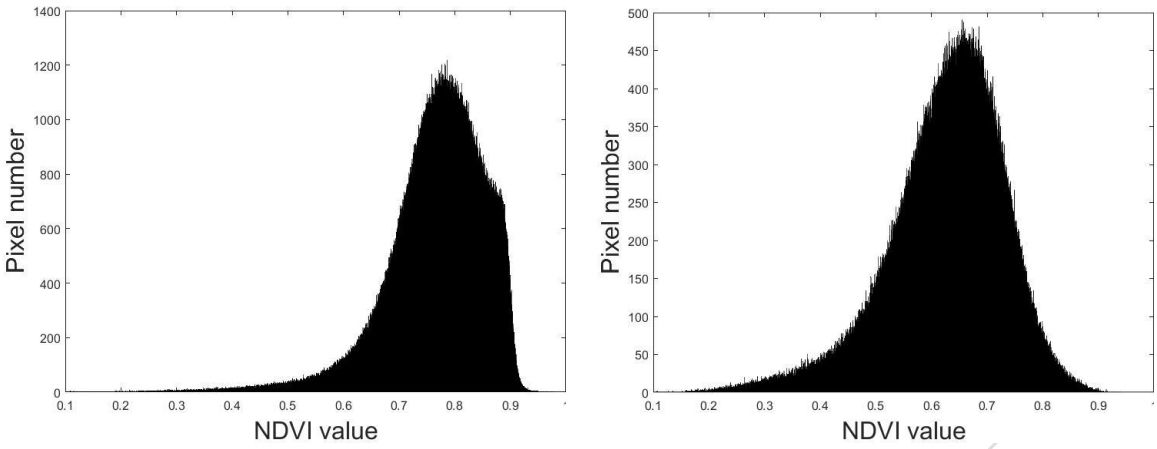

(c) Developed open space (d) Low intensity urban

Fig. 3. Histograms of NDVI values for (a) medium/high intensity urban; (b) vegetation (forests and agriculture); (c) low intensity urban; (d) developed open space

Detection of no-change pixels

NLCD data have relatively high accuracy for medium-high intensity urban class (Irwin and Bockstael, 2007), but change pixels identified from NLCD 2001-2011 may still include false positives. Each of the three NDVI change detection methods could potentially identify those false detections from NLCD data. For the minimum-value method, if the NDVI-derived change year located outside of the period of 2001-2011, we label the pixel as no-change. For the break-point method, a negative value of μ1- μ2 signals an increase of NDVI value in the time-series so it is reasonable to label the corresponding pixel as no-change. For simple-threshold identification, the no-change pixel can be determined based on a pre-defined threshold (e.g., 0.6). For a given NDVI time-series, if all NDVI values within the 2001-2011 window are higher than the threshold value of 0.6, the pixel could be labeled as no-change.

2.5 Accuracy assessment

We conducted detailed accuracy assessments for two change pixel groups: (1) an urbanization group that includes all pixels changed from non-urban land cover classes to medium-high intensity urban, and (2) an urban intensification group that includes pixels changed from open space or low intensity urban to medium-high intensity urban. We systematically selected a total of 400 pixels for accuracy assessment: 200 for the urbanization group and 200 for the urban intensification group. Within the urban intensification group, 100 pixels were selected for open space to medium-high intensity urban change and low intensity to medium-high intensity urban change, respectively.

Each selected change pixel was pinpointed on Google Earth and the actual urban change year was recorded by visual interpretation of Google Earth's High-Resolution Imagery Archive. The conversion of forest/agriculture cover to urban cover can be a multi-year process from the beginning of clear-cutting to the completion of construction. We used beginning of clear-cutting as the 'ground truth' of urban change. In some cases, it was difficult to detect the starting point of clear-cutting due to limited availability of historical satellite images. For example, an ongoing construction was observed in the March of 2005 Google imagery and the previous July 2003 Google image showing forest/agricultural cover, the middle temporal point (year 2004) was then selected as the urban change year. For pixels without sufficient high-resolution imagery as reference (i.e., imaging gap > 2 years), we simply excluded them from the accuracy assessment because we could not define a 'ground truth' or observed urban change year. About 29 pixels were removed because of their ineligibility for the accuracy assessment, and replenished pixels were selected by simple random sampling. The same method was applied to the urban

intensification pixel group for determining change years. The only difference is that there might not be a clear-cutting event so the observed urban intensification year should be the year when construction started.

The urban change years estimated from the NDVI time series analyses were compared with the Google Earth-derived data, pixel-by-pixel. Due to image availability issues, the Google Earth-derived urban change year could have a one-year deviation from the actual urban change year, therefore, one-year difference between the NDVI-estimated change year and the Google Earth-derived change year was considered as a 'correct' change detection. Overall accuracies were computed to compare three change detection algorithms using such a one-year deviation assessment. Additional two-year deviation assessments were conducted for thoroughness.

3. Results

3.1 Accuracy assessment for urbanization pixels

Table 1 shows the error matrix of accuracy assessment for change and no-change pixels using Google Earth as reference. Note all 200 pixels were previously identified as change pixels (from other land cover classes to medium-high intensity urban) by comparing NLCD 2001 and 2011. Among the 200 selected pixels, 196 pixels were visually interpreted as change pixels using high resolution Google Earth imagery, suggesting very high accuracy of NLCD in determining other land cover classes (e.g., forest and agricultural lands) to medium-high intensity urban change. Using 1998-2014 NDVI time-series data as input, all three time-series methods performed well on the separation of change and no-change pixels, and the minimum-value method had the highest overall accuracy of 98.5% (kappa=0.56). Simple-threshold identification performed

worst by falsely identifying no-change pixels, leading to a high commission error of 71.4%. The use of longer time-series NDVI (1988-2017) resulted in almost identical overall accuracy (difference < 1%) so the detailed error matrix is not presented here.

Table 1. Error matrices of change and no-change for urbanization pixels using reference data derived from Google Earth.

Time series 1998-2014

	Reference from Google Earth				
	No change	**Change**	**Total**	**%Correct**	**%Commission**
Minimum-value method					
No change	**2**	1	3	66.7	32.3
Change	2	**195**	197	99.0	1.0
Total	4	196	200	**98.5**	**(n=200)**
%Correct	50.0	99.5			
%Omission	50.0	0.5			**Kappa=0.56**
Break-point method					
No change	**2**	6	8	25.0	75.0
Change	2	**190**	192	99.0	1.0
Total	4	196	200	**96.0**	**(n=200)**
%Correct	50.0	97.0			
%Omission	50.0	3.0			**Kappa=0.32**
Simple-threshold (t=0.6)					
No change	**4**	14	18	22.2	77.8
Change	0	**182**	182	100.0	0
Total	4	196	200	**92.2**	**(n=200)**
%Correct	100.0	92.6			
%Omission	0	7.4			**Kappa=0.34**

Table 1 summarizes general accuracy statistics for change and no-change pixels only. Fig. 4 shows a scatter plot comparing the NDVI-derived and the Google Earth-derived change year, pixel-by-pixel. For simplicity, we used results from the break-point algorithm as an example to

demonstrate the comparison. Among 200 randomly selected points, ten were interpreted as non-change pixels either from Google Earth or from the algorithm. The remaining points were plotted with different colors representing different frequencies of occurrence in the accuracy assessment. One-year deviation from the observed urbanization year from Google Earth is colored in yellow. It appears that a large majority of points (90.6%) lie within the one-year deviation zone, indicating good overall accuracy (R^2 is 0.74 and RMSE value is 1.01 year).

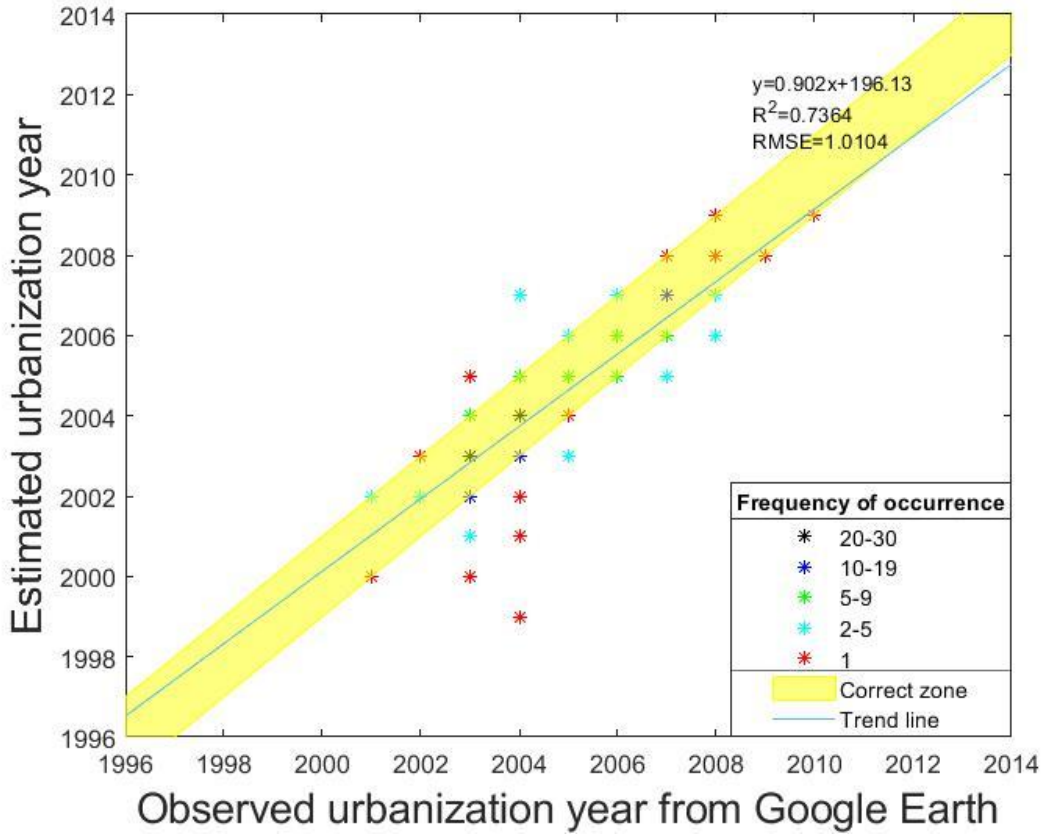

Fig. 4. Scatter plot of observed urbanization year v.s. estimated urbanization year for break-point method using MVC NDVI time series 1998 to 2014

Based on one-year deviation definition as well as the classification of change and non-change pixels, pixels can be grouped into two categories of correct or wrong classification and overall

accuracy can be calculated for each algorithm. Table 2 summarizes overall accuracies for three change detection algorithms. Using 1998-2014 time series data as input, the break-point algorithm generated the highest overall accuracy of 88.0% for the one-year deviation accuracy assessment. The minimum-value and simple-threshold (threshold = 0.6) algorithms had the same accuracy of 82.5%. For the simple-threshold algorithm, variation of threshold value to 0.5 and 0.7 led to reduced overall accuracy to 53.5% and 65.0%, respectively. Differences among three change detection algorithms declined when the tolerance level increased to two years of deviation. All three algorithms generated above 90% of overall accuracy; the break-point algorithm had the highest overall accuracy of 94%.

Table 2. The overall accuracies for urbanization pixel group

	Time series 1998-2014	Time series 1988-2017
±1 year:		
minimum-value	82.5%	85.0%
break-point	88.0%	83.5%
simple-threshold (t=0.6)	82.5%	82.0%
±2 year:		
minimum-value	92.0%	88.5%
break-point	94.0%	91.5%
simple-threshold (t=0.6)	90.0%	89.0%

The accuracy of change detection generally decreased when the longer time series (1988-2017) were used as input, except for the minimum-value algorithm in the one-year-deviation assessment. For example, the overall accuracy for break-point algorithm decreased to 83.5% compared to 88.0% resulted from 1998-2014 change detection. Longer time series data may be associated with more complicated NDVI trends involving longer-term NDVI increase/decrease

patterns. Our selected change detection algorithms thus can falsely identify change years located beyond the 2001-2011 time period.

3.2 Accuracy assessment for urban-intensification pixels

The classification accuracy of NLCD for urban-intensification pixels was much lower than that for urbanization pixels (Table 3). Among 200 randomly selected change pixels, only 168 pixels (84%) appeared to be actual change pixels based on Google Earth imagery and the remaining 32 pixels (16%) should be labeled as no-change pixels. Among three change detection algorithms, the break-point method achieved the highest overall accuracy of 86.5% (kappa = 0.49) while simple-threshold method performed worst with an overall accuracy of 63.0% (kappa=0.25).

Table 3. Error matrices of change and no-change for urban-intensification pixels

Time series 1998-2014					
	Google Earth Reference				
	No-change	Change	Total	%Correct	%Commission
Minimum-value method					
No change	**7**	5	12	58	42
Change	25	**163**	188	87	13
Total	32	168	200	**85**	(n=200)
%Correct	22	97			
%Omission	78	3			**kappa=0.25**
Break-point method					
No change	**18**	13	31	58	42
Change	14	**155**	169	91.7	8.3
Total	32	168	200	**86.5**	(n=200)
%Correct	56.3	92.3			
%Omission	43.7	7.7			**Kappa=0.49**
Simple-threshold identification					
No change	**28**	70	98	28.6	71.4
Change	4	**98**	102	96.1	3.9

Total	32	168	200	**63**	(n-200)
%Correct	87.5	58.3			
%Omission	12.5	41.7			**kappa=0.25**

Fig. 5 shows scatter plots comparing the results from the break-point algorithm (best performing one) and the visual interpretation of Google Earth imagery. A total of 45 pixels out of 200 were identified as no-change pixels either from Google Earth or from the algorithm, so were not displayed on the scatter plot. Compared to the urbanization pixel group, the distribution of the scatterplot for urban intensification is more scattered. A much smaller portion of the points lies within the correct zone (76.6%), and there are more outliers located further away from the correct zone, indicating an inferior estimation of urban change year when compared with urbanization pixel group. The R^2 (0.54) is much lower than that of urbanization pixel group while the RMSE (1.47 year) here is higher.

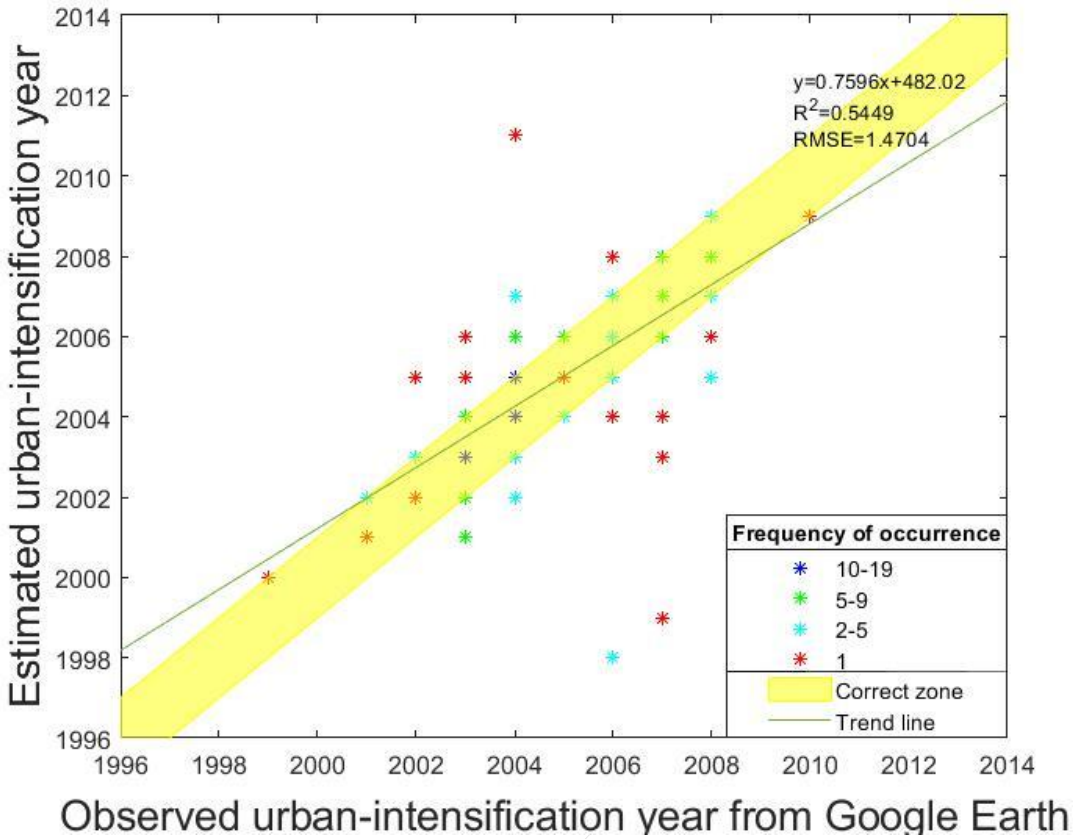

Fig. 5. Scatterplot of observed urban intensification year v.s. estimated urban intensification year for break-point method using MVC NDVI time series 1998 to 2014.

Overall accuracies of urban intensification for the three change detection methods are shown in Table 4. Within the urban intensification group, we further divided the change pixels into two sub-groups depending on initial 2001 land cover types: subgroup21 represents change pixels with initial land cover class of open space (NLCD class 21) and subgroup22 represents change pixels with initial land cover class of low intensity urban (NLCD class 22). Using 1998-2014 time series data as input and one-year-deviation accuracy assessment, the break-point algorithm resulted in the highest overall accuracy of 76% for subgroup21 change detection. The other two algorithms generated relatively lower accuracies of 59% and 65%, respectively. For

subgroup22, the minimum-value algorithm performed best (65.0%), although break-point algorithm's performance was only 4% lower. The simple-threshold identification (threshold=0.6) performed worst on subgroup22 change detection. The overall accuracy of 35.0% for subgroup22 using simple-threshold identification was substantially lower than accuracy statistics derived from other algorithms. We did additional sensitivity analyses by varying threshold values from 0.5 to 0.7, the best overall accuracy achieved was only around 55.0%. This result suggested poor overall performance of this change detection algorithm.

Table 4. Overall accuracies for urban intensification pixel group

	Subgroup21		Subgroup22	
	Time series 1998-2014	Time series 1988-2017	Time series 1998-2014	Time series 1988-2017
±1 year:				
minimum-value	59.0%	59.0%	65.0%	66.0%
break-point	76.0%	71.0%	61.0%	64.0%
simple-threshold (t=0.6)	65.0%	73.0%	35.0%	38.0%
±2 year:				
minimum-value	84.0%	85.0%	75.0%	77.0%
break-point	88.0%	83.0%	68.0%	71.0%
simple-threshold (t=0.6)	71.0%	78.0%	38.0%	42.0%

Comparing overall accuracies for two subgroups suggests that the subgroup22 is more challenging for annual change detection. This was expected because the initial land cover type for subgroup22 is low intensity developed urban which has about 40-49% of impervious cover within each 30m Landsat pixel. Although all pixels within the subgroup22 experienced urban intensification during the 2001-2011 time period, it was difficult to pinpoint the specific year of

intensification through time series NDVI analysis.

For both subgroup21 and subgroup22, overall accuracies generally increased when the length of the time series was expanded to 1988-2017, with the exception of break-point algorithm for subgropu21 change detection. This was the opposite of the result observed for urbanization pixels (i.e., non-urban to NLCD 23/24). This may be explained by the fact that certain algorithms' ability to distinguish between non-change pixels from change pixels had a much higher weight on the overall accuracy calculation. A significant portion (16%) of 200 randomly selected pixels were actual non-change pixels (i.e., falsely identified by NLCD). When using time series 1998 to 2014 as data input, the minimum-value method would falsely assign an urban change year to a non-change pixel. By using a much longer time series as input data, more pixels would be assigned an urban change year outside the study time period, thus potentially increasing overall accuracy. A longer time series did not improve the performance of the break-point method, because the break-point method detects the point where means of the time series change the most, and is less sensitive to length of the time series when compared with other methods.

3.3 Urban change maps

Urban change years for both urbanized pixels and urban-intensification pixels obtained from the optimal method (break-point) are shown in Fig. 6. In this figure, we grouped pixels with similar urban change years and assigned different colors to each group. To illustrate effects more clearly, Fig. 6 shows only a subset of the study area. As we have expected, pixels with the same or closer urban change years tend to be clustered together on the map. A part of the Washington Dulles Airport development can be seen as the L-shaped structure in the center of figure. All the

pixels for this airport have similar urban change years from 2005 to 2008. Figure 7 summarizes total numbers of urban change pixels by year. It is clear that the urban change rate increased from 1998 to 2003 and then slowly decreased year by year. Overall, a majority of urban development in our study area occurred between 2002 and 2007.

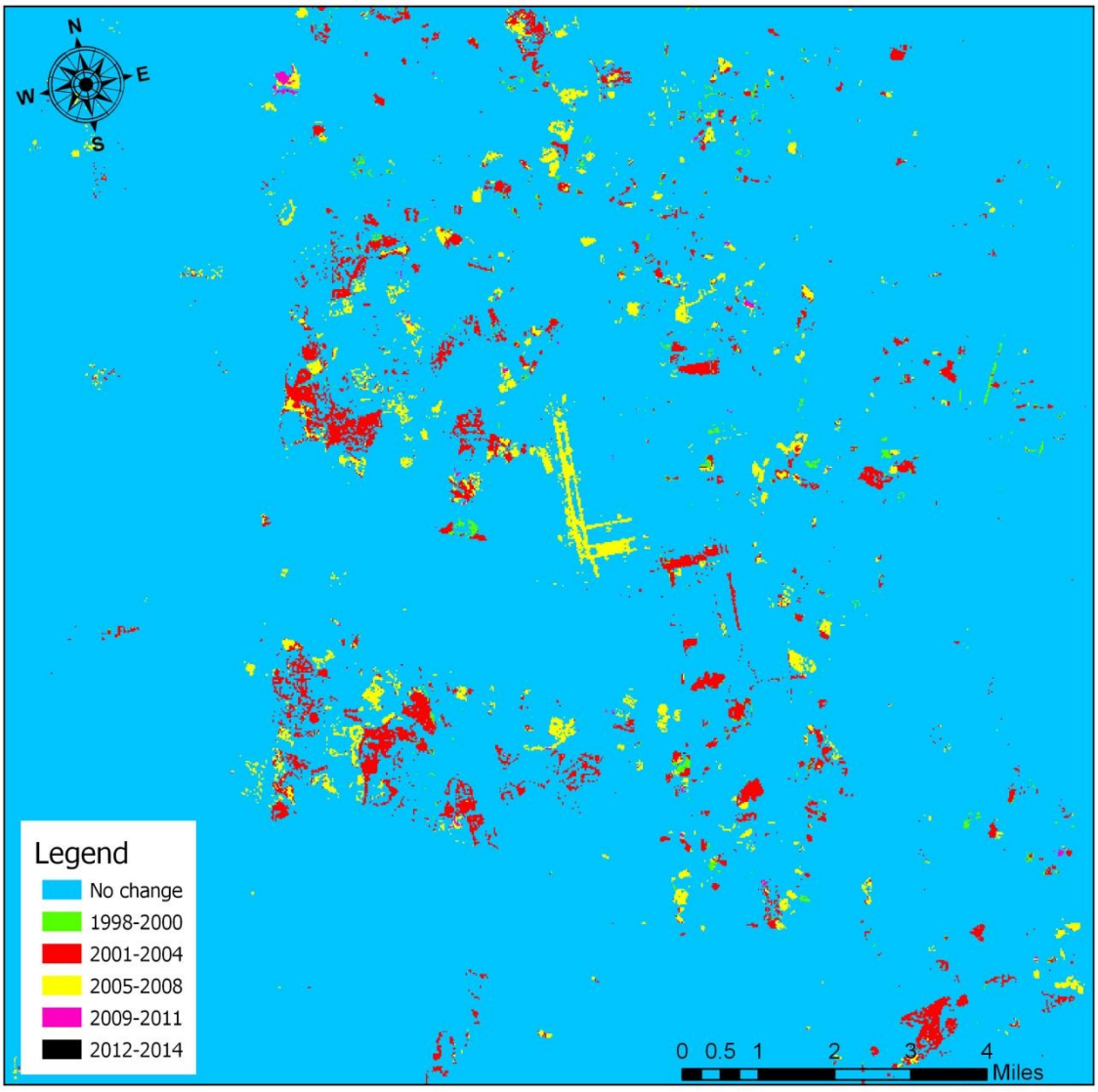

Fig. 6. Urban change years: pixels were grouped into 5 categories for better visualization

purpose.

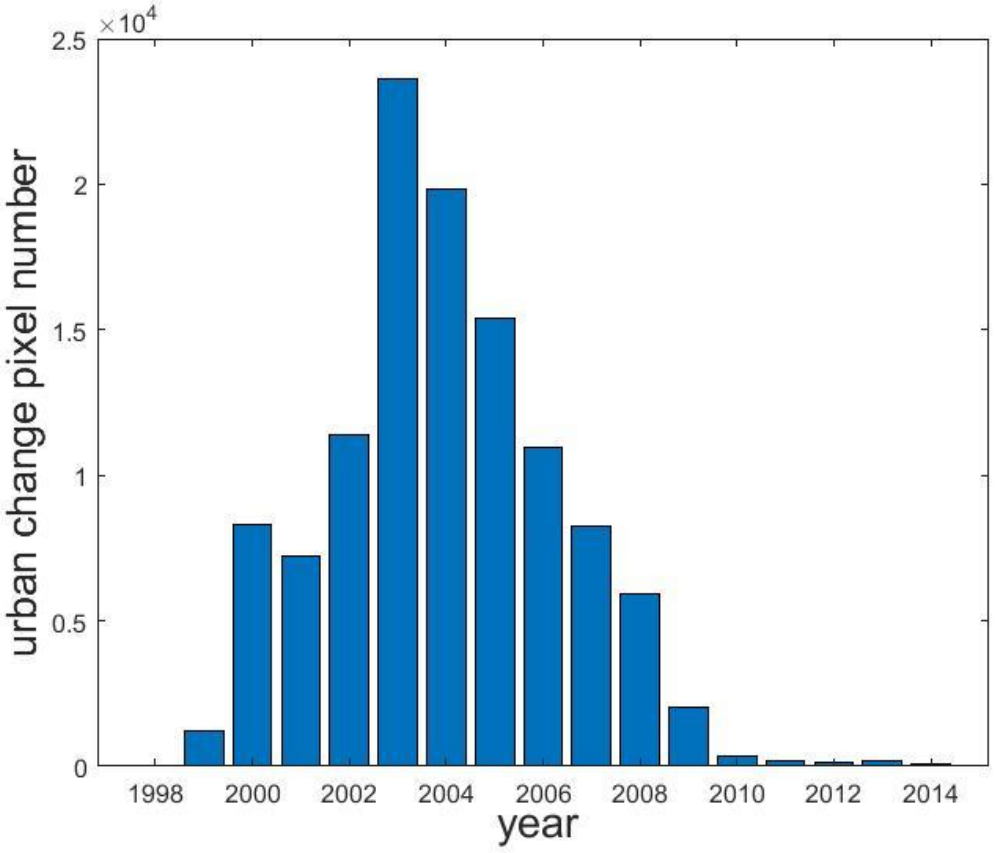

Fig. 7. Frequency distribution of annual urban change.

3.4 Novelty and limitation

In our time series analysis, a maximum value composite (MVC) algorithm was applied to the Landsat NDVI time series to develop the annual MVC NDVI time series. The use of annual MVC NDVI time series has greatly reduced data volume, and at the same time, removed most of the noise in the original NDVI time series. For our accuracy assessment, we divided change pixels into two groups, urbanization and urban intensification. Separation of the accuracy assessment could provide more detailed information on the performance of our change detection

algorithms.

Among three selected change detection algorithms, the break-point algorithm can be considered as optimal, based on two main reasons. First, the break-point algorithm is fully automated without user intervention while the simple-threshold identification and minimum-value algorithm both need different levels of calibration or threshold tuning.

A fully automated method is much preferred when it is applied for a different study region or time-period. Second, the break-point algorithm finds the point at which the mean of the NDVI time-series changes the most significantly, thus it is less sensitive to data noise, contributing to higher overall detection accuracies.

Our change detection methods, combined with the readily available NLCDs and Landsat Analysis Ready Data, can be directly applied to other fast-growing urban regions in the US to derive annual urban changes. The annual urban change maps contribute to NLCD impacts. More importantly, the high temporal urban change information could potentially improve our understanding of urban development patterns/trends. For example, the linkage between urban development and population dynamics (or other socio-economic factors) could be examined in a more continuous modelling framework.

The main limitation for our change detection algorithms is their poor performance in dealing with subgroup22 (pixels changed from low intensity to medium-high intensity urban). However, we note that the number of pixels in the subgroup22 pixels is much smaller than those of other urban change categories, thus our change detection methods would maintain relatively high

overall accuracies when all change pixels are included for accuracy assessment. Future study needs to focus on improving change detection accuracy for subgroup 22. Potential solution may include exploring other spectral and spatial indices in addition to the commonly used NDVI time-series. Newly developed change detection algorithms, especially those dealing with high dimensional time-series data (e.g., Cho and Fryzlewicz 2015), could be explored in the future. Another limitation for our analytical approach is that annual mapping of urban areas could not be accomplished without the support from NLCD. For this study, NLCD 2001 and 2011 served as the input data to derive urban change masks. In our future studies, we plan to update our annual urban maps to include all study years from 1992 to 2016. The NLCD Retrofit data (1992-2001 change) and NLCD 2016 data will be used as references for the longer term time-series analysis.

4. Conclusion

This study was designed for characterizing annual urban changes using time series Landsat and NLCD data. We examined both 17-year and 30-year Landsat-derived annual MVC NDVI time series using three different change detection algorithms to determine optimal combinations for annual urban change mapping. Using Google Earth's high resolution imagery as reference, detailed accuracy assessment was implemented for urbanization and urban-intensification pixel groups, defined by the initial land cover types of change pixels. The result showed that the combination of break-point algorithm with a time series of 1998-2014 reached the highest overall accuracy for estimating both urbanization years (overall accuracy of 88%) and urban-intensification years (overall accuracies of 76% and 61% for subgroup 21 and subgroup 22, respectively). The relatively low overall accuracy for subgroup 22 suggests that it is particularly challenging in determining urban intensification years for pixels labeled as low-intensity urban in

the NLCD data. Pixels with the same or close urban change years identified by the break-point algorithm tend to be clustered together on the map, further validating the overall good performance. In addition, the break-point algorithm is easy to implement and can be fully automated without user adjustment. It could be generalized to other fast-growing urban regions for annual urban change mapping across the US.

REFERENCES

Alston, K.P., Richardson, D.M., 2006. The roles of habitat features, disturbance, and distance from putative source populations in structuring alien plant invasions at the urban/wildland interface on the Cape Peninsula, South Africa, *Biological Conservation*, 132: 183–198.

Banskota, A., Kayastha, N., Falkowski, M.J., Wulder, M.A., Froese, R.E., White, J.C., 2014. Forest monitoring using Landsat time series data: A review, *Canadian Journal of Remote Sensing*, 40: 362–384.

Barnsley, M.J., Møller-Jensen, L., Barr, S.L., 2003. Inferring urban land use by spatial and structural pattern recognition, *Remote Sensing and Urban Analysis*, 9: 115–144.

Chen, J., Gong, P., He, C., Pu, R., Shi, P., 2003. Land-use/land-cover change detection using improved change-vector analysis, *Photogrammetric Engineering & Remote Sensing*, 69: 369–379.

Chen, J., Jönsson, P., Tamura, M., Gu, Z., Matsushita, B., Eklundh, L., 2004. A simple method for reconstructing a high-quality NDVI time series data set based on the Savitzky–Golay filter, *Remote sensing of Environment*, 91: 332–344.

Chen, J., Chen, J., Liao, A., Cao, X., Chen, L., Chen, X., He, C., Han, G., Peng, S., Lu, M., 2015.

Global land cover mapping at 30 m resolution: A POK-based operational approach, *ISPRS Journal of Photogrammetry and Remote Sensing*, 103: 7–27.

Cho, H. and Fryzlewicz, P., 2015. Multiple-change-point detection for high dimensional time series via sparsified binary segmentation. Journal of the Royal Statistical Society: Series B (Statistical Methodology), 77(2), pp.475-507.

Cohen, J.E., 2003. Human population: the next half century, *science*, 302: 1172-1175.

DeFries, R.S., Asner, G.P., Houghton, R., 2004. Trade-offs in land-use decisions: towards a framework for assessing multiple ecosystem responses to land use change, *Ecosystems and Land Use Change*, 153: 1–9.

Deng, X., Güneralp, B., Su, H., 2014. Observations and modeling of the climatic impact of land-use changes, *Advances in Meteorology*, 2014.

Foley, J.A., DeFries, R., Asner, G.P., Barford, C., Bonan, G., Carpenter, S.R., Chapin, F.S., Coe, M.T., Daily, G.C., Gibbs, H.K., 2005, *Global Consequences of Land Use* Science, 309: 570–574.

Fung, T., 1992. Land use and land cover change detection with Landsat MSS and SPOT HRV data in Hong Kong, *Geocarto International*, 7: 33–40.

Herold, M., Scepan, J., Clarke, K.C., 2002. The use of remote sensing and landscape metrics to describe structures and changes in urban land uses, *Environment and Planning A*, 34: 1443–1458.

Holben, B.N., 1986. Characteristics of maximum-value composite images from temporal AVHRR data, *International Journal of Remote Sensing*, 7: 1417–1434.

Homer, C., Dewitz, J., Fry, J., Coan, M., Hossain, N., Larson, C., Herold, N., McKerrow, A., VanDriel, J.N., Wickham, J., 2007. Completion of the 2001 national land cover database

for the counterminous United States, *Photogrammetric Engineering & Remote Sensing*, 73: 337.

Homer, C., Dewitz, J., Yang, L., Jin, S., Danielson, P., Xian, G., Coulston, J., Herold, N., Wickham, J., Megown, K., 2015. Completion of the 2011 National Land Cover Database for the conterminous United States–representing a decade of land cover change information, *Photogrammetric Engineering & Remote Sensing*, 81: 345–354.

Huete, A., Didan, K., Miura, T., Rodriguez, E.P., Gao, X., Ferreira, L.G., 2002. Overview of the radiometric and biophysical performance of the MODIS vegetation indices, *Remote Sensing of Environment*, 83: 195–213.

Huang, C., Goward, S.N., Masek, J.G., Gao, F., Vermote, E.F., Thomas, N., Schleeweis, K., Kennedy, R.E., Zhu, Z., Eidenshink, J.C., 2009. Development of time series stacks of Landsat images for reconstructing forest disturbance history, *International Journal of Digital Earth*, 2: 195–218.

Huang, C., Goward, S.N., Masek, J.G., Thomas, N., Zhu, Z., Vogelmann, J.E., 2010. An automated approach for reconstructing recent forest disturbance history using dense Landsat time series stacks, *Remote Sensing of Environment*, 114: 183–198.

Irwin, E.G., Bockstael, N.E., 2007. The evolution of urban sprawl: Evidence of spatial heterogeneity and increasing land fragmentation, *Proceedings of the National Academy of Sciences*, 104: 20672–20677.

Jia, K., Liang, S., Zhang, N., Wei, X., Gu, X., Zhao, X., Yao, Y. and Xie, X., 2014. Land cover classification of finer resolution remote sensing data integrating temporal features from time series coarser resolution data, *ISPRS Journal of Photogrammetry and Remote Sensing*, 93: 49-55.

Kalnay, E., Cai, M., 2003. Impact of urbanization and land-use change on climate, *Nature*, 423: 528-531.

Lo, C.P., Choi, J., 2004. A hybrid approach to urban land use/cover mapping using Landsat 7 Enhanced Thematic Mapper Plus (ETM+) images, *International Journal of Remote Sensing*, 25: 2687–2700.

Lu, D., Moran, E. and Hetrick, S., 2011. Detection of impervious surface change with multitemporal Landsat images in an urban–rural frontier, *ISPRS Journal of Photogrammetry and Remote Sensing*, 66(3): 298-306.

Lunetta, R.S., Knight, J.F., Ediriwickrema, J., Lyon, J.G., Worthy, L.D., 2006. Land-cover change detection using multi-temporal MODIS NDVI data, *Remote Sensing of Environment*, 105: 142–154.

Masek, J.G., Lindsay, F.E., Goward, S.N., 2000. Dynamics of urban growth in the Washington DC metropolitan area, 1973-1996, from Landsat observations, *International Journal of Remote Sensing*, 21: 3473–3486.

McKinney, M.L., 2002. Urbanization, Biodiversity, and Conservation: The impacts of urbanization on native species are poorly studied, but educating a highly urbanized human population about these impacts can greatly improve species conservation in all ecosystems, *Bioscience*, 52: 883–890.

Messina, J.P., Walsh, S.J., 2001. Simulating land use and land cover dynamics in the Ecuadorian Amazon through cellular automata approaches and an integrated GIS, in: *Open Meeting of the Human Dimensions of Global Environmental Change Research Community*, 6-8 October 2001, Rio de Janeiro, Brazil.

Maimaitiyiming, M., Ghulam, A., Tiyip, T., Pla, F., Latorre-Carmona, P., Halik, Ü., Sawut, M.

and Caetano, M., 2014. Effects of green space spatial pattern on land surface temperature: Implications for sustainable urban planning and climate change adaptation, *ISPRS Journal of Photogrammetry and Remote Sensing*, 89: 59-66.

Muñoz-Rojas, M., Jordán, A., Zavala, L.M., De la Rosa, D., Abd-Elmabod, S.K., Anaya-Romero, M., 2015. Impact of land use and land cover changes on organic carbon stocks in Mediterranean soils (1956–2007), *Land Degradation & Development*, 26: 168–179.

Pontius, R.G., Boersma, W., Castella, J.-C., Clarke, K., de Nijs, T., Dietzel, C., Duan, Z., Fotsing, E., Goldstein, N., Kok, K., 2008. Comparing the input, output, and validation maps for several models of land change, *The Annals of Regional Science*, 42: 11–37.

Radeloff, V.C., Hammer, R.B., Stewart, S.I., Fried, J.S., Holcomb, S.S., McKeefry, J.F., 2005. The wildland–urban interface in the United States, *Ecological Applications*, 15: 799–805.

Roy, A., Srivastava, V.K., 2012. Geospatial approach to identification of potential hotspots of land-use and land-cover change for biodiversity conservation, *Current Science*, 102(8): 1174–1180.

Seto, K.C., Fragkias, M., 2005. Quantifying spatiotemporal patterns of urban land-use change in four cities of China with time series landscape metrics, *Landscape ecology*, 20: 871–888.

Seto, K.C., Shepherd, J.M., 2009. Global urban land-use trends and climate impacts, *Current Opinion in Environmental Sustainability*, 1: 89–95.

Seto, K.C., Güneralp, B., Hutyra, L.R., 2012. Global forecasts of urban expansion to 2030 and direct impacts on biodiversity and carbon pools, *Proceedings of the National Academy of Sciences*, 109: 16083–16088.

Sexton, J.O., Song, X.-P., Huang, C., Channan, S., Baker, M.E., Townshend, J.R., 2013. Urban growth of the Washington, DC–Baltimore, MD metropolitan region from 1984 to 2010

by annual, Landsat-based estimates of impervious cover, *Remote Sensing of Environment*, 129: 42–53.

Shao, Y., Lunetta, R.S., 2011. Sub-pixel mapping of tree canopy, impervious surfaces, and cropland in the Laurentian Great Lakes Basin using MODIS time series data, *IEEE Journal of Selected Topics in Applied Earth Observations and Remote Sensing*, 4: 336.

Shao, Y., Lunetta, R.S., Wheeler, B., Iiames, J.S., Campbell, J.B., 2016. An evaluation of time series smoothing algorithms for land-cover classifications using MODIS-NDVI multi-temporal data, *Remote Sensing of Environment*, 174: 258–265.

Staudt, A., Leidner, A.K., Howard, J., Brauman, K.A., Dukes, J.S., Hansen, L.J., Paukert, C., Sabo, J., Solórzano, L.A., 2013. The added complications of climate change: understanding and managing biodiversity and ecosystems, *Frontiers in Ecology and the Environment*, 11: 494–501.

Taubenböck, H., Esch, T., Felbier, A., Wiesner, M., Roth, A., Dech, S., 2012. Monitoring urbanization in mega cities from space, *Remote Sensing of Environment*, 117: 162–176.

U.S. Landsat Analysis Ready Data (ARD), n.d., URL: https://landsat.usgs.gov/ard (last date accessed: 11 September 2018).

Wang, H., Shao, Y. and Kennedy, L.M., 2014. Temporal generalization of sub-pixel vegetation mapping with multiple machine learning and atmospheric correction algorithms, *International Journal of Remote Sensing*, 35(20): 7118-7135.

Welch, R., 1982. Spatial resolution requirements for urban studies, *International Journal of Remote Sensing*, 3: 139–146.

Weng, Q., Lu, D., Schubring, J., 2004. Estimation of land surface temperature–vegetation abundance relationship for urban heat island studies, *Remote sensing of Environment*, 89:

467–483.

Weng, Q., 2009. Thermal infrared remote sensing for urban climate and environmental studies: Methods, applications, and trends, *ISPRS Journal of Photogrammetry and Remote Sensing*, 64(4): 335-344.

Wickham, J.D., Stehman, S.V., Fry, J.A., Smith, J.H., Homer, C.G., 2010. Thematic accuracy of the NLCD 2001 land cover for the conterminous United States, *Remote Sensing of Environment*, 114: 1286–1296.

Winz, I., Brierley, G., Trowsdale, S., 2009. The use of system dynamics simulation in water resources management, *Water resources management*, 23: 1301–1323.

Wu, Y. and Chin, L.S., 2016. A simplified training data collection method for sequential remote sensing image classification, *Fourth International Workshop on Earth Observation and Remote Sensing Applications (EORSA)*, 4-6 July, 2016, Guangzhou, China, pp. 329-332.

Woodcock, C.E., Allen, R., Anderson, M., Belward, A., Bindschadler, R., Cohen, W., Gao, F., Goward, S.N., Helder, D., Helmer, E., 2008. Free access to Landsat imagery, *Science*, 320: 1011–1011.

Xian, G., Crane, M., 2006. An analysis of urban thermal characteristics and associated land cover in Tampa Bay and Las Vegas using Landsat satellite data, *Remote Sensing of environment*, 104: 147–156.

Xian, G., Homer, C., Fry, J., 2009. Updating the 2001 National Land Cover Database land cover classification to 2006 by using Landsat imagery change detection methods, *Remote Sensing of Environment*, 113: 1133–1147.

Yuan, F., Sawaya, K.E., Loeffelholz, B.C., Bauer, M.E., 2005. Land cover classification and change analysis of the Twin Cities (Minnesota) Metropolitan Area by multitemporal

Landsat remote sensing, *Remote sensing of Environment*, 98: 317–328.

Yuan, F., 2008. Land-cover change and environmental impact analysis in the Greater Mankato area of Minnesota using remote sensing and GIS modelling, *International Journal of Remote Sensing*, 29: 1169–1184.

Zha, Y., Gao, J., Ni, S., 2003. Use of normalized difference built-up index in automatically mapping urban areas from TM imagery, *International Journal of Remote Sensing*, 24: 583–594.

Zhang, L. and Weng, Q., 2016. Annual dynamics of impervious surface in the Pearl River Delta, China, from 1988 to 2013, using time series Landsat imagery, *ISPRS Journal of Photogrammetry and Remote Sensing*, 113: 86-96.

Zhu, Z., Woodcock, C.E., Rogan, J., Kellndorfer, J., 2012. Assessment of spectral, polarimetric, temporal, and spatial dimensions for urban and peri-urban land cover classification using Landsat and SAR data, *Remote Sensing of Environment*, 117: 72–82.

Chapter 3. Near real-time urban change detection through machine learning

3.1 INTRODUCTION

In this chapter, we processed a decadal long Landsat-derived NDVI time series data by using machine learning algorithms to achieve near real-time urban change detection. Different machine learning algorithms, such as random forest and artificial neural networks, have been tested and compared to find out the optimal method.

3.2 MANUSCRIPT

The manuscript for this chapter is in preparation for submission and is shown below:

Near real-time urban change identification through machine learning

Abstract

Urbanization is the most intensive Land Use Land Cover Change (LULCC) type, resulting in biodiversity loss, degradation of water and air quality, alteration of climate patterns, and changes in hydrologic cycles. Monitoring past and current urban growth could help us have a better understanding of urbanization processes, thus supporting ecosystem service evaluation, urban planning, and policy making. In this study, machine learning-based classification models, including the random forest classifier and Artificial Neural Networks (ANN), were tested and compared to find out the optimal algorithm for near real-time urban change detection. Ten-year-annual-maximum NDVI time series data were used as data inputs in the classification models. Because the number of no-change pixels is much greater than that of urban change pixels, we are dealing with an extremely imbalanced dataset, thus different ratios between the number of no-change pixels and that of urban change pixels were tested. Cross validations determined that a ratio of 1:200 between urban change pixels and no-change pixels worked best for urban change detection, and ANN achieved higher overall classification accuracy and with a faster computation speed than random forest classifier. By using high-resolution imagery archives in Google Earth as reference, accuracy assessments for the optimal classification model were conducted in three different sampling areas, including urban core, suburb area, and rural area. The results indicate that our model works well in urban setting environment, with overall accuracies of 95% and 92% for urban core and suburb area, respectively. However, its performance is inferior in rural areas where forest clearing could be induced by both urban change and forest harvest. Future research should seek to add more data inputs, such as distance

to existing urban, elevation and slope in our classification model to better distinguish urban change from forest harvest in rural areas.

1. Introduction

Land Use Land Cover Change (LULCC) causes huge impacts on the environment, including the alteration of the hydrologic cycle, climate patterns, air and water quality, biodiversity, and biogeochemical fluxes (Homdee et al., 2011; Lawrence et al., 2012; Mahmood et al., 2010; Martínez et al., 2009; Wilson and Weng, 2010; Wu et al., 2012). Urbanization is considered to be the most irreversible and human-dominated LULCC type, and likely the most intensive one, given the resulting environment impacts at local, regional scales, and global scale (Seto et al., 2011). In the past decades, urban areas have expanded at a fast rate due to rising population and migration from rural to urban areas (Angel et al., 2005). Seto et al. (2011) reported a world-wide urban growth of 58,000 km^2 from 1970 to 2000. The world's urban population has surpassed its rural counterpart since 2007, and it is predicted that over two-thirds of the world's population will be living in urban areas by 2050 (Dye, 2008; Kammen and Sunter, 2016). This dramatic increase in urban population will continue boosting the expansion of urban growth in the following decades.

Monitoring past and current urban extent could enable a better understanding of urban growth processes, including urban growth rates and patterns, thus supporting ecosystem services assessment, urban planning and policy-making (Harts et al., 2003). Numerous studies have quantified urban growth at local, regional, and global scales using remote sensing data, especially satellite imagery (Schneider et al., 2009; Trianni et al., 2015; Xian and Crane, 2005).

Landsat imagery is widely used one for urban growth monitoring due to its high spatial resolution (30m), high temporal resolution (approximately every 16 days), rich historic archives and open access (Woodcock et al., 2008). In the U.S., Landsat imagery, together with a series of ancillary datasets (e.g., topography, census and agricultural statistics, soil characteristics, wetlands, and other land cover maps), are used to derive the National Land Cover Database (NLCD), which provides land use land cover data for the entire U.S. (Homer et al., 2015). Due to its high overall accuracy of around 85% and its broad coverage across the whole nation, NLCD has been widely used for providing high spatial resolution (30-m) land use land cover data in numerous models (Homer et al., 2015). However, the five-year time gap between each NLCD product has limited its applications in some models requiring higher temporal resolution of land use land cover data (Winz et al., 2009).

Image classification and change detection techniques are widely used for urban mapping and urban change detection (Jensen, 1981; Thapa and Murayama, 2009). One commonly used method is to conduct individual image classification for each satellite image obtained in each mapping year, and then urban change areas could be simply derived based on comparisons. But the intrinsic classification errors in each mapping year would accumulate through time, making this mapping method a low accuracy approach (Chen et al., 2003). Another method for annual urban mapping is to update the existing urban map products (e.g., NLCD) to an annual temporal resolution. Using NLCD as baseline could ensure a relatively higher accuracy for the derived annual urban map products, and these products could be utilized by a broader users since they are the continuations of NLCD. Wan et al. (2019) has proposed one method for annual urban mapping by using NLCD and Landsat-derived maximum annual Normalized Difference

Vegetation Index (NDVI) time series data. Here, annual urban mapping is to find out the urban change years for both urbanization pixels and urban intensification pixels, with the former one represents pixels changing from non-urban categories to medium/high-intensity urban and the latter one represents pixels changing from open space/low-intensity urban to medium/high-intensity urban. The overall accuracy for detecting urban change years of urbanization pixels has reached a high level of 89%. There are two major steps in this method: First, NLCD from two different years (e.g., NLCD2001 and NLCD2011) are compared to identify all the urban change pixels (both urbanization pixels and urban intensification pixels) during this time period; Then, urban change year for each identified pixel is determined by analyzing Landsat-derived maximum annual NDVI time series data. One major limitation of this method is that it relies heavily on NLCD, and it could not be used for recent years where there's no land cover data support from NLCD. To be specific, currently, the most up-to-date version of NLCD is for the year of 2016, and this method is not applicable for the years after 2016 (e.g., 2017, 2018, 2019) because urban change pixels after 2016 could not be identified due to the lack of NLCD data. Finding out pixels experienced with urbanization and urban intensification in recent years is considered as near real-time urban change detection.

Urban change detection for recent years can be treated as a classification problem, where areas that have experienced urban change are represented by urban change pixels that can be distinguished from no-change pixels. Machine learning-based classification models, such as the random forest classifier and Artificial Neural Networks (ANN), could be the solution for this near real-time urban change detection problem (Feng et al., 2015; Liu and Lathrop, 2002). The classification process of these machine learning-based classification models is a black box where

classification mechanism is unknown, but these models normally outperform traditional statistical models in terms of overall classification accuracy (Breiman, 2001).

The purpose of this study is to compare methods for achieving near real-time urban change detection using machine learning-based classification models. Specifically, I tested and compared random forest and ANN to determine the optimal method for urban change detection. To test the optimal model's prediction capability on different land cover settings, accuracy assessments will be conducted for three different sapling areas, including urban core, suburb area, and rural area.

2. Methods

2.1 Study area

Landsat scene (path: 27, row: 9) shown in figure 1 is selected as the study area. The study area has a total area of 22,500 km^2, and includes the northwestern part of the Washington D.C. metropolitan area, northern Virginia, and a small portion of West Virginia. Washington D.C. metropolitan area is considered as one of the fastest growing urban areas in U.S., with an average urban growth rate of 11±2 km^2/year (Sexton et al., 2013). The dramatic urban expansion processes in the study area during the past decades is the prerequisite condition for testing our near real-time urban change detection methods. Based on NLCD 2001, the study area consists of 2.83% water, 16.88% urban and barren land, 49.05% forest, 2.45% shrub and grassland, 25.29% agriculture, and 3.48% wetlands. The diversity in land cover types in the study area is another advantage of the selected scene because it allows us to test the classification accuracy of the optimal method at different land cover settings. Finally, a rich time series of high-resolution

images for the study area are available on Google Earth's High-Resolution Imagery Archive, which facilitated the accuracy assessment of our method.

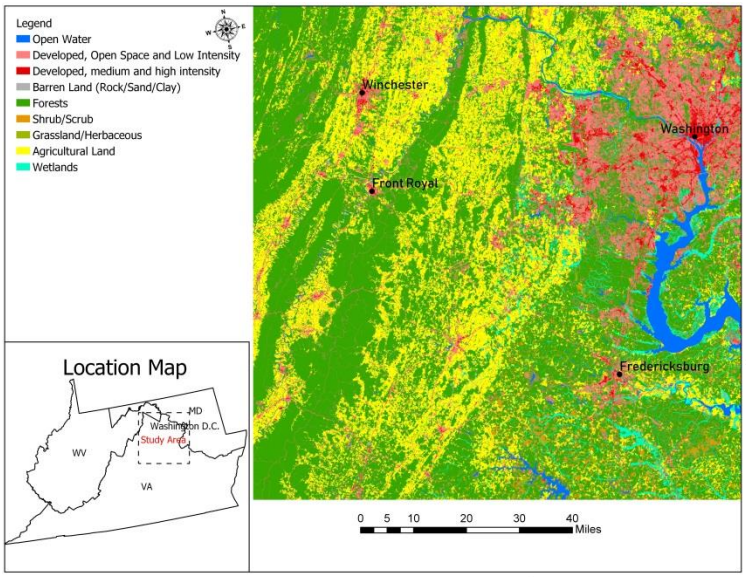

Figure1. Study area and associated NLCD classes

2.2 Data

A total of 1,084 Landsat Analysis Ready Data (ARD) (h027v009, ARD tile) surface reflectance imagery from 1994 to 2019 were downloaded from the USGS EarthExplorer (https://earthexplorer.usgs.gov). The downloaded dataset included all the Landsat 5, 7, and 8 ARD imagery within the designated time domain regardless of its cloud-contamination conditions since the cloud-free part of the image could still provide valuable information. Each image is composed of 5,000 by 5,000 pixels of 30-m resolution. In addition to Landsat ARD imagery, four NLCD map products (NLCD2001, NLCD2006, NLCD2011, and NLCD2016) were also downloaded from the Multi-Resolution Land Characteristics Consortium (http://www.mrlc.gov/). NLCD products have high overall accuracies of around 85%, with individual class accuracies ranging from 79% to 91% for Anderson Level I classes (Wickham et al., 2010).

2.3 Data preprocessing

NDVI is commonly used as an index for the characterization of urban growth because urbanization is always accompanied by a huge drop in NDVI value (Liu et al., 2010). Therefore, NDVI was derived for each satellite image, forming a dense NDVI time series stack from 1994 to 2019. Converting Landsat imagery into NDVI could also reduce data dimensionality, which better facilitated further data analytics. NDVI was directly calculated based on red band and near-infrared band of the Landsat ARD imagery, and no additional data preprocessing steps were needed before the calculation because ARD data has already been processed to the highest scientific standards.

The resulted dense NDVI time series stack contained cloud contamination and noise, which should be removed before proceeding to further data analysis. To reduce cloud contamination and noise, Maximum Value Composite (MVC) algorithm was applied to the NDVI time series stack at an annual interval (Holben, 1986). For each pixel in the study area, its maximum NDVI value for each year from 1994 to 2019 was selected as the representation of the NDVI value for that year, thus forming a 26 years of maximum NDVI time series stack. This MVC algorithm not only reduced cloud contamination and noise, but also decreased data dimensionality, making data analytics less computationally-intensive.This maximum annual NDVI time series stack could be further used in machine learning-based classifier training and near real-time urban change identification.

2.4 Preparing training samples

The basic idea of this research is to achieve near real-time urban change identification based on

machine learning algorithms, including random forest and ANN. The constructed machine learning-based models should automatically distinguish pixels experienced with urban change at the targeted year from pixels of no-change by using ten-years-annual-maximum NDVI time series (NDVI values from eight years before the mapping year, the mapping year, and the following one year) as data inputs. For instance, if we want to identify all the urban change pixels in 2015, ten annual maximum NDVI time series values from 2007 to 2016 shall be used as the data inputs in the classification models. Figure 2 shows the annual maximum NDVI time series examples for both urban change pixel and no-change pixel. It is rather simple to detect the difference between these two time series.

The most important step for constructing a machine learning-based classifier is to obtain enough training samples. Wan et al. (2019) proposed a method for detecting the specific year of urban change based on NLCD and Landsat-derived annual maximum NDVI time series data. This method could be applied to prepare training samples for urban change pixels. By the comparison of NLCD 2001 and NLCD2011, all the urban change pixels in this time period were identified, and Wan et al (2019) mapped out urban change year for each identified urban change pixel by using annual maximum NDVI time series data from 1998 to 2014. Based on the histogram of the urban change years, the majority of the urban changes happened in the middle portion of the time period. This phenomenon may reflect the intrinsic urban growth reality in the study area, but it may also be resulted from the intrinsic flaw of this method, which may omit some urban change pixels towards two ends of the time series. To enhance data quality, urban change pixels from the former three years (2001, 2002, and 2003) and the latter three years (2009, 2010, and 2011) of the time series were excluded, and only the middle five years' urban change pixels were

selected. To increase training samples for urban change pixels, another annual maximum NDVI time series data ranging from 2003 to 2019 were analyzed to pinpoint urban change years from 2006 to 2016. The incorporation of more urban change pixels from other years could contribute to a classification model with better generalization capability over time. We also only take the middle five years (2009, 2010, 2011, 2012, and 2013) of urban change pixels as training samples for a better accuracy. By combining the two data sets, we now have identified all the urban change pixels from 2004 to 2013 with their urban change years known. There are a total of 76,456 urban change pixels. For each identified urban change pixel, its corresponding 10-years-annual-maximum NDVI time series values will be serving as data inputs in classification models.

The preparation for pixels of no-change is much easier, and we can simply identify all the no-change pixels by the comparison of NLCD products. To exclude noises from other land cover categories, we are only sampling no-change pixels from agricultural land and forests because the majority of the urbanization in the study area is converted from agricultural land and forests. To be compatible with the urban change pixels, all the no-change pixels shall be sampled from the same years, ranging from 2004 to 2013. There are a total of 183,346,290 no-change pixels. For each no-change pixel, its corresponding 10 years-annual-maximum NDVI time series values will be serving as data inputs in classification models.

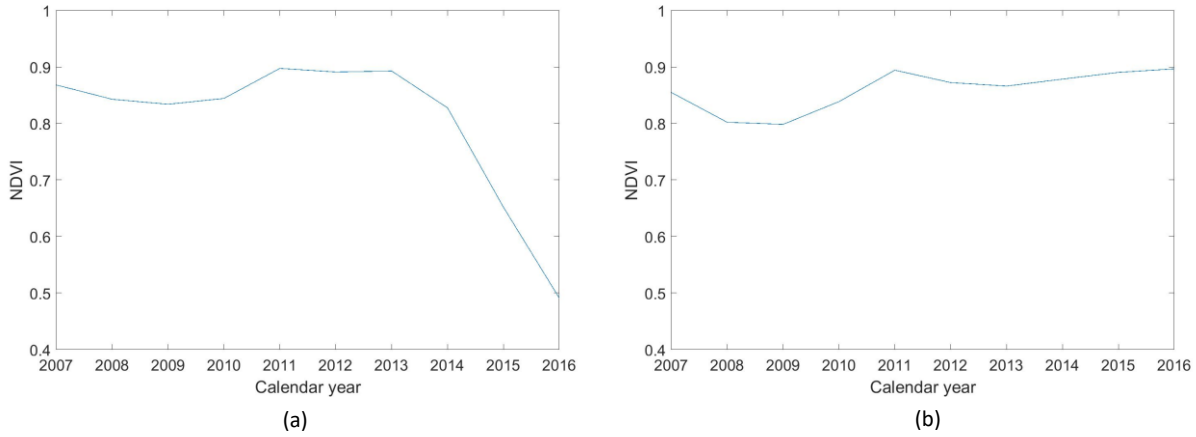

Figure 2. NDVI time series examples for: (a) pixel urbanized in 2015; (b) no-change pixel.

2.5 Training of machine learning-based classification models

Cross validation was implemented for parameter-tuning and model selection. The dataset combing urban change pixels and no-change pixels was divided into a training dataset (80% of total dataset) and a testing dataset (20% of total dataset). Different machine learning algorithms have been tested and compared to find out the optima method, including random forest classifier and ANN. The ratio between the number of urban change pixels and that of no-change pixels is approximately 1:2400, indicating that we are dealing with an extremely imbalanced dataset classification problem, thus different ratios shall be tested when training the classification model. The change of ratio was accomplished by undersampling the no-change pixel group while keeping all the urban change pixels.

2.6 Urban change identification for the year of 2017

The constructed optimal classification model could be used for the detection of urban change pixels in the year of 2017 and 2018. In this study, we only used the constructed model for

identifying urban changes in the year of 2017, which should be sufficient for the justification of this proposed method. Annual maximum NDVI time series values from 2008 to 2018 were used as data inputs in the classification model to automatically detect urban change pixels in 2017. After classification, NLCD 2016 was used to mask out all the medium and high-intensity urban areas in 2016. All the identified urban change patches smaller than 4 pixels were also removed to exclude potential classification errors.

2.7 Accuracy assessment

Historic high-resolution imagery on Google Earth was used for the accuracy assessment of this study. We have designed three sampling squares (500 by 500 pixel; figure 3) representing urban core, suburb area, and rural area in the study area to test the classification capability of the optimal model under different land cover settings. Within each sampling square, we have randomly sampled 50 pixels for urban change pixel and no-change pixel, respectively. The selected sampling pixels were pinpointed on Google Earth, and its reference urban change year was determined by observing the historic high-resolution imagery archive. The conversion from agriculture/forest to urban can be a process which lasts for several years, and the reference urban change year was defined as the year where the clear cut starts because clear cut can decrease NDVI value instantly. Due to the lack of historic high-resolution imagery, the starting time of clear cut for some pixels may not be observed, and the middle temporal time point shall be estimated as the urban change year. For example, an ongoing construction was observed for the targeted pixel on June, 2018 from the Google Imagery. The previous Google Imagery for this pixel was obtained on September, 2016, showing this pixel was forest on that time. Under this circumstance, we could not know the exact time of clear cut, thus the middle temporal time point

(2017) was estimated as the reference urban change year. For pixels with insufficient historic high-resolution imagery (i.e., imaging gap > 2 years), the middle temporal time point may not be a good estimation of its true urban change year, thus we simply exclude those pixels in our accuracy assessment. The reference urban change year estimated from the middle-temporal-time-point method might have a one-year-deviation from its true urban change year, thus, one-year-difference between the reference urban change year and the designated urban change year (2017) shall be tolerated and treated as a 'correct' change detection. Exclusions are for those pixels with abundant historic high-resolution imagery, which could be used to determine their accurate urban change years. Under this circumstance, even if the difference between the reference urban change year and the designated urban change year is one-year, it is still considered as 'incorrect' change detection since the obtained reference urban change year is accurate enough to reject the classification result.

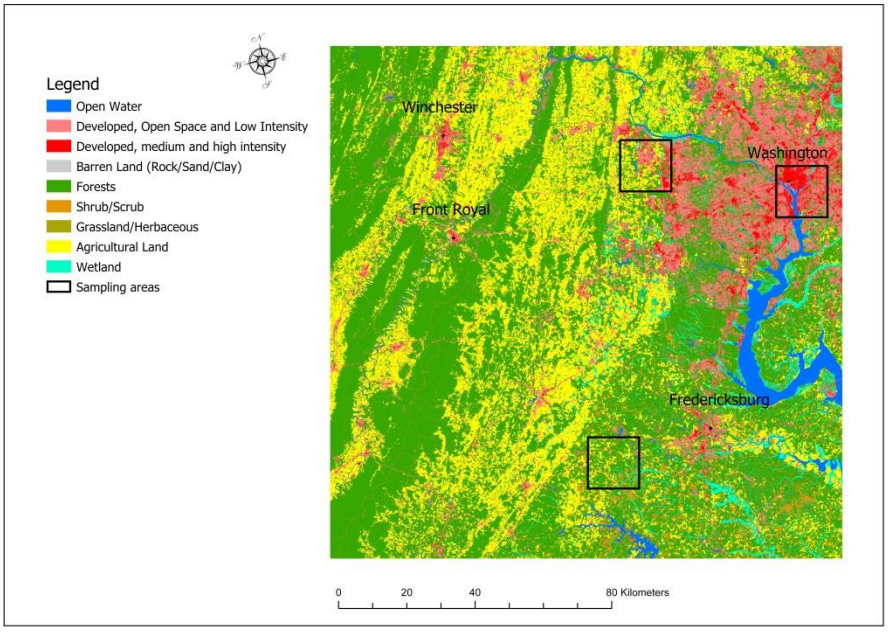

Figure3. Sampling areas

3. Results

3.1 Model selection

In this study, ANN outperformed random forest classifier in terms of overall classification accuracy and calculation speed, and the ratio of 1:200 between the number of urban change pixel and the number of no-change pixel produced the best result. This ANN model was considered as the optimal classification model and was then used for the urban change detection in 2017. Table 1 shows the confusion matrix for the validation result. The omission error for the detection of urban change pixel is around 17% while the commission error is 64%. The high commission error for detecting urban change pixels indicates that a large portion of no-change pixels (based on NLCD) were classified incorrectly as urban change pixels. Detailed analysis on the NDVI time series data of these misclassified pixels showed that they actually match the general pattern of those urban change pixels (showing a dramatic drop of NDVI value in the final years). This may indicate that these no-change pixels are actually mislabeled in the reference data, and the high commission error is because of the inaccuracy of the reference data (NLCD). So, this validation result could not be used to represent the true power of the classification models, and the final accuracy should be based on a more robust method.

Table1. Confusion matrix for the validation result

	Reference			
	No-change	Change	Total	% Commission
No-change	**36646366**	2586	36648952	0.01%
Change	22892	**12705**	35597	**64.31%**
Total	36669258	15291		

% Omission	0.06%	**16.91%**	**Overall = 99.93%**	**Kappa = 0.5**

3.2 Accuracy assessment

Accuracy assessments were individually conducted for three sampling areas (500 by 500 pixels) representing urban core, suburban, and rural environments within the study area. There were 163 urban change pixels identified by our classification model for urban core sampling area, and this number for suburb sampling area and rural sampling area were 4,135 and 498, respectively. Accuracy assessment result for each sampling area and three areas combined were shown in Table 2.

Urban core has the highest overall accuracy and Cohen's Kappa Coefficient among the three sampling areas. This sampling area is mainly focusing on Washington D.C., and it also has the most abundant historic high-resolution imagery in support for accuracy assessment, thus the accuracy assessment result for this sampling area is the most robust one. Because this area is highly urbanized, almost all the urban change events identified here were urban intensification. The overall accuracy and Cohen's Kappa Coefficient for suburb area is in the middle level among the three. This area received moderate but sufficient amount of high-resolution imagery for accuracy assessment, and the result was reliable.

Performance of the classification model was lowest in t in the rural area, with an overall accuracy of 91.3%. The accuracy assessment in this area is the least robust one because the related high-resolution imagery is limited here. We defined a large amount of pixels as urban change pixels from Google Earth because these pixels underwent clear cut in 2017. But actually we could not determine whether these clear cut events are related to urban change or forest

harvest because the most recent imagery for this area is obtained in October, 2017, and no further imagery could be found to observe the future changes of these pixels. Therefore, accuracy assessment result for this area has a low credibility.

Table2. Error matrices of change and no-change pixels in 2017.

	Reference from Google Earth				
	No-change	Change	Total	%Correct	%Commission
Urban core					
No-change	**50**	0	50	100	0
Change	5	**45**	50	90	10
Total	55	45with	100	**95**	**(n=100)**
%Correct	90.9	100			
%Omission	9.1	0			**kappa=0.9**
Suburb area					
No-change	**49**	1	50	98	2
Change	7	**43**	50	86	14
Total	56	44	100	**92**	**(n=100)**
%Correct	87.5	97.7			
%Omission	12.5	2.3			**Kappa=0.84**
Rural area					
No-change	**39**	11	50	78	
Change	2	**48**	50	96	
Total	41	59		**87**	**(n=100)**
%Correct	95.1	81.4			
%Omission	4.9	18.6			**kappa=0.74**
All 3 areas					
No-change	**138**	12	150	92	
Change	14	**136**	150	90.7	
Total	152	148		**91.3**	**(n=300)**
%Correct	90.8	91.9			
%Omission	9.2	8.1			**Kappa=0.83**

4. Discussion

4.1 High commission error for detecting urban change pixels in model validation

This study has explored the potential of using machine learning-based classification model in achieving near real-time urban change identification. ANN outperformed random forest in terms of accuracy and calculation speed. The validation result showed a satisfying omission error rate of approximately 17% in detecting urban change pixels, although the commission error was unacceptably high, at a rate of 64%. This high commission error rate might not be representative of our model's ability in correctly detecting urban change pixels because it is heavily biased due to the extreme imbalanced ratio between the number of no-change pixels and that of change pixels in the testing dataset. Based on NLCD, there are 36,669,258 no-change pixels in the testing dataset while the number for urban change pixel is only 15,291. We know that NLCD could not be 100% correct, and suppose only 0.1% of no-change pixels determined by NLCD are wrong, then there would be 36,669 pixels that are wrongly labeled as no-change pixels. The number of wrongly-labeled pixels is two times larger than that of urban change pixels, thus causing a huge increase in commission error.

4.2 Generalization capability of the model

The near real-time urban change identification method proposed in this study detects urban change by identifying the corresponding abrupt NDVI decrease using ANN-based classification models. This method works well in urban setting environment because almost all the abrupt NDVI decreases were related to urbanization and urban intensification. However, its accuracy is inferior working in rural areas where forest harvest could be misinterpreted as urban change event. In this study, the lack of high-resolution imagery for rural area limited our ability to distinguish urban change from forest harvest, thus the accuracy assessment conducted in this area could not be trusted. In future works, more reliable data (such as ground survey data) from this

area should be gathered for a more robust accuracy assessment.

Even if we currently do not have a trustworthy accuracy assessment result for this rural area, I would still suspect that the method proposed in this study doesn't perform well in rural areas. The data inputs for training the classification model only involve NDVI values, thus it is impossible for the current model to distinguish urban change events from forest harvest events. In this study, the sampling rural area is far away from existing urban areas, and detailed observations found out that the clear cut patch sizes are mostly very large. Therefore, it is highly possible that these clear cut events are mostly related to forest harvest, which means the accuracy assessment result for this sampling rural area is an overestimation of the true capacity of our model in detecting urban change pixels.

To improve the performance of our model in rural areas, future research works should seek for adding more data inputs for classification model training so that urban change could be separated from forest harvest. Distance from existing urban area, elevation, slope, and change patch size could be the potential candidates.

5. Conclusion

Machine learning-based classification models using annual maximum NDVI time series values as data inputs were tested and compared to deal with near real-time urban change detection problem. ANN outperformed random forest classifier in terms of both accuracy and calculation speed. Accuracy assessments were conducted by using high resolution imagery archives from Google Earth. To assess the model's ability in different land cover settings, accuracy

assessments were conducted in three different areas, including urban core, suburb area, and rural area. The results found out that our model worked quite well in urban core and suburb areas, with an overall accuracy of 95% and 92%, respectively. As for in rural area, the accuracy assessment result is not reliable due to the lack of high-resolution imagery in this region. Although the overall accuracy for this area is 87%, it's not trustworthy because of our model's inability to distinguish urban change from forest harvest, both of which starts with clear cut. Future work should seek for adding for data inputs, such as distance from existing urban, elevation and slope, to strengthen our model's ability in distinguishing urban change pixels from forest harvest in rural areas.

References:

Angel, S., Sheppard, S., Civco, D.L., Buckley, R., Chabaeva, A., Gitlin, L., Kraley, A., Parent, J., Perlin, M., 2005. The dynamics of global urban expansion. Citeseer.

Breiman, L., 2001. Statistical modeling: The two cultures (with comments and a rejoinder by the author). Statistical science 16, 199–231.

Chen, J., Gong, P., He, C., Pu, R., Shi, P., 2003. Land-use/land-cover change detection using improved change-vector analysis, *Photogrammetric Engineering & Remote Sensing*, 69: 369–379.

Dye, C., 2008. Health and urban living. Science 319, 766–769.

Feng, Q., Liu, J., Gong, J., 2015. UAV remote sensing for urban vegetation mapping using random forest and texture analysis. Remote sensing 7, 1074–1094.

Harts, J., Maat, K., Ottens, H., 2003. An urbanisation monitoring system for strategic planning, in: Planning Support Systems in Practice. Springer, pp. 315–329.

Holben, B.N., 1986. Characteristics of maximum-value composite images from temporal AVHRR data, *International Journal of Remote Sensing*, 7: 1417–1434.

Homer, C., Dewitz, J., Yang, L., Jin, S., Danielson, P., Xian, G., Coulston, J., Herold, N., Wickham, J., Megown, K., 2015. Completion of the 2011 National Land Cover Database for the conterminous United States–representing a decade of land cover change information. Photogrammetric Engineering & Remote Sensing 81, 345–354.

Homer, C., Dewitz, J., Yang, L., Jin, S., Danielson, P., Xian, G., Coulston, J., Herold, N., Wickham, J., Megown, K., 2015. Completion of the 2011 National Land Cover Database for the conterminous United States–representing a decade of land cover change information. Photogrammetric Engineering & Remote Sensing 81, 345–354.

Homdee, T., Pongput, K., Kanae, S., 2011. Impacts of land cover changes on hydrologic responses: a case study of Chi River Basin, Thailand. Journal of Japan Society of Civil Engineers, Ser. B1 (Hydraulic Engineering) 67, I_31–I_36.

Jensen, J.R., 1981. Urban change detection mapping using Landsat digital data. The American Cartographer 8, 127–147.

Kammen, D.M., Sunter, D.A., 2016. City-integrated renewable energy for urban sustainability. Science 352, 922–928.

Lawrence, P.J., Feddema, J.J., Bonan, G.B., Meehl, G.A., O'Neill, B.C., Oleson, K.W., Levis, S., Lawrence, D.M., Kluzek, E., Lindsay, K., 2012. Simulating the biogeochemical and biogeophysical impacts of transient land cover change and wood harvest in the Community Climate System Model (CCSM4) from 1850 to 2100. Journal of Climate 25, 3071–3095.

Liu, X., Lathrop Jr, R.G., 2002. Urban change detection based on an artificial neural network.

International Journal of Remote Sensing 23, 2513–2518.

Liu, Y., Wang, Q., Bi, J., Zhang, M., Xing, Q., Shi, P., 2010. The analysis of NDVI trends in the coastal zone based on Mann-Kendall test: a case in the Jiaodong Peninsula. Acta Oceanologica Sinica 32, 79–87.

Mahmood, R., Pielke Sr, R.A., Hubbard, K.G., Niyogi, D., Bonan, G., Lawrence, P., McNider, R., McAlpine, C., Etter, A., Gameda, S., 2010. Impacts of land use/land cover change on climate and future research priorities. Bulletin of the American Meteorological Society 91, 37–46.

Martínez, M.L., Pérez-Maqueo, O., Vázquez, G., Castillo-Campos, G., García-Franco, J., Mehltreter, K., Equihua, M., Landgrave, R., 2009. Effects of land use change on biodiversity and ecosystem services in tropical montane cloud forests of Mexico. Forest Ecology and management 258, 1856–1863.

Schneider, A., Friedl, M.A., Potere, D., 2009. A new map of global urban extent from MODIS satellite data. Environmental research letters 4, 044003.

Seto, K.C., Fragkias, M., Güneralp, B., Reilly, M.K., 2011. A meta-analysis of global urban land expansion. PloS one 6.

Sexton, J.O., Song, X.-P., Huang, C., Channan, S., Baker, M.E., Townshend, J.R., 2013. Urban growth of the Washington, DC–Baltimore, MD metropolitan region from 1984 to 2010 by annual, Landsat-based estimates of impervious cover. Remote Sensing of Environment 129, 42–53.

Thapa, R.B., Murayama, Y., 2009. Urban mapping, accuracy, & image classification: A comparison of multiple approaches in Tsukuba City, Japan. Applied geography 29, 135–144.

Trianni, G., Lisini, G., Angiuli, E., Moreno, E.A., Dondi, P., Gaggia, A., Gamba, P., 2015. Scaling up to national/regional urban extent mapping using Landsat data. IEEE Journal of Selected Topics in Applied Earth Observations and Remote Sensing 8, 3710–3719.

Wan, H., Shao, Y., Campbell, J.B., Deng, X., 2019. Mapping Annual Urban Change Using Time Series Landsat and NLCD. Photogrammetric Engineering & Remote Sensing 85, 715–724.

Wickham, J.D., Stehman, S.V., Fry, J.A., Smith, J.H., Homer, C.G., 2010. Thematic accuracy of the NLCD 2001 land cover for the conterminous United States, *Remote Sensing of Environment*, 114: 1286–1296.

Wilson, C., Weng, Q., 2010. Assessing surface water quality and its relation with urban land cover changes in the Lake Calumet Area, Greater Chicago. Environmental Management 45, 1096–1111.

Winz, I., Brierley, G., Trowsdale, S., 2009. The use of system dynamics simulation in water resources management, *Water resources management*, 23: 1301–1323.

Woodcock, C.E., Allen, R., Anderson, M., Belward, A., Bindschadler, R., Cohen, W., Gao, F., Goward, S.N., Helder, D., Helmer, E., 2008. Free access to Landsat imagery, *Science*, 320: 1011–1011.

Wu, S., Mickley, L.J., Kaplan, J.O., Jacob, D.J., 2012. Impacts of changes in land use and land cover on atmospheric chemistry and air quality over the 21st century. Atmospheric Chemistry and Physics.

Xian, G., Crane, M., 2005. Assessments of urban growth in the Tampa Bay watershed using remote sensing data. Remote sensing of environment 97, 203–215.

Chapter 4. Assessing urbanization's impacts on evapotranspiration

4.1 INTRODUCTION

In chapter 4, we generated spatially-explicit annual ET data for Virginia Beach using daily ET data derived from Landsat imagery and METRIC (Mapping evapotranspiration at high resolution with internalized calibration) model, and then assessed evapotranspiration changes under different land use land cover change scenarios. The drivers of evapotranspiration are also explored.

4.2 MANUSCRIPT

Wan, H., McLaughlin, D.L., Shao, Y., Eerden, B.V., Raganathan, S., Deng, X., 2020. Remotely-sensed evapotranspiration for informed urban forest management. Under review at *Journal of Environmental Management*.

The manuscript for this chapter has been submitted to *Journal of Environmental Management* for review on April 24th, 2020. The manuscript is shown below:

Remotely-sensed Evapotranspiration for Informed Urban Forest Management

Heng Wan[a], Daniel McLaughlin[b], Yang Shao[a], Brian van Eerden[c], Shyam Ranganathan[d], Xinwei Deng[d]

[a] Virginia Tech, Department of Geography, 238 Wallace Hall, Blacksburg, VA 24061, USA

[b]Virginia Tech, Department of Forest Resources and Environmental Conservation, 313 Cheatham Hall, Blacksburg, VA 24061, USA

[c]Virginia Pinelands Program, The Nature Conservancy

[d] Virginia Tech, Department of Statistics, 211 Hutcheson Hall, Blacksburg, VA 24061, USA

*Corresponding Author (e-mail: mclaugd@vt.edu; Tel: 540-231-6616)

Abstract

Evapotranspiration (ET) is a major terrestrial water loss, particularly from forested systems. As such, forest patches within urban landscapes can play an important role in stormwater flood reduction and urban heat island mitigation. Effective incorporation of urban forests into stormwater planning and green infrastructure design thus requires methods that can quantify ET across large, mixed-land use landscapes but with sufficient spatial resolution for parcel-specific rates. Here, we take advantage of Landsat-derived ET observations (via the METRIC model) to estimate ET rates at a 30-m resolution across the City of Virginia Beach, USA, a large (640 km^2) mixed land-use landscape with increasing flood concerns. Our objectives were to compare ET rates across land cover types, with particular attention to forest covers, and then identify land cover attributes and models to explain spatial ET variation. Both upland and wetland forest covers had higher ET compared to urban areas, where wetland forest, the dominant forest in our

study area, had annual ET rates 3-4 times that of urban and contributed ca. 40% of the total landscape ET despite covering only 20% of the area. Urban areas had the lowest mean annual ET among all land classes indicating the consequences of urbanization, which we verified when parsing ET data between time periods in the context of newly urbanized locations. Relationships between ET rates and aggregated, higher resolution land attribute data indicated key drivers, where annual ET increased with canopy cover and decreased with impervious cover and depth to water table. A regression model combining these drivers explained approximately 70% of the total annual ET variation, providing potential means to downscale ET estimates. Our study highlights the disproportional role forests play in ET-associated functions (runoff reduction, urban heat island mitigation) in urban landscapes and provides an approach to guide local and landscape decisions regarding urban forest conservation and management.
Keywords: flood reduction, green infrastructure, forest conservation

1.0 INTRODUCTION

Evapotranspiration (ET) is an important component in the hydrologic cycle and represents a major water loss in the landscape (Irmak and Haman, 2003; Rothfuss et al., 2010). Regional ET differences are largely driven by climate variables such as temperature and humidity (e.g., potential evapotranspiration; PET) (Adnan et al., 2017; Teuling et al., 2009). However, local ET can vary widely based on land cover, vegetation types, and available water (e.g., soil moisture and depth to water table) (Copper et al., 2006; Zhang et al., 2001). Generally, ET in urban settings is much lower compared to forest landscapes (Taha, 1997; Liu et al., 2010), whereas annual forest ET can be as much as 60-90% of incoming precipitation (McLaughlin et al., 2013). Relatively lower ET rates in urbanized areas can result in a higher probability of stormwater

flooding (De Roo et al., 2003; Berland et al., 2017; Kuehler et al., 2017) and also contribute to urban heat island effects by reducing latent heat exchange (Qiu et al., 2013).

Numerous studies document the roles of green infrastructure (e.g., green roofs, vegetated swales) in flood reduction and mitigation of urban overheating (Block et al., 2012; Emmanuel and Loconsole, 2015; Lennon et al., 2014; Liu et al., 2014). Until recently, however, green infrastructure practices have mainly focused on infiltration-based technologies (e.g., rain garden, permeable pavements) and "street" tree planting and conservation. Larger, urban forest patches can be a common feature embedded within otherwise mostly urban areas (Nowak et al., 2001), and thus deserve more attention as a green component due to their potentially higher water storage capacity (e.g., via canopy interception and soil infiltration) and subsequent water losses via ET (Berland et al., 2017). While some research has focused on interception and infiltration within urban forests, less attention has focused on water removal through ET (Kuehler et al., 2017). Within urban forests, ET rates can vary substantially, depending on soil type, depth to water table, and vegetation characteristics (El Maayar and Chen, 2006). Yet, few studies have quantified ET rates at land-parcel scales (e.g., 1 hectare; Berland et. al., 2017), a spatial scale necessary to inform urban planning decisions and green infrastructure design.

Methods for parcel-scale ET measurement (e.g., eddy covariance towers, sap flow sensors, and lysimeter system) are costly and limited in spatial representation (Drexler et al., 2004; Glenn et. al., 2011). For example, eddy covariance methods are considered as the leading approach for accurate ET estimation but can cost over $50,000 and only provide data over ca. 1-2 km^2 (Baldocchi et al., 1996), thus limiting application across large, mixed land-use landscapes. In

contrast, remotely sensed-based approaches have been increasingly used to estimate ET at high spatial resolution while also over large spatial extents (Courault et al., 2005; Gowda et al. 2007; Gonzalez-Dugo and Neale, 2009). For example, using Landsat imagery data as main input, the Mapping Evapotranspiration at high Resolution with Internalized Calibration (METRIC) model (Allen et al., 2011) has been widely implemented for local and regional applications (Allen et al., 2007; French et al., 2015; Trezza et al., 2013). Currently, 30-m resolution ET map products can be readily accessed from METRIC-EEFLUX at Google Earth Engine, and together with detailed land cover data may provide insights into ET differences between urban forests and other land covers and thus potential consequences of various land change scenarios.

For urban and suburban environments, vegetation surfaces are spatially dispersed and often mixed with other land covers (e.g., impervious surface) when they are observed at 30-m spatial resolution (Wu and Murray et al., 2003; Shao et al., 2015). ET values (30-m pixels) derived from Landsat data thus intrinsically represent mixed signals from sub-pixel land cover components. Statistical modeling of ET using sub-pixel land cover composition can improve our understanding of ET drivers in urban settings and potentially enable downscaling of ET estimates. Previous ET regression models have been largely based on either several site-specific locations or aggregated analytical units (e.g., watershed scale and regional scale) (Kişi, Ö., 2006; Kişi, Ö., 2011; Lu et. al., 2003; Sanford and Selnick, 2013). Until recently, however, ET statistical modeling with sub-pixel land cover data has been rare, mainly due to the availability of very high resolution land cover data.

Here, we use Landsat-derived, 30-m ET data to compare annual ET rates among land cover types

in Virginia Beach, USA. Using higher-resolution land use, topographic, and groundwater data, we also explore potential drivers and associated predictive models of annual ET rates. We focus on Virginia Beach because the area has growing concerns related to stormwater flooding and increasing efforts to incorporate a portfolio of solutions, including green infrastructure, for flood reduction. Understanding ET differences and associated drivers among land cover types will help such efforts in Virginia Beach and is broadly relevant to green infrastructure design and forest conservation in other urban landscapes.

2.0 METHODS

2.1 Study Area

The City of Virginia Beach encompasses ca. 640 km^2, with a population of 450,189 as of 2018 and with an estimated 2.8% increase in population since 2010 (U.S. Census Bureau). According to the National Land Cover Database 2011, Virginia Beach land cover types include (Figure 1): urban ("developed") (39.3%), forested ("woody") and herbaceous wetlands (28.3%), water bodies (12%), agricultural (14.1%), upland forests and shrubs (4.8%), and minimal amounts of other covers (e.g., grasslands & barren land). By comparing NCLD2001 and NLCD2011 datasets, the newly urbanized area in this decadal time period was approximately 13 km^2, with a slow annual urbanization rate (< 1%). Soils in the study area are dominated by silt loam or loam (50% of the area), with smaller extents of sandy clay loam (35%) (NRCS SSURGO Database). The landscape is relatively flat, with a mean slope of 2.4%. The climate is considered humid subtropical, with annual precipitation of 1143 mm and annual potential evapotranspiration (PET) of 838 mm (for nearby Norfolk; Univ. of Virginia Climatology Office).

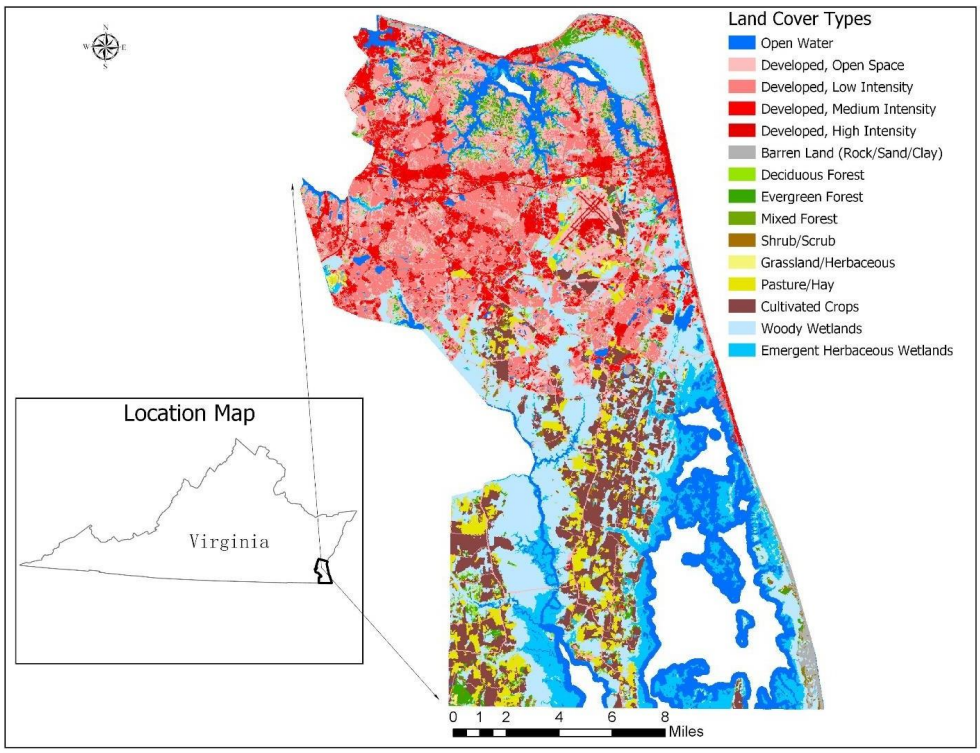

Figure 1. Study area along with land use/land cover data from National Land Cover Database 2011.

2.2 Data Processing

2.2.1 Pre-processing METRIC-derived Daily ET Rates

To estimate ET across our study area required remotely sensed data that cover the required spatial scale as well as include enough observations over time to determine annual ET rates while accounting for seasonal variability. To do so, we used the METRIC model developed at the University of Idaho. This model is based on the previous Surface Energy Balance Algorithms for Land (SEBAL) model and is a mature, operational surface energy balance model capable of producing reliable ET estimation with high resolution for large spatial scales (Allen et al., 2011; Foolad et al., 2018). The model utilizes Landsat satellite thermal

data and ground-based weather data (for calibration) to estimate daily ET (mm) at a 30-m resolution for each satellite fly-over date (16-day frequency); see example of daily ET observations in Figure 2, indicating lower ET values in northern, more urban locations (Figure 1). We used the Earth Engine Evapotranspiration Flux (EEFLUX) tool, which estimates and calibrates these 30-m ET data using the METRIC model and Landsat imagery archived on Google Earth Engine Platform (Allen et al., 2015).

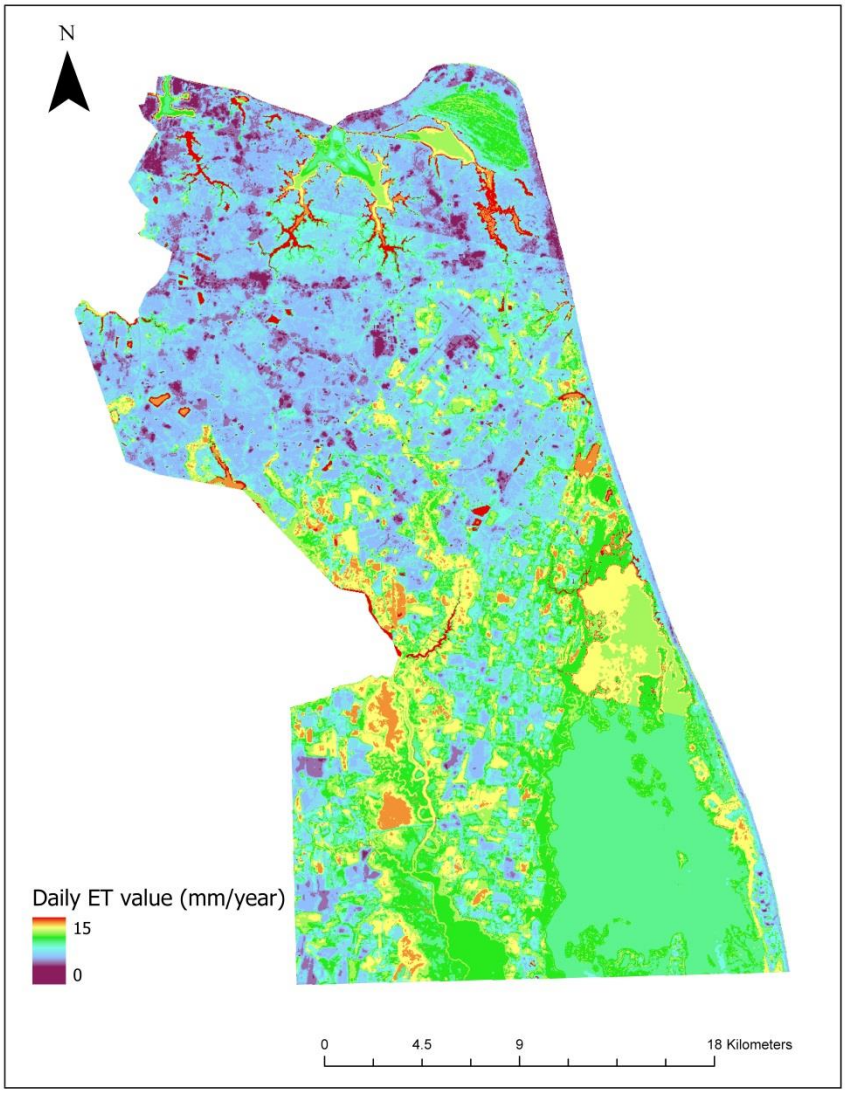

Figure2. Example of METRIC-derived daily ET from Landsat flyover on March 14th, 2013, obtained from EEFLUX.

Daily ET data for 30-m pixels between 2000 and 2018 were downloaded from EEFLUX website (https://eeflux-level1.appspot.com/). Our study area encompasses two Landsat scenes, thus daily ET data for each scene were downloaded separately and then merged into one integrated dataset. These daily ET data were then manually checked to exclude scenes with a total cloud coverage over 30%, as reported in the EEFLUX output data. For the remaining scenes (n=301), we downloaded the corresponding original Landsat scenes (Landsat Level 1 collection products, including 5, 7, and 8 imagery) from Earth Explorer (https://earthexplorer.usgs.gov/). Then, these Landsat imagery data were processed by Fmask 4.0, a software capable of recognizing clouds and shadows, to generate cloud masks (Qiu et al., 2019). The daily ET data and their corresponding cloud mask were integrated to exclude cloud-contaminated pixels, providing a time series of cloud-free daily ET data for each 30-m pixel.

2.2.2 Statistical Processing to Derive Annual ET rates

Before deriving annual ET rates, cloud-free daily ET data were further processed to exclude outliers and decrease uncertainty in two steps. First, outliers were corrected by truncation using the long-term temporal distributions for each pixel, with the reasonable daily ET value range for each pixel defined based on the interquartile range rule:

$$Q_1 - 1.5*IQR \leq \text{daily ET} \leq Q_3 + 1.5*IQR \quad [1]$$

where Q_1 was the first quartile, IQR was the interquartile range, and Q_3 was the third quartile for the targeting pixel. All the daily ET values beyond this reasonable range were regarded as outliers, which were reclassified as the corresponding upper/lower limit value. Second, to reduce uncertainty for pixels with limited or highly variable observations in a specific month, processed

data were further corrected by borrowing strength from other pixels from the same land cover and month using Bayesian Posterior Processing (see S1).

With corrected daily ET rates, we determined average daily ET for each pixel and month using data between 2000 and 2018; these month-specific daily means were then converted to average annual rates (mm/year) for each pixel using number of days in each month. Annual means were compared among five major land cover types, as well as subcategories within urban and forested categories. We note that removing cloudy days and pixels was a necessary and commonly applied step (due to increased uncertainty under such conditions; Chen and Yang, 2012; Hwang and Choi, 2013) but that this results in a consistent bias to high (cloud-free) ET days. As such, derived annual estimates are likely overestimated; however, relative comparisons among land cover types should not be affected since this bias is equally applied across all pixels and land cover types.

2.3 Exploring Potential ET changes Due to Land Use Change

The data range used here (2000-2018) was chosen to maximize data availability. For pixels experiencing land use (and associated ET) changes over this period, average annual ET rates from the full data range may not reflect current conditions. However, a comparison of NLCD 2001 and NLCD 2011 datasets demonstrated a slow annual urban growth rate (< 1%), suggesting that generating the annual ET layer based on ET data from 2000 to 2018 is reasonable. However, we did compare average annual ET separately for the 2000-2010 and 2010-2018 periods to explore potential changes in ET due to land use change over time. To do so, we identified two groups of pixels: ones that changed from a non-urban cover to an urban cover (i.e., newly urbanized) and those that did not experience land use change between the

evaluated time periods. Differences in annual ET between the two time periods were then compared between the two groups using the non-parametric Mann-Whitney-Wilcoxon Test.

2.4 Drivers and Models of Annual ET

To explain ET differences among pixels, we obtained land attribute data for expected drivers, including impervious cover, canopy cover, and depth to water table. These data are available at higher resolution than the ET data, allowing us to understand aggregate controls on 30-m ET observations. For impervious cover and canopy cover, we used 0.5-m resolution land cover data acquired from the Tree Canopy Assessment for Virginia Beach (O'Neil-Dunne, 2019). In addition to higher resolution, these data are also independent observations from Landsat imagery (used for NCLD datasets) from which our derived ET were based. For depth to water table, we combined LiDAR-derived bare earth digital elevation model (DEM) (3-m spatial resolution) from Virginia Information Technologies Agency (VITA; https://www.vita.virginia.gov/integrated-services/vgin-geospatial-services/elevation---lidar/) and USGS groundwater well observations (https://waterdata.usgs.gov/va/nwis/gw) to construct a interpolated 3-m raster set. To do so, we used 10 USGS wells, which had overlapping (sub-daily) data from 2012 to 2016, and calculated mean annual water table depth for each well. Using ground elevation of each well (from the LiDAR DEM), we then converted the mean water table depth at each well to water level elevation; these mean water level elevations were then spatially interpolated among well locations using inverse distance weighted interpolation to produce a continuous groundwater level layer for the entire study domain. With this layer and the DEM, we then calculated depth to water table for each 3-m pixel. Data for impervious and canopy covers (0.5-m resolution) and depth to water table (3-m) were then resampled to 30-m resolution data,

concordant with ET data.

For each dataset, we conducted regression analysis using all pixels (n=713,754), with annual ET (for the full data record, 2000-2018) as our response variable. We report the significance and goodness-of-fit (R^2) for these relationships using all ET pixels but also illustrate the general trend in pairwise plots using a subset of 200 pixels, which were randomly sampled and equally (n=50) from each of four major land use categories: urban, upland forest, wetland forest, and agriculture. We also conducted multiple regression to develop a predictive model of ET using all three expected drivers. To address potential nonlinearity, we explored several functional forms for both separate and multiple regression models, including quadratic polynomial and linear regressions applied with different transformation methods.

3.0 RESULTS

3.1 Annual ET Comparison among Land Covers

Figure 3 illustrates the distribution of annual ET values from all pixels and categorized by major land cover types. Differences among land cover types are distinct, with wetland forest having the highest annual ET while urban has the lowest.

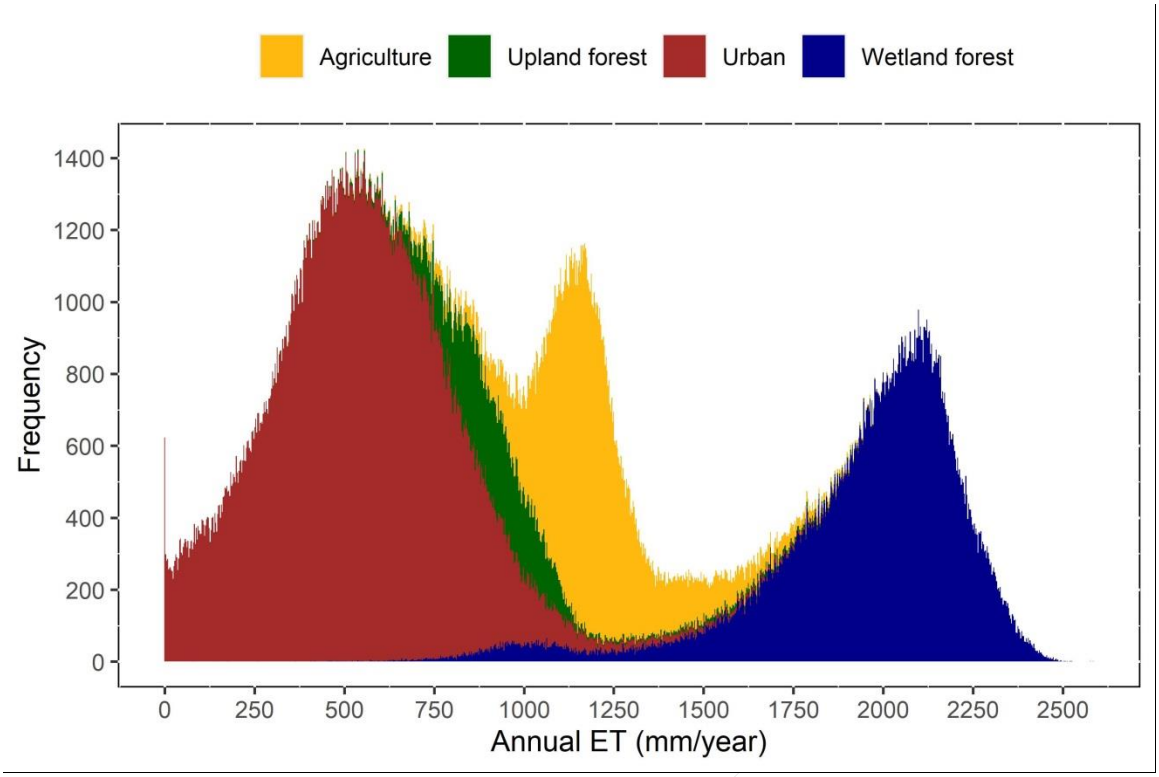

Figure 3. Frequency distribution of annual ET values from all pixels categorized by major land use/cover.

Urban land uses have the lowest average annual ET rates and thus contribute only 23% of the total landscape ET, despite disproportionally higher amounts of area coverage (45%) (Table 1). Mean upland forest annual ET is almost twice that of urban, but with its very low coverage (5.5%) contributes the least to the total cumulative ET (4.7%). Among all the land cover types, forested wetlands have the highest mean annual ET value (ca. 3.5 times that of urban covers) and contribute the highest amount to cumulative landscape ET. We critically note that this contribution (42%) by wetland forests is disproportionally higher (almost by a factor of 2) than their area coverage (23%). Herbaceous wetlands also have high mean annual ET and contribute 13.4% of the total cumulative ET. Agriculture has intermediate ET values relative

to the other land uses and contributes 17.7% of the total cumulative ET, a percentage similar to its area proportion.

Table 1. Percent of land area and mean, cumulative, and percent contributions of ET for major land use/cover types, where the percentages of land area and contributions are relative to the total landscape values. Grassland and barren land are excluded from the table due to their small area percentage (0.4% and 1%, respectively).

	Urban	Agriculture	Upland Forest	Forested Wetland	Herbaceous Wetland
Area (%)	45.42	16.42	5.48	23.46	9.22
Evapotranspiration					
Mean (mm)	546	1189	937	1945	1583
Cumulative (m^3)	1.74×10^8	1.36×10^8	3.62×10^7	3.20×10^8	1.03×10^8
Contribution (%)	22.62	17.68	4.71	41.60	13.39

A forest-specific analysis demonstrates that all forest types other than forested wetlands have similar mean ET rates (920-961 mm; Table 2). Forested wetlands constitute 81% of the total forested area but contribute ca. 90% of the cumulative ET provided by all forest cover types. For urban subcategories, the range of mean annual ET rates was large (195 to 740 mm), with higher values in open space and low-intensity urban as expected due to lower impervious cover (Table 3).

Table 2. Percent land area and mean, cumulative, and percent contributions for ET, soil water storage, and depressional storage of each forest sub-types, where the percentages of land area and contributions are relative to the total forest cover.

	Deciduous Forest	Evergreen Forest	Mixed Forest	Shrub/ scrub	Forested Wetland
Area (%)	5.29	7.87	1.57	4.27	81.01
Evapotranspiration					
Mean (mm)	949	920	961	948	1945
Cumulative (m^3)	1.02×10^7	1.47×10^7	3.07×10^6	8.22×10^6	3.20×10^8
Contribution (%)	2.86	4.13	0.86	2.31	89.84

Table 3. Percent land area and mean, cumulative, and percent contributions for ET, soil water storage, and depressional storage of each urban sub-types, where the percentages of land area and contributions are relative to the total urban cover.

	Developed, Open Space	Developed, Low-Intensity	Developed, Medium-Intensity	Developed, High-Intensity
Area (%)	34.55	41.66	18.76	5.03
Evapotranspiration				
Mean (mm)	740	523	332	195
Cumulative (m^3)	8.15×10^7	6.95×10^7	1.98×10^7	3.12×10^6
Contribution (%)	46.86	39.96	11.38	1.80

3.2 Changes in Annual ET from Land Use Change

We also generated two different mean annual rates (one for 2000 to 2009 and one for 2010 to 2018) to assess changes between these two time periods. Figure 4A illustrates the pixel-specific differences between these two periods (2010-2018 minus 2000-2009), where positive values indicate ET increases. The change is relatively small across the study area, which is concordant with the documented small change in land use during these two periods.

However, there are some evident areas, albeit limited in spatial extent, with ET decreases (blue colors in Figure 4A) likely reflecting conversion to urban cover. Indeed, ET changes for newly-urbanized pixels were significantly higher (and importantly negative) compared to the no-change pixel group (Figure 4B). That is, urbanization generally resulted in lower ET values, explaining such locations in Figure 4A, whereas the no-change pixels exhibited ET changes centered around zero. There were also some locations with ET increases between these two time periods, but to a lesser magnitude than the observed ET declines; such locations primarily represent wetland and agriculture areas, suggestive of changes in weather variables or water availability that warrants further investigation.

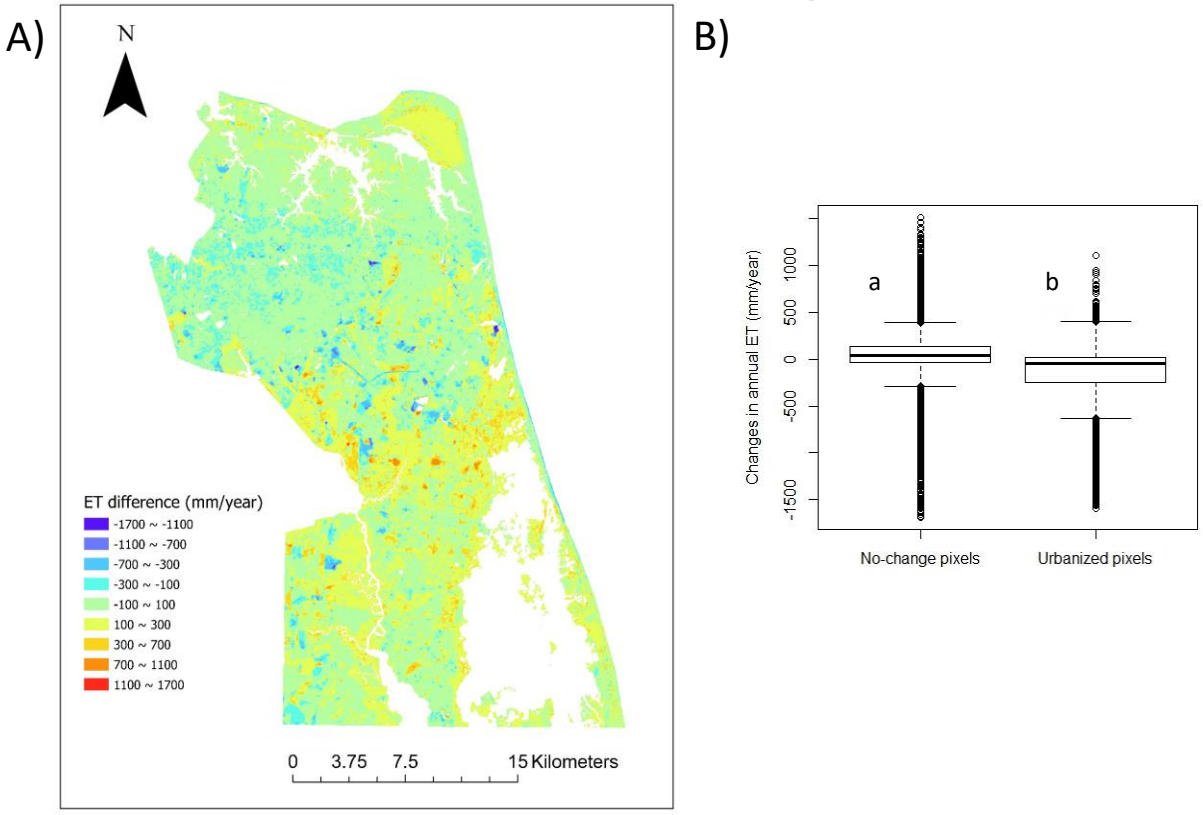

Figure 4. A) Change in mean annual ET between 2000-2009 and 2010-2018, where positive values indicate ET increases (warm colors) and negative values indicate decreases (coolcolors). B) Distribution of ET change values between 2000-2009 and 2010-2018 for

pixels with no-change in land use and pixels that were newly urbanized between these two time periods. Letters denote significant difference between pixel groups via Mann-Whitney-Wilcoxon Test.

3.3 Drivers and Models of Annual ET

Among tested regression models, quadratic polynomial regression performed best for each predictor variable. There was a strong and significant ($R^2 = 0.5$, $p < 0.001$) negative relationship between annual ET and impervious cover. Figure 5A illustrates this negative trend using a random subset of 200 pixels (50 for each major land use cover denoted with different colors), with a similar, albeit lower, R^2 (0.34) to that of the entire dataset. As expected, urban areas have a high impervious cover and associated low ET rates. Interestingly, the other three groups have similar (and very low) impervious covers but clearly different ET values; however, the separation by land cover is clear, again with wetland forest exhibiting the highest annual ET rates. Differences among these groups are likely due to other land cover attributes (canopy cover, depth to water table) that drive ET.

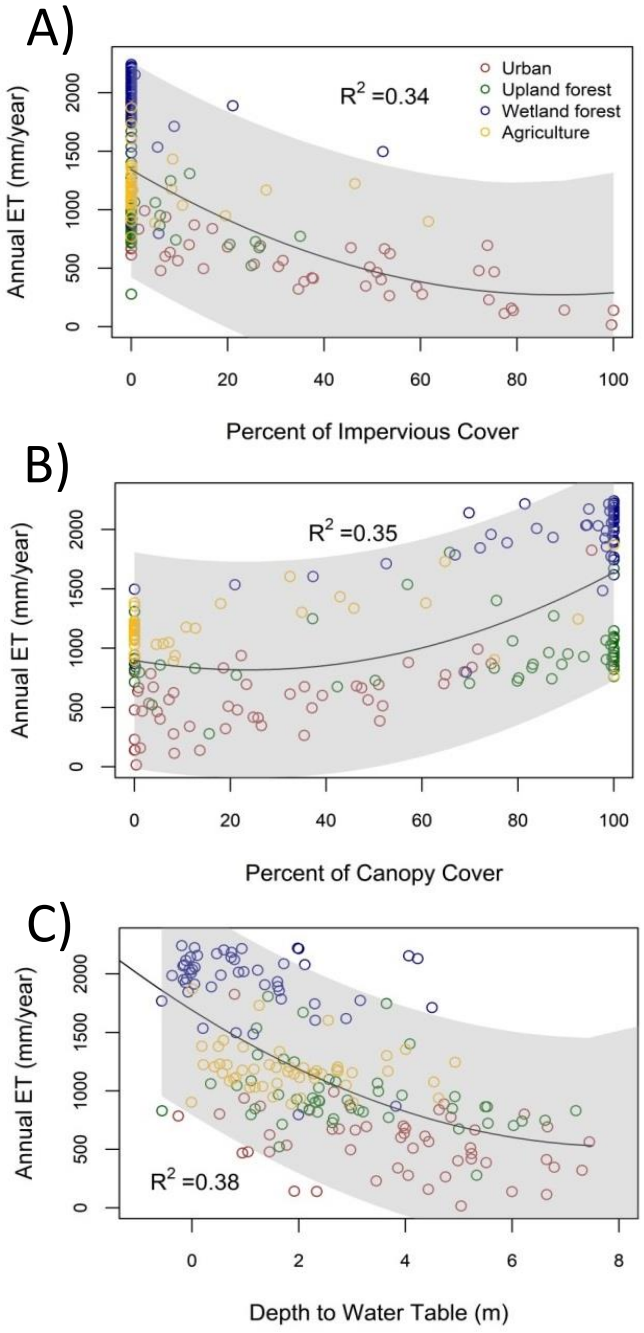

Figure 5. Mean annual ET versus A) percent impervious cover, B) percent canopy cover, and C) depth to water table for a subset of 200 randomly sampled pixels and equally from four major land uses (denoted by colors). Note that a negative depth to water table value represents standing water. Gray area represents 95% confidence interval.

There was a positive, significant relationship ($R^2 = 0.4$, $p < 0.001$) between mean annual ET and canopy cover percent, shown in Figure 5B with a subset of 200 pixels and an R^2 (0.35) similar to that of the entire dataset. Despite this general positive trend, land cover groups group together and clearly differ in ET even at similar canopy covers. Wetland forests have similar percent canopy cover compared to upland forests but much higher ET rates, likely due to shallow water tables and thus more water availability. Similarly, canopy cover percent is often similar between urban and agriculture pixels, but agriculture clearly has higher ET rates due to crop (not tree canopy) water use.

There was a negative and moderate ($R^2 = 0.38$, $p<0.001$) relationship between mean annual ET and depth to water table, suggesting that shallow water tables (small water table depth values) generally increase ET. The subset of 200 pixels illustrates this trend and with a same R^2 value (0.38; Figure 5C). Of the four major land covers, wetland forest generally has the smallest depths to water table (i.e., high water availability) and thus the highest ET values. However, there are some occurrences of upland forest and agriculture pixels with similar depth to water tables as wetland forest but with lower ET values; this is likely due to differences in canopy cover (see Figure 5B). Likewise, urban pixels span similar ranges of water table depths as other categories but have substantially lower ET rates due to impervious cover. Together, these results highlight the interacting influences of multiple attributes (impervious cover, canopy cover, and water availability) on ET rates.

The best-fit multiple regression model for ET using impervious cover, canopy cover, and depth to water table is shown in Table 4. The resulting model had an $R^2 = 0.71$, with all variables significant and similar degree of importance. Figure 6 illustrates this model with a subset of 100 pairs of predicted and observed values, with a similar R^2 value to that when using the entire pixel set.

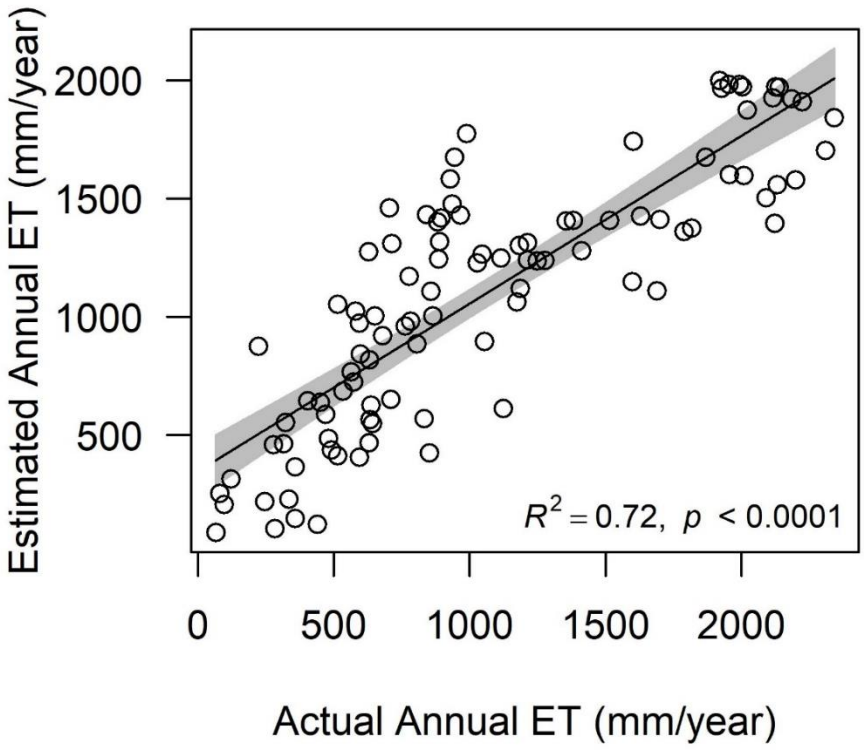

Figure 6. Modeled versus actual annual ET for a subset of 100 randomly selected pixels, where the modeled values were produced using the developed statistical model and data for impervious cover, canopy cover, and depth to water table.

Table 4. Summary of the quadratic polynomial regression model predicting mean annual ET with three predictor variables: impervious cover, canopy cover, and depth to water table. The Relative Importance metric represents the relative R^2 contribution among regressors following Lindemen et al. (1980).

Summary of Fit					
Multiple R Square	0.71				
Adjusted R Square	0.71				
Residual Standard Error	337.9				
Observations	713754				
Parameter Estimates					
Term	Estimate	Std Error	t-value	Prob > |t|	Relative Importance
Intercept	1368	0.81	1685.26	<0.0001	
Impervious cover percent	-13.44	0.056	-238.94	<0.0001	0.17
Impervious cover percent^2	0.068	0.00068	99.95	<0.0001	0.10
Water table depth	-119.5	0.27	-450.98	<0.0001	0.17
Water table depth^2	2.79	0.016	172.07	<0.0001	0.023
Canopy cover percent	-5.24	0.049	-107.28	<0.0001	0.10
Canopy cover percent^2	0.11	0.0005	223.07	<0.0001	0.14

4.0 DISCUSSION

Using remotely sensed daily ET rates over a ca. 20-year time period, we compared annual ET among land cover types in Virginia Beach, a large, mixed-land use urban landscape with growing stormwater flooding concerns. Such data enable ET estimation at both the spatial scales and resolution (30-m) necessary to inform urban planning and green infrastructure focused on ET-associated services, such as flood reduction and urban overheating mitigation. We found lower ET from urban covers and disproportional contributions from forest covers to total landscape ET, particularly from wetland forests (i.e., ca. 40% of total land ET despite 20% of land area). Integrating higher resolution land use data, we were able to explain drivers of ET

variation and develop predictive models for potential downscaling ET estimates. As such, our work both points to the value of urban forests in Virginia Beach as well as demonstrates an approach for similar application in other urban landscapes to inform incorporation of urban forests into green infrastructure design.

4.1 Remotely Sensed ET Data for Annual Estimates

Landsat-based ET data (via the METRIC model) provide daily estimates since 1985, at a frequency ca. 16 days, and over large extents (34,225 km^2 for each scene) with relatively high resolution (30-m) (Allen et al., 2015); however, there are several considerations for deriving annual rates. Specifically, we screened both cloudy scenes and cloud-contaminated pixels to remove associated errors in ET estimates. While this is typically conducted (Tsouni et al., 2008; Senay et al., 2016), it results in a systematic bias for high ET days since cloud cover decreases solar radiation and increases relative humidity, both of which result in lower daily ET rates (Zhang et. al., 2016). Indeed, some of our annual rates for wetland forests approached 2,500 mm/yr, representing extreme values (compared to PET = 800 – 900 mm/yr in the region). Observed ET rates can often exceed PET due to such phenomena as the clothesline and oasis effects (Drexler et al., 2004), where advection of dry, hot air from impervious covers stimulates ET in adjacent wet, vegetated land covers. Nonetheless, our annual rates likely remain overestimates by biasing our dataset to cloud-free days. Such bias can be reduced by constructing pixel-specific relationships between (cloud-free) daily ET observations and climate-based PET estimates, where developed relationships and daily PET are then subsequently used to estimate daily ET time series (e.g., Singh et al., 2012). However, given our objective, we decided against this approach, suggesting it may introduce additional uncertainty (Lepot et al.,

2017). That is, our objective was to compare ET rates among land covers in one landscape, and we contend that relative differences in ET (via annual estimates solely using cloud-free days) are maintained and informative in understanding ET drivers and differences among land covers. Where absolute annual ET estimates are the objective (e.g., for water budget calculations, hydrologic model inputs, and comparisons to other regions), developing ET-PET relationships for estimating complete daily ET time series is the more appropriate approach.

4.2 ET Differences Among and Within Land Cover Types

Relative differences in annual ET among land covers were evident, particularly when assessing the proportional contribution to total landscape ET from each land cover type (Table 1). As expected, urban rates had the lowest ET among all major land covers, consistent with other studies using remotely sensed estimates (Sun et al., 2004; Liu et al., 2010) as well as others using on-the-ground approaches (Liu et al., 2008). As a consequence, urban cover in Virginia Beach contributes only 23% of the total ET despite being the dominant land use (45% of area). To that end, we found significant ET decreases for newly urbanized pixels when parsing the ET dataset into two time periods (Fig. 4). Yet, there were also clear differences among urban sub-categories that highlight consequences of development intensity and continued changes thereof within urban areas. For example, ET values for open space and low intensity were 3.8 and 2.7 times higher compared to high intensity developed, respectively, and more comparable to (but less than) upland ET values (Tables 2 and 3). In Virginia Beach, and many other large mixed-land use localities, lower intensity urban areas can be dominant (approximately 35% of land area in Virginia Beach), suggesting their relative contribution to ET-associated functions and implications of continued development. These findings are supported by our regression analysis,

where impervious cover decreased ET (Fig. 5A), and are in accordance with other studies exploring ET drivers in urban settings (Grimmond and Oke, 1999; Haase, 2009; Liu et al., 2010). Upland and wetland forest covers exhibited much higher ET compared to urban areas, indicating the relative role of such forest patches in supporting ET-associated functions. In locations such as Virginia Beach and many others, growing stormwater flooding concerns are motivating both engineered and green infrastructure solutions (Soz et al., 2016). The importance of "street" trees in runoff reduction has been recognized (Stovin et al., 2008), but larger forest patches have received less attention as potential locations for flood mitigation services. Of particular note in our study area, wetland forests represent a major land cover (23% of the area) and are often adjacent to urban, flood-prone areas. We found that wetland forest covers have ET rates ca. 3.5 times that of urban, and thus disproportionately contribute to total landscape ET. Upland forests also exhibit higher rates than urban but lower than wetland forests, indicating important differences among forest cover types similar to those within the broad urban cover class. Regression analysis highlighted the influence of water table depth on ET (Fig. 5c), helping to explain higher ET in wetland forests where water availability increases ET rates. Canopy cover can also exert a strong control on forest ET rates (Fig. 5B), and accordingly many ET predictive models are largely based on such forest structural attributes, including basal area and leaf area index (Yan et al., 2012; McLaughlin et al., 2013). However, such efforts and targeted urban forest conservation may benefit from a better representation of the differences among forest types due to forest composition, structure, and water availability.

4.3 Tools to Guide Urban Forest Conservation

Our results enable estimates of ET change with forest loss scenarios and thus demonstrate the

value of forest conservation as an important green infrastructure strategy. As of 2020, approximately half of Virginia Beach forests are either protected (reported by the Virginia Department of Conservation and Recreation) or controlled by the City of Virginia Beach. For the remaining "unprotected" forests, replacing annual ET observations for those pixels with mean values for different urban subcategories yields annual ET losses of 11% - 32% compared to current total forest ET, the range of which depends on development intensity (data not shown). While this scenario assessment is not surprising, and is supported by empirical studies (e.g., Teuling et al., 2019; Owen et al., 1998), it helps to emphasize the importance of forest conservation. Going forward, pixel-specific ET observations and mean land cover rates can support such scenario analyses but at scales and particular settings relevant for specific land planning decisions.

Integrating ET observations with higher resolution land attribute data can further guide planning decisions at smaller spatial scales and potentially inform stormwater models and policies. Aggregating data for impervious and canopy covers (0.5 m resolution) and water table depth (3-m) resulted in a multiple regression model that explained 71% of the variation in 30-m annual ET estimates. While this model indicates the key, and expected, drivers of ET, it also can be used to potentially downscale ET estimates. Most predictive ET models either focus at larger, often watershed scales (Billah et al., 2015; Lu et al., 2003) or are more generalizable across regions (e.g., Isaac et al., 2004; Sun et al., 2008; Buttafuoco et al., 2010). Clearly, there are benefits to such tools, such as streamflow predictions and across-region assessments, but we contend that regional variation in relationships among ET, vegetation, and soil water availability suggests that site-specific models may be more appropriate when informing site-specific decisions. To that

end, our predictive model for the Virginia Beach area has the potential to use fine-scale land attribute data to inform such actions as stormwater credit programs, which often occurs at sub-30 m scales (Nowak, 2016). Given that such data are available for other regions, similar efforts could be applied, and comparing modeled parameters across regions may also provide insights to ET controls and their potential variability across regional climates, soils, and vegetation composition.

We largely focused on ET services in the context of flood reduction given the pressing stormwater concerns in Virginia Beach, yet urban forest ET supports additional functions. For example, urban forest patches have been shown to mitigate urban overheating, largely due to elevated ET and thus latent heat exchange (Hiemstra et al., 2017). As such, urban forests can serve as "cool spots", the extent to which can be indicated by relative ET estimates compared to other land covers. Further, ET, particularly in vegetated covers where transpiration dominates the flux, is directly linked to carbon uptake rates (Scott et al., 2006) thereby indicating potential carbon sequestration rates. Thus, our work and others (e.g., Nowak et al., 2001) focusing on urban forest ET has direct relevance to valuing multiple ecosystem services. Last, and not necessarily linked to ET, urban forests provide additional functions (e.g., habitat provision, recreation, water quality; Mörtberg, 2001; Arnberger, 2006; Livesley et al., 2016), and quantified ET rates can help add to the portfolio of urban forest services and thus guide urban forest conservation and management.

4.4 Limitations and Future Work

We note two limitations of our approach. First, we derived mean annual estimates using a long-

term data set (ca. 20 years, with 16-day frequency) to account for: i) natural interannual ET variation (e.g., from climate and water availability variation; Zha et al., 2010), ii) limited data for some years due to cloud-contamination (removal of approximately 53% of pixel observations), and iii) inherent uncertainty in individual observations (Kilic et al., 2016). To do so, however, required the assumption that minimal land cover change occurred over the data record, which is a reasonable assumption for our study area (i.e., less than 1% annual increase in urban area between 2001 and 2011). For other study sites, annual ET estimates may not reflect current conditions where dramatic land cover conversions have occurred in the study area. The limited data availability from METRIC for any particular year may also preclude analysis of land use or climate change-induced temporal differences in ET (Allen et al., 2007), but such could be assessed using larger timesteps (10 years in our case; Fig. 4).

Second, and important in the context of flood reduction services, our work estimated relative differences in annual ET among land uses but did not quantify the runoff reductions that may be realized. While runoff reduction is expected with higher ET (Rossi et al., 2016), specifically within urban forests, the degree to which annual ET estimates affect runoff reduction remains largely unknown, particularly at storm-event scales. In low-relief landscapes such as Virginia Beach, saturation excess runoff (i.e., shallow water tables limiting infiltration) can be the dominant form of runoff (Appels et al., 2016). As such, runoff potential for any given storm event is determined by antecedent water table and soil moisture levels (Hernandez et al., 2003), which are largely regulated by preceding ET water losses (Gerla, 1992). This supports the notion that higher ET will lead to runoff reduction and underscores a need to better parameterize commonly used stormwater models (e.g., Storm Water Management Model; SWMM) to

represent ET differences and drivers among land cover types. Indeed, most applications of SWIMM simulate time-varying ET using climate data and apply the same rate across the model domain, failing to represent land cover ET controls (but see Feng and Burian, 2016). To do so will require daily ET time series and thus ET-PET modeling as discussed above. Thus, our estimates of annual ET differences only point to that research need and the potential for forest runoff reduction services, but do not provide the requisite data for such stormwater modeling efforts.

Conclusions

In this work, we used remotely sensed ET data in a large, mixed-land use urban landscape (Virginia Beach, USA) and demonstrated large differences in annual ET values across land cover types. In particular, wetland forests, the dominant forest cover in our study area, have the highest ET rates among all land cover types (roughly 3.5 times that of urban) and contribute ca. 40% of the cumulative landscape ET but only ca. 20% of the land area. Upland forests also have higher ET values compared to urban areas but their estimated area coverage is low (ca 5%), likely due to past urbanization and land use change. While land use change, specifically urbanization, was relatively slow (annual rate <1%) over the ET data record used here (2000-2018), we found significant ET reductions in locations with conversion to urban land use categories. As such, our analysis demonstrates the role of forests in providing ET-related function such as stormwater flood reduction, a service of specific interest in our study area and other flood-prone urban settings. Observed ET differences among land covers can further be used in scenarios of land use change to inform and prioritize urban planning and forest conservation decisions. We also found significant relationships with expected attributes that drive ET and characterize different

land covers, where ET decreased with impervious cover and water table depth and increased with canopy cover. Statistical modeling using high-resolution data for all three attributes provides a potential approach to downscale ET estimates and thus further inform urban planning at smaller spatial scales, including such policies as stormwater crediting. To quantify potential runoff reduction driven by forest ET requires future work to derive daily ET time series and to better represent land cover differences in commonly used stormwater models. Our work may help to motivate such work in the future but hopefully, at hand, will guide urban forest conservation efforts as part of the increasing use of green infrastructure solutions for multiple ecosystem services.

Supplemental 1: Bayesian Posterior Processing

To reduce uncertainty for pixels with limited or highly variable observations in a specific month, processed data (outliers removed) were further corrected by borrowing strength from other pixels from the same land cover and month using Bayesian Posterior Processing. All pixels were first categorized into groups based on their land cover types and image-acquired months, leading to a total of 144 pixel groups (i.e., 12 land cover types and 12 months). Using the z-score for each pixel and month to maintain relative temporal variability, we then corrected pixel, month-specific daily means using information from other pixels in that pixel's group (land cover and month). To do so, the grand mean and grand standard deviation for each pixel group were calculated and then used to calculate the corrected month-specific mean for each pixel by using the Bayesian posterior mean formula:

$$CM = \frac{\frac{s_p^2}{n}}{\frac{s_p^2}{n}+s_g^2} * GM + \frac{s_g^2}{\frac{s_p^2}{n}+s_g^2} * M, \quad [1]$$

where *CM* is the corrected pixel month-mean of daily ET values, s_p is the pixel standard deviation of daily ET values within specific month, M is the pixel month-mean of daily ET values, *n* is the number of observations for each pixel within that month, *GM* is the pixel group grand mean of daily ET values, and S_g is the pixel group grand standard deviation of daily ET values.

Corrected month-specific daily means for each pixel are thus the weighted sum of the pixel month-means and the pixel group grand mean. When there are a large number of observations for any particular pixel and month, or if these observations are consistent (i.e., low standard deviation for that pixel and month), then the group grand mean has a smaller weight. If these two conditions are not met, it indicates low confidence in the pixel month-specific daily mean estimate and hence the need to borrow strength from other pixels from the same group (month and land cover).

The corrected daily ET values within a specific month are then calculated as:

$$ET_{corr} = CM + s_p * z, \quad [2]$$

where ET_{corr} is the corrected daily ET values for each pixel and month, CM is the corrected pixel month-specific mean of daily ET values, s_p is the pixel standard deviation, and z is the z-score value of daily ET values for each pixel and month. Note that, in this step, we assume that the standard deviation and the relative variability of each pixel over time is reasonably well estimated and hence do not attempt to correct for these values.

References

Adnan, S., Ullah, K., Khan, A.H., Gao, S., 2017. Meteorological impacts on evapotranspiration in different climatic zones of Pakistan. J. Arid Land 9, 938–952. https://doi.org/10.1007/s40333-017-0107-2.

Allen, R.G., Tasumi, M., Morse, A., Trezza, R., Wright, J.L., Bastiaanssen, W., Kramber, W., Lorite, I., Robison, C.W., 2007. Satellite-based energy balance for mapping evapotranspiration with internalized calibration (METRIC)—Applications. Journal of Irrigation and Drainage Engineering 133, 395–406.

Allen, R., Irmak, A., Trezza, R., Hendrickx, J.M., Bastiaanssen, W., Kjaersgaard, J., 2011. Satellite-based ET estimation in agriculture using SEBAL and METRIC. Hydrological Processes 25, 4011–4027.

Allen, R.G., Morton, C., Kamble, B., Kilic, A., Huntington, J., Thau, D., Gorelick, N., Erickson, T., Moore, R., Trezza, R., 2015. EEFlux: A Landsat-based evapotranspiration mapping tool on the Google Earth Engine, in: 2015 ASABE/IA Irrigation Symposium: Emerging Technologies for Sustainable Irrigation-A Tribute to the Career of Terry Howell, Sr. Conference Proceedings. American Society of Agricultural and Biological Engineers, pp. 1–11.

Appels, W.M., Bogaart, P.W., van der Zee, S.E., 2016. Surface runoff in flat terrain: How field topography and runoff generating processes control hydrological connectivity. Journal of Hydrology 534, 493–504.

Arnberger, A., 2006. Recreation use of urban forests: An inter-area comparison. Urban Forestry & Urban Greening 4, 135–144.

Baldocchi, D., Valentini, R., Running, S., Oechel, W., Dahlman, R., 1996. Strategies for

measuring and modelling carbon dioxide and water vapour fluxes over terrestrial ecosystems. Global Change Biology 2, 159–168.

Berland, A., Shiflett, S.A., Shuster, W.D., Garmestani, A.S., Goddard, H.C., Herrmann, D.L., Hopton, M.E., 2017. The role of trees in urban stormwater management. Landscape and Urban Planning 162, 167–177.

Billah, M.M., Goodall, J.L., Narayan, U., Reager, J.T., Lakshmi, V., Famiglietti, J.S., 2015. A methodology for evaluating evapotranspiration estimates at the watershed-scale using GRACE. Journal of Hydrology 523, 574–586.

Block, A.H., Livesley, S.J., Williams, N.S., 2012. Responding to the urban heat island: a review of the potential of green infrastructure. Victorian Centre for Climate Change adaptation Research, Melbourne.

Buttafuoco, G., Caloiero, T., Coscarelli, R., 2010. Spatial uncertainty assessment in modelling reference evapotranspiration at regional scale. Hydrology and Earth System Sciences 14, 2319.

Chen, H., Yang, D., 2012. Remote sensing based continuous estimation of regional evapotranspiration by improved SEBS model, in: Land Surface Remote Sensing. International Society for Optics and Photonics, p. 85240M.

Cooper, D.J., Sanderson, J.S., Stannard, D.I., Groeneveld, D.P., 2006. Effects of long-term water table drawdown on evapotranspiration and vegetation in an arid region phreatophyte community. Journal of Hydrology 325, 21–34. https://doi.org/10.1016/j.jhydrol.2005.09.035.

Courault, D., Seguin, B., Olioso, A., 2005. Review on estimation of evapotranspiration from remote sensing data: From empirical to numerical modeling approaches. Irrigation and

Drainage Systems 19, 223–249.

De Roo, A., Schmuck, G., Perdigao, V., Thielen, J., 2003. The influence of historic land use changes and future planned land use scenarios on floods in the Oder catchment. Physics and Chemistry of the Earth, Parts A/B/C 28, 1291–1300.

Drexler, J.Z., Snyder, R.L., Spano, D., Paw U, K.T., 2004. A review of models and micrometeorological methods used to estimate wetland evapotranspiration. Hydrological Processes 18, 2071–2101.

El Maayar, M., Chen, J.M., 2006. Spatial scaling of evapotranspiration as affected by heterogeneities in vegetation, topography, and soil texture. Remote Sensing of Environment 102, 33–51.

Emmanuel, R., Loconsole, A., 2015. Green infrastructure as an adaptation approach to tackling urban overheating in the Glasgow Clyde Valley Region, UK. Landscape and Urban Planning 138, 71–86.

Foolad, F., Blankenau, P., Kilic, A., Allen, R.G., Huntington, J.L., Erickson, T.A., Ozturk, D., Morton, C.G., Ortega, S., Ratcliffe, I., 2018. Comparison of the automatically calibrated google evapotranspiration application—EEFlux and the manually calibrated METRIC application.

Feng, Y., Burian, S., 2016. Improving evapotranspiration mechanisms in the U.S. Environmental Protection Agency's Storm Water Management Model. Journal of Hydrologic Engineering 12: 06016007.

French, A.N., Hunsaker, D.J., Thorp, K.R., 2015. Remote sensing of evapotranspiration over cotton using the TSEB and METRIC energy balance models. Remote Sensing of Environment 158, 281–294.

Gerla, P.J., 1992. The relationship of water-table changes to the capillary fringe, evapotranspiration, and precipitation in intermittent wetlands. Wetlands 12, 91–98.

Glenn, E.P., Doody, T.M., Guerschman, J.P., Huete, A.R., King, E.A., McVicar, T.R., Van Dijk, A.I., Van Niel, T.G., Yebra, M., Zhang, Y., 2011. Actual evapotranspiration estimation by ground and remote sensing methods: the Australian experience. Hydrological Processes 25, 4103–4116.

Gonzalez-Dugo, M.P., Neale, C.M.U., Mateos, L., Kustas, W.P., Prueger, J.H., Anderson, M.C., Li, F., 2009. A comparison of operational remote sensing-based models for estimating crop evapotranspiration. Agricultural and Forest Meteorology 149, 1843–1853.

Gowda, P.H., Chavez, J.L., Colaizzi, P.D., Evett, S.R., Howell, T.A., Tolk, J.A., 2007. Remote sensing based energy balance algorithms for mapping ET: Current status and future challenges. Transactions of the ASABE 50, 1639–1644.

Grimmond, C.S.B., Oke, T.R., 1999. Evapotranspiration rates in urban areas. IAHS Publication 259, 235–244.

Haase, D., 2009. Effects of urbanisation on the water balance–A long-term trajectory. Environmental Impact Assessment Review 29, 211–219.

Hernandez, T., Nachabe, M., Ross, M., Obeysekera, J., 2003. Modeling runoff from variable source areas in humid, shallow water table environments. Journal of the American Water Resources Association 39, 75–85.

Hiemstra, J.A., Saaroni, H., Amorim, J.H., 2017. The urban heat Island: Thermal comfort and the role of urban greening, in: The Urban Forest. Springer, pp. 7–19.

Hwang, K., Choi, M., 2013. Seasonal trends of satellite-based evapotranspiration algorithms over a complex ecosystem in East Asia. Remote Sensing of Environment 137, 244–263.

Irmak, S., Haman, D.Z., 2003. Evapotranspiration: potential or reference. IFAS Extension, ABE 343.

Isaac, P.R., Leuning, R., Hacker, J.M., Cleugh, H.A., Coppin, P.A., Denmead, O.T., Raupach, M.R., 2004. Estimation of regional evapotranspiration by combining aircraft and ground-based measurements. Boundary-Layer Meteorology 110, 69–98.

Kilic, A., Allen, R., Trezza, R., Ratcliffe, I., Kamble, B., Robison, C., Ozturk, D., 2016. Sensitivity of evapotranspiration retrievals from the METRIC processing algorithm to improved radiometric resolution of Landsat 8 thermal data and to calibration bias in Landsat 7 and 8 surface temperature. Remote Sensing of Environment 185, 198–209.

KIŞI, Ö., 2006. Generalized regression neural networks for evapotranspiration modelling. Hydrological Sciences Journal 51, 1092–1105.

Kişi, Ö., 2011. Evapotranspiration modeling using a wavelet regression model. Irrigation Science 29, 241–252.

Kuehler, E., Hathaway, J., Tirpak, A., 2017. Quantifying the benefits of urban forest systems as a component of the green infrastructure stormwater treatment network. Ecohydrology 10: doi.org/10.1002./eco.1813.

Lennon, M., Scott, M., O'Neill, E., 2014. Urban design and adapting to flood risk: the role of green infrastructure. Journal of Urban Design 19, 745–758.

Lepot, M., Aubin, J.-B., Clemens, F.H., 2017. Interpolation in time series: An introductive overview of existing methods, their performance criteria and uncertainty assessment. Water 9, 796.

Liu, M., Tian, H., Chen, G., Ren, W., Zhang, C., Liu, J., 2008. Effects of Land-Use and Land-Cover Change on Evapotranspiration and Water Yield in China During 1900-2000 1.

JAWRA Journal of the American Water Resources Association 44, 1193–1207.

Liu, W., Hong, Y., Khan, S.I., Huang, M., Vieux, B., Caliskan, S., Grout, T., 2010. Actual evapotranspiration estimation for different land use and land cover in urban regions using Landsat 5 data. Journal of Applied Remote Sensing 4, 041873.

Liu, W., Chen, W., Peng, C., 2014. Assessing the effectiveness of green infrastructures on urban flooding reduction: A community scale study. Ecological Modelling 291, 6–14.

Livesley, S.J., McPherson, E.G., Calfapietra, C., 2016. The urban forest and ecosystem services: impacts on urban water, heat, and pollution cycles at the tree, street, and city scale. Journal of Environmental Quality 45, 119–124.

Lu, J., Sun, G., McNulty, S.G., Amatya, D.M., 2003. Modeling actual evapotranspiration from forested watersheds across the Southeastern United States. Journal of the American Water Resources Association 39, 886–896.

McLaughlin, D.L., Kaplan, D.A., Cohen, M.J., 2013. Managing forests for increased regional water yield in the southeastern US Coastal Plain. JAWRA Journal of the American Water Resources Association 49, 953–965.

Mörtberg, U.M., 2001. Resident bird species in urban forest remnants; landscape and habitat perspectives. Landscape Ecology 16, 193–203.

Nowak, D.J., Noble, M.H., Sisinni, S.M., Dwyer, J.F., 2001. People and trees: assessing the US urban forest resource. Journal of Forestry 99, 37–42.

Nowak, D., 2016. Urban forests. In: Robertson, G.; Mason, A., eds. Assessing the sustainability of agricultural and urban forests in the United States. USDA Forest Service FS-1067, Washington, DC: 37-52. 37–52.

[dataset] Soil Survey Staff, Natural Resources Conservation Service, Unites States Departmengt

of Agriculture. Soil Survey Geographic (SSURGO) Database. https://sdmdataaccess.sc.egov.usda.gov. (accessed 10 September, 2019).

O'Neil-Dunne. 2019. Tree Canopy Change Assessment, Virginia Beach, 2012-2018. Study by the University of Vermont.

Owen, T.W., Carlson, T.N., Gillies, R.R., 1998. An assessment of satellite remotely-sensed land cover parameters in quantitatively describing the climatic effect of urbanization. International Journal of Remote Sensing 19, 1663–1681.

Qiu, S., Zhu, Z., He, B., 2019. Fmask 4.0: Improved cloud and cloud shadow detection in Landsats 4–8 and Sentinel-2 imagery. Remote Sensing of Environment 231, 111205.

Qiu, G., Li, H., Zhang, Q., Chen, W., Liang, X., Li, X., 2013. Effects of Evapotranspiration on Mitigation of Urban Temperature by Vegetation and Urban Agriculture. Journal of Integrative Agriculture 12, 1307–1315. https://doi.org/10.1016/S2095-3119(13)60543-2.

Rossi, M.W., Whipple, K.X., Vivoni, E.R., 2016. Precipitation and evapotranspiration controls on daily runoff variability in the contiguous United States and Puerto Rico. Journal of Geophysical Research: Earth Surface 121, 128–145.

Rothfuss, Y., Biron, P., Braud, I., Canale, L., Durand, J.-L., Gaudet, J.-P., Richard, P., Vauclin, M., Bariac, T., 2010. Partitioning evapotranspiration fluxes into soil evaporation and plant transpiration using water stable isotopes under controlled conditions. Hydrological Processes 24, 3177–3194. https://doi.org/10.1002/hyp.7743.

Sanford, W.E., Selnick, D.L., 2013. Estimation of evapotranspiration across the conterminous United States using a regression with climate and land-cover data 1. JAWRA Journal of the American Water Resources Association 49, 217–230.

Scott, R.L., Huxman, T.E., Cable, W.L., Emmerich, W.E., 2006. Partitioning of

evapotranspiration and its relation to carbon dioxide exchange in a Chihuahuan Desert shrubland. Hydrological Processes: An International Journal 20, 3227–3243.

Senay, G.B., Friedrichs, M., Singh, R.K., Velpuri, N.M., 2016. Evaluating Landsat 8 evapotranspiration for water use mapping in the Colorado River Basin. Remote Sensing of Environment 185, 171–185.

Shao, Y., Li, G.L., Guenther, E., Campbell, J.B., 2015. Evaluation of topographic correction on subpixel impervious cover mapping with CBERS-2B data. IEEE Geoscience and Remote Sensing Letters 12, 1675–1679.

Singh, R.K., Liu, S., Tieszen, L.L., Suyker, A.E., Verma, S.B., 2012. Estimating seasonal evapotranspiration from temporal satellite images. Irrigation Science 30, 303–313.

Soz, S.A., Kryspin-Watson, J., Stanton-Geddes, Z., 2016. The role of green infrastructure solutions in urban flood risk management. Washington, DC: World Bank.

Stovin, V.R., Jorgensen, A., Clayden, A., 2008. Street trees and stormwater management. Arboricultural Journal 30, 297–310.

Sun, R., Chen, J.M., Zhu, Q., Zhou, Y., Liu, J., Li, J., Liu, S., Yan, G., Tang, S., 2004. Spatial distribution of net primary productivity and evapotranspiration in Changbaishan Natural Reserve, China, using Landsat ETM+ data. Canadian Journal of Remote Sensing 30, 731–742.

Sun G., McNulty, J., Moore Myers, J., Cohen, E., 2008. Impacts of multiple stresses on water demand and supply across the southeastern United States. Journal of America Water Resources Association 44: 1441-1457.

Taha, H., 1997. Urban climates and heat islands: albedo, evapotranspiration, and anthropogenic heat. Energy and Buildings 25, 99–103.

Teuling, A.J., Hirschi, M., Ohmura, A., Wild, M., Reichstein, M., Ciais, P., Buchmann, N., Ammann, C., Montagnani, L., Richardson, A.D., 2009. A regional perspective on trends in continental evaporation. Geophysical Research Letters 36, L02404.

Teuling, A.J., De Badts, E.A., Jansen, F.A., Fuchs, R., Buitink, J., Van Dijke, A.J.H., Sterling, S.M., 2019. Climate change, reforestation/afforestation, and urbanization impacts on evapotranspiration and streamflow in Europe. Hydrology and Earth System Sciences 23, 3631–3652.

Trezza, R., Allen, R.G., Tasumi, M., 2013. Estimation of actual evapotranspiration along the Middle Rio Grande of New Mexico using MODIS and landsat imagery with the METRIC model. Remote Sensing 5, 5397–5423.

Tsouni, A., Kontoes, C., Koutsoyiannis, D., Elias, P., Mamassis, N., 2008. Estimation of actual evapotranspiration by remote sensing: Application in Thessaly Plain, Greece. Sensors 8, 3586–3600.

[dataset] U.S. Census Bureau QuickFacts: Virginia Beach city, Virginia (County), n.d. https://www.census.gov/quickfacts/virginiabeachcityvirginiacounty (accessed 23, May, 2019).

Wu, C., Murray, A.T., 2003. Estimating impervious surface distribution by spectral mixture analysis. Remote Sensing of Environment 84, 493–505.

Yan, H., Wang, S.Q., Billesbach, D., Oechel, W., Zhang, J.H., Meyers, T., Martin, T.A., Matamala, R., Baldocchi, D., Bohrer, G., 2012. Global estimation of evapotranspiration using a leaf area index-based surface energy and water balance model. Remote Sensing of Environment 124, 581–595.

Zha, T., Barr, A.G., van der Kamp, G., Black, T.A., McCaughey, J.H., Flanagan, L.B., 2010.

Interannual variation of evapotranspiration from forest and grassland ecosystems in western Canada in relation to drought. Agricultural and Forest Meteorology 150, 1476–1484.

Zhang, L., Dawes, W.R., Walker, G.R., 2001. Response of mean annual evapotranspiration to vegetation changes at catchment scale. Water Resources Research 37, 701–708. https://doi.org/10.1029/2000WR

Zhang, Q., Wang, W., Wang, S., Zhang, L., 2016. Increasing trend of pan evaporation over the semiarid loess plateau under a warming climate. Journal of Applied Meteorology and Climatology 55, 2007–2020

Chapter 5. Conclusions

Monitoring past and current urban growth rates and patterns can help us better understand urbanization processes and provide valuable information for urban planners and policy-makers. Mapping urban extent at annual frequency could also be beneficial for those environmental models requiring land cover data at high temporal resolution. Such high temporal resolution urban change data could also facilitate analyzing the consequences of urban growth on the environment. Using Washington D.C. metropolitan area and Virginia Beach as case study, this dissertation has focused on 1)Mapping annual urban change by analyzing Landsat-derived NDVI time series data and NLCD; 2) Identifying near real-time urban change using machine learning; 3) Assessing urban growth's impacts on evapotranspiration.

First, this dissertation designed and compared three different methods for mapping annual urban change by analyzing Landsat-derived NDVI time series data from 1998 to 2014 and NLCD. Break-point method detects the year where the mean and standard deviation of the time series signal changes the most as the urban change year, and is proven as the optimal method among all the three. This method is better at detecting urbanization years rather than urban intensification years, and future research efforts might be focusing on improving the accuracy of detecting urban intensification years.

Second, this dissertation achieved near real-time urban change identification by using machine learning-based classification. Landsat-derived NDVI time series data for ten years were used as data input in machine learning classifiers, and the training dataset for urban change pixels were derived based on the method introduced in Chapter 2. Random forest classifier and Artificial Neural Networks (ANN) were compared, and the result found out ANN produced better result than random forest. Our model works well in urban settings, with overall accuracies of 95% and

93% for urban core and suburb area, respectively, but its performance is inferior in rural areas where urban change is hard to be distinguished from forest harvest.

Last, this dissertation compared annual ET rates among major land cover types to assess the impacts of urban growth on evapotranspiration. The result found out that urban has the lowest ET rate of approximately 550 mm/year while wetland forest, the major forest type in Virginia Beach, has the highest ET rate of around 2000 mm/year. Wetland forest contributed approximately 40% of the total ET by only constituting 20% of the total terrestrial land area. Converting forest or agricultural land to urban would result in a huge decrease in ET, thus increasing flood probability. Some land attribute data, such as impervious cover, canopy cover, and water table depth were used to explain the spatial variations of ET, and the result found out ET would increase with the increase of canopy cover and would decrease with the increase of impervious cover or water table depth. A polynomial regression model combing all the tree land attributes was constructed for the estimation of annual ET, and the R^2 has reached around 0.7, indicating its good estimation capability.

Overall, this dissertation proposed novel and accurate methods for annual urban mapping as well as ET quantification, and these methods could be potentially be applied elsewhere to provide valuable information for local urban planners and policy-makers.